DEPARTMENT OF MATHEMATICS & STATISTICS
COLLEGE OF ENGINEERING AND TECHNOLOGY
OLD DOMINION UNIVERSITY
NORFOLK, VIRGINIA 23529

THE REDUCTION OF DUCTED FAN ENGINE NOISE VIA A BOUNDARY INTEGRAL EQUATION METHOD

By
Principal Investigator:
Dr. J. Tweed

and

Co-Principal Investigator:
Dr. M. Dunn

Final Report
For the period April 1996 through April 1997

Prepared for
National Aeronautics and Space Administration
Lewis Research Center
Attn.: Dennis Huff, Technical Officer
Mail Stop 77-6
21000 Brookpark Road
Cleveland, OH 44135

Under
Grant Number NCC-3-469
ODURF #136161

February 1997

Final Report: April 1996 - April 1997

The Reduction of Ducted Fan Engine Noise Via a Boundary Integral Equation Method

M.H. Dunn and J. Tweed
Department of Mathematics and Statistics
Old Dominion University

Introduction

The development of a Boundary Integral Equation Method (BEM) for the prediction of ducted fan engine noise is discussed. The method is motivated by the need for an efficient and versatile computational tool to assist in parametric noise reduction studies. In this research, the work in reference 1 was extended to include passive noise control treatment on the duct interior.

The BEM considers the scattering of incident sound generated by spinning point thrust dipoles in a uniform flow field by a thin cylindrical duct. The acoustic field is written as a superposition of spinning modes. Modal coefficients of acoustic pressure are calculated term by term.

The BEM theoretical framework is based on Helmholtz potential theory. A boundary value problem is converted to a boundary integral equation formulation with unknown single and double layer densities on the duct wall. After solving for the unknown densities, the acoustic field is easily calculated.

The main feature of the BIEM is the ability to compute any portion of the sound field without the need to compute the entire field. Other noise prediction methods such as CFD and Finite Element methods lack this property. Additional BIEM attributes include versatility, ease of use, rapid noise predictions, coupling of propagation and radiation both forward and aft, implementable on midrange personal computers, and valid over a wide range of frequencies.

Accomplishments

Given a locally reacting, segmented liner model on the duct interior, a system of boundary integro-differential equations for the scattered acoustic pressure field was derived (references 2 and 3). The equations are hypersingular and require special analytical and computational techniques to solve. These methods are near completion.

For small inflow Mach numbers ($M<0.4$), the complexity of the integra equations can be significantly reduced. The small Mach number BIEM has been determined to be valid at takeoff and approach. Mathematical details of the derivation and solution techniques will in reference 2.

BIEM methodology and several passive and active noise control studies were presented at the NASA AST Engine/Nacelle Noise Workshop (reference 3). In this presentation, the accuracy, versatility and simplicity of the BEM were demonstrated.

A computer program for predicting ducted fan engine noise (TBEM3D) and user manual (reference 4) has been written. The TBEM3D code was designed for general use by the aeroacoustics community and is available electronically.

BIEM methods were applied to sound radiation and propagation in two dimensions. The resulting methodology is valid for the shielding of sound by thin strips (wings) and the radiation and propagation of sound in a finite length channel. The 2-D channel configuration is an excellent tool for studying the effects of a scarfed inlet on noise directivity (see reference 5). A general use 2D noise prediction computer program (TBIEM2D) and user manual are near completion.

Conclusions

The effectiveness of BIEM as a tool for active and passive noise control has been clearly demonstrated. Due to the simplicity, speed, accuracy, and versatility of BIEM, TBEM3D is far superior to wave envelope and CFD codes for conducting parametric noise reduction studies.

The implicit coupling of sound radiation and propagation both forward and aft are unique features of BIEM. In addition, the far field radiation condition is satisfied implicitly. Consequently, special boundary conditions at an artificial far field boundary and at the duct's inlet and exhaust planes are not required. These theoretical niceties further enhance the simplicity of BEM.

References

1. M.H. Dunn, J. Tweed, and F. Farassat: The Prediction of Ducted Fan Engine Noise Via a Boundary Integral Equation Method; AIM Paper 96-1770, State College, PA, 1996.

2. M.H. Dunn, J. Tweed, and F. Farassat: Acoustic Radiation and Propagation for an Acoustically Treated Engine Duct Via a Boundary Integral Equation Method. to be submitted to Journal of Sound and Vibration; final version in progress

3. M.H. Dunn, J. Tweed, and F. Farassat: Rapid Ducted Fan Noise Prediction Via a Boundary Integral Equation Method; AST Engine/Nacelle Noise Workshop, Volume III: Fan Analysis/Prediction, Compendium of Presentation Viewgraphs.

4. M.H. Dunn: TBIEM3D - A Computer Program for Predicting Ducted Fan Engine Noise; to be submitted as a NASA Contractor Report (see attachment)

5. M.H. Dunn and R. St. John: A Study of Noise Radiation from a Two Dimensional Scarf Duct; to be submitted as a NASA Contractor Report (see attachment)

AIAA-96-1770

The Prediction of Ducted Fan Engine Noise Via a Boundary Integral Equation Method

M.H. Dunn and J. Tweed
Old Dominion University, Norfolk, Va.

F. Farassat
NASA Langley Research Center, Hampton, Va.

2nd AIAA/CEAS Aeroacoustics Conference
May 6-8,1996/State College, PA

THE PREDICTION OF DUCTED FAN ENGINE NOISE VIA A BOUNDARY INTEGRAL EQUATION METHOD

M. H. Dunn* and J. Tweed†
Old Dominion University
Norfolk, VA

F. Farassat‡
NASA Langley Research Center
Hampton, VA

Abstract

A computationally efficient Boundary Integral Equation Method (BIEM) for the prediction of ducted fan engine noise is presented. The key features of the BIEM are its versatility and the ability to compute rapidly any portion of the sound field without the need to compute the entire field. Governing equations for the BIEM are based on the assumptions that all acoustic processes are linear, generate spinning modes, and occur in a uniform flow field. An exterior boundary value problem (BVP) is defined that describes the scattering of incident sound by an engine duct with arbitrary profile. Boundary conditions on the duct walls are derived that allow for passive noise control treatment. The BVP is recast as a system of hypersingular boundary integral equations for the unknown duct surface quantities. BIEM solution methodology is demonstrated for the scattering of incident sound by a thin cylindrical duct with hard walls. Numerical studies are conducted for various engine parameters and continuous portions of the total pressure field are computed. Radiation and duct propagation results obtained are in agreement with the classical results of spinning mode theory for infinite ducts.

Notation

~	denotes that a quantity is dimensional when appearing over a variable
(r, ψ, z)	cylindrical coordinates - stationary frame
t	time
Z	axial coordinate - stretched, moving frame
$\tilde{r}_{max}$	maximum fan radius
$r_D^{\pm}$	radial coordinate of duct exterior (interior) profile
$\tilde{\rho}_0$	ambient density
$\tilde{c}$, c	ambient sound speed
V_F	forward flight speed
M_F	$= V_F/c$ forward flight Mach number
β	$= \sqrt{1-M_F^2}$ stretching parameter
N_B	number of fan blades
$\tilde{\Omega}, \Omega$	shaft speed
M_{TIP}	$= \tilde{r}_{max}\tilde{\Omega}/\tilde{c}$ tip Mach number
a	axial coordinate of duct trailing edge in stretched, moving frame
b	axial coordinate of duct leading edge in stretched, moving frame
L_D	ratio of duct length to duct diameter
m	circumferential mode number
k	$= mM_{TIP}$ characteristic wave number of m-th circumferential mode
k_z	axial wave number for first radial mode and m-th circumferential mode
κ	$= k/\beta$ modified wave number
p_t'	Eulerian description of total acoustic pressure field
p_s'	Eulerian description of scattered acoustic pressure field
p_i'	Eulerian description of incident acoustic pressure field
u_n	Eulerian description of normal component of acoustic velocity field
$\partial/\partial n$	normal derivative operator in stationary frame (with respect to outward facing normal to duct surface)
$\partial/\partial N$	normal derivative operator in stretched, moving frame (with respect to outward facing normal to stretched duct surface)
$\zeta^{\pm}$	surface acoustic impedance for duct exterior (interior)

---

* Research Associate Professor, AIAA Member
† Chairman, Department of Mathematics and Statistics
‡ Senior Research Scientist, AIAA Associate Fellow

Introduction

Ducted fan engine noise is dominated by the fan component at takeoff and approach. Community exposure to the high levels of radiated fan noise at these conditions is significant. The reduction of tonal noise produced by the rotating components of high bypass turbofan engines is therefore of primary concern to the aeroacoustician. The design of active and passive noise abatement technology can be facilitated by advanced analytical tools for predicting the radiated sound from engine ducts. To be useful in design studies, prediction tools should be fast, versatile, accurate, and implementable on mainstream computer systems. The ability to compute only a portion of the sound field without the need to calculate the entire field is an important attribute in conducting rapid noise predictions. Computational approaches such as Finite Element Methods (FEM) and Computational Aeroacoustics (CAA) methods lack this property. For this reason, farfield noise calculations using FEM or CAA require vast amounts of computational time and computer storage. Therefore, the use of FEM and CAA for parametric studies in noise abatement research is limited.

In this paper, a Boundary Integral Equation Method for the prediction of ducted fan engine noise is presented. The method is based on the equations of linearized acoustics with uniform inflow. A scattering approach is adopted in which the acoustic pressure field is split into known incident and unknown scattered components. The source process is assumed to generate an incident pressure field that can be represented by a superposition of spinning modes. In a frame of reference moving with the engine duct and in regions of space not occupied by acoustic sources or scattering surfaces, the components of acoustic pressure are governed by Helmholtz' equation. An exterior boundary value problem is obtained by the inclusion of boundary conditions on the duct surfaces. The most general form of the boundary conditions allows for a spatially varying, locally reacting liner model on the duct surface.

By considering special values of the specific acoustic impedance in the boundary conditions, the classical Dirichlet and Neumann boundary values are obtained. The boundary value problem is then solved by expressing the scattered pressure field in terms of double and single layer Helmholtz potentials with unknown densities that are related to surface pressure and the normal derivative of surface pressure, respectively. Application of the boundary conditions to the layer representation yields a system of one-dimensional, hypersingular boundary integral equations for the unknown layer densities. The source terms for the system are related to the known incident pressure and its normal derivative. This system of boundary integral equations and method of solution comprise the BIEM.

The system of boundary integral equations is valid for engine ducts with arbitrary profile. If, however, the duct is approximated by an infinitesimally thin cylindrical tube, the complexity of the integral equation kernels is substantially reduced.

Analytical results will be presented that separate the singular and logarithmic portions of the integral equation kernels from the bounded parts. This analysis is significant because calculations involving singular and logarithmic integrals are available in closed form, thus avoiding time consuming, customized numerical integration techniques.

To demonstrate the BIEM, the solution procedure for a thin pipe geometry with hard wall boundary conditions is presented. A collection of spinning point dipoles located inside the duct are used to simulate the loading component of the fan noise and generate the incident pressure field. Several sets of engine operating parameters are considered in this study. Various researchers[1-5] have employed boundary integral techniques to solve this problem. Differences in the present work relative to the referenced works appear in the conclusions section of this paper.

Boundary Value Problem Derivation

In the analysis that follows, all quantities have been nondimensionalized; length by $\tilde{r}_{max}$, mass by $\tilde{\rho}_0 \tilde{r}_{max}^3$, and time by $\tilde{\Omega}^{-1}$.

We consider an engine fan surrounded by an axisymmetric, nondeformable duct of arbitrary profile translating in the +z (axial) direction with uniform speed V_F (see figure 1). The fan is composed of N_B equally spaced blades and rotates with shaft speed Ω. The incident acoustic pressure field generated by the fan is known. Linear conditions are assumed to apply and the inflow is uniform.

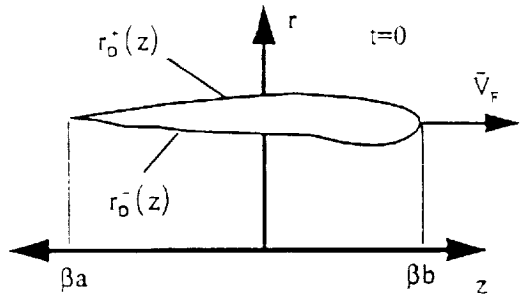

Figure 1: Duct Geometry
(Cylindrical, Stationary Coordinates)

Governing Differential Equations

The total acoustic pressure in the sound field is written as a sum of incident and scattered parts.

$$p'_t(r,\psi,z,t) = p'_i(r,\psi,z,t) + p'_s(r,\psi,z,t) \quad (1)$$

In regions of space that contain no scattering surfaces, p'_s is governed by the homogeneous wave equation.

$$\left[\frac{1}{c^2}\frac{\partial^2}{\partial t^2} - \frac{1}{r}\frac{\partial}{\partial r}\left(r\frac{\partial}{\partial r}\right) - \frac{1}{r^2}\frac{\partial^2}{\partial \psi^2} - \frac{\partial^2}{\partial z^2}\right] p'_s = 0 \quad (2)$$

Total acoustic pressure and acoustic velocity are related through the normal component of the acoustic momentum equation.

$$\frac{\partial u_n(r,\psi,z,t)}{\partial t} + \frac{\partial p'_t(r,\psi,z,t)}{\partial n} = 0 \quad (3)$$

In a frame of reference moving with the duct, all dependent acoustic variables can be expressed as linear superpositions of spinning modes. For example, the scattered pressure has the form

$$p'_s(r,\psi,Z,t) = \sum_{m/N_B=-\infty}^{\infty} P_s^m(r,Z)\, e^{im(\Omega t-\psi)} \quad (4a)$$

and the acoustic velocity is written

$$u_n(r,\psi,Z,t) = \sum_{m/N_B=-\infty}^{\infty} U_N^m(r,Z)\, e^{im(\Omega t-\psi)}, \quad (4b)$$

where the stretched, moving axial coordinate Z is given by

$$Z = \frac{z - V_F t}{\beta}. \quad (5)$$

The BIEM calculates modal amplitudes in (4) term by term. For notational convenience, the superscript m on the modal coefficients is dropped hereafter.

Define the dependent variables Q_s and Φ_N by

$$Q_s(r,Z) = P_s(r,Z)\, e^{i\kappa M_r Z} \quad (6a)$$

and

$$\Phi_N(r,Z) = U_N(r,Z)\, e^{i\kappa M_r Z}, \quad (6b)$$

with similar definitions for the total and incident pressures. Combining (4-6) with (2) yields the two dimensional Helmholtz equation

$$\left[\frac{1}{r}\frac{\partial}{\partial r}\left(r\frac{\partial}{\partial r}\right) + \frac{\partial^2}{\partial Z^2} - \frac{m^2}{r^2} + \kappa^2\right] Q_s = 0 \quad (7)$$

for the m-th coefficient. Using the definitions in (6), the momentum equation (3) can be written as

$$\Phi_N(r,Z) = \frac{1}{c} e^{i\frac{\kappa}{M_r}Z} \times \int_{-\infty}^{Z} e^{-i\frac{\kappa}{M_r}Z'}\left[\frac{\beta}{M_F}\frac{\partial Q_t}{\partial N'} - i\kappa M_F N'_Z Q_t\right] dZ', \quad (8)$$

where N'_Z is the axial component of the outward facing, unit normal to the stretched duct surface. Equation (8) is valid for $M_F > 0$. If the duct is stationary ($M_F = 0$), then (7) and (8) reduce to

$$\left[\frac{1}{r}\frac{\partial}{\partial r}\left(r\frac{\partial}{\partial r}\right) + \frac{\partial^2}{\partial z^2} - \frac{m^2}{r^2} + k^2\right] P_s = 0 \quad (9)$$

and

$$U_n(r,Z) + \frac{1}{ick}\frac{\partial P_t(r,Z)}{\partial n} = 0. \quad (10)$$

Equations (7-10) are valid for points not lying on the surface of the stretched duct.

Boundary Conditions

To meet noise certification levels it is necessary to treat the engine duct with passive noise suppression technology. In this work, the duct treatment is modeled by a locally reacting, axially varying liner.

Define the surface functions $Q_t^{\pm}$ and $\Phi_N^{\pm}$ by

$$Q_t^{\pm}(Z) = \lim_{r\to r_0^{\pm}(Z)} Q_t(r,Z) \quad Z\in[a,b] \quad (11a)$$

and

$$\Phi_N^{\pm}(Z) = \lim_{r\to r_0^{\pm}(Z)} \Phi_N(r,Z) \quad Z\in[a,b] \quad (11b)$$

with similar definitions for $Q_s^{\pm}$, $Q_i^{\pm}$, normal velocity, and all pressure components.

Myers[6] has shown that if $\zeta^{\pm}(Z)$ represents the specific acoustic surface impedance, then, in the stretched, moving frame of reference, the modal coefficients of velocity and pressure satisfy the boundary equation

$$\Phi_N^{\pm}(Z) + \left(1 + \frac{M_F^2}{\beta}\frac{\partial}{\partial Z}\right)\frac{Q_t^{\pm}(Z)}{\zeta^{\pm}(Z)} = 0 \quad Z\in[a,b]. \quad (12)$$

Equation (12) represents two boundary conditions, one for the exterior surface and the other for the interior surface. The boundary conditions for the stationary case reduce to

$$U_N^{\pm}(Z)+\frac{P_t^{\pm}(Z)}{\zeta^{\pm}(Z)}=0 \quad Z\in[a,b]. \tag{13}$$

By considering special values for the functions $\zeta^{\pm}$ in (12) and (13), several boundary conditions of interest are derivable. Total sound absorption is achieved if

$$\zeta^{+}=\zeta^{-}=\text{constant}\to 0. \tag{14}$$

Total sound reflection (hard walls) arises for

$$\zeta^{+}=\zeta^{-}=\text{constant}\to \infty. \tag{15}$$

Of particular relevance to actual engine ducts, is the case of a hard exterior surface ($\zeta^{+}\to\infty$) and lined interior. The boundary conditions for this situation are

$$\Phi_N^{+}(Z)=0 \quad Z\in[a,b] \tag{16a}$$

and

$$\Phi_N^{-}(Z)+\left(1+\frac{M_F^2}{\beta}\frac{\partial}{\partial Z}\right)\frac{Q_t^{-}(Z)}{\zeta^{-}(Z)}=0 \quad Z\in[a,b]. \tag{16b}$$

We now evaluate the momentum equation on the duct surface to obtain a relation between surface pressure and surface velocity. Let

$$\left(\frac{\partial Q_t}{\partial N}\right)^{\pm}(Z)=\lim_{r\to\zeta^{\pm}(Z)}\frac{\partial Q_t(r,Z)}{\partial N}, \tag{17}$$

with normal derivatives of other dependent acoustic variables evaluated on the duct surfaces similarly defined. Then from (8), (10), and (11) we get

$$\Phi_N^{\pm}(Z)=\frac{1}{c}e^{-i\frac{\kappa}{M_F}Z}\times$$

$$\int_{-\infty}^{Z}e^{-i\frac{\kappa}{M_F}Z'}\left[\frac{\beta}{M_F}\left(\frac{\partial Q_t}{\partial N'}\right)^{\pm}-ikM_F N_Z' Q_t^{\pm}\right]dZ' \tag{18}$$

$$Z\in[a,b] \quad M_F>0$$

and

$$U_t^{\pm}(Z)=-\frac{1}{ick}\left(\frac{\partial P_t}{\partial n}\right)^{\pm}(Z) \tag{19}$$

$$Z\in[a,b] \quad M_F=0$$

Classical boundary conditions are obtained for the stationary case. Combining (13) and (19) yields the Robin's boundary conditions

$$\frac{P_t^{\pm}(Z)}{\zeta^{\pm}(Z)}-\frac{1}{ick}\left(\frac{\partial P_t}{\partial n}\right)^{\pm}=0 \quad Z\in[a,b]. \tag{20}$$

Dirichlet or Neumann conditions are obtained by application of (14) or (15), respectively, to (20).

We complete the derivation of the boundary value problem by requiring the dependent acoustic variables to satisfy the appropriate Sommerfeld radiation condition. Additional conditions may apply depending on the smoothness of the duct walls. If there are points on the duct that do not possess continuously turning tangent planes, then edge conditions specifying the behavior of the acoustic pressure at these points must be provided[7]. Edge behavior is determined from the physics of the problem together with an asymptotic analysis of the governing equations in a neighborhood of the edge. This problem occurs at the leading and trailing edges of the thin pipe approximation, for example.

Summary

The above analysis describes a uniquely solvable two dimensional boundary value problem for the scattered acoustic pressure in the sound field. For the stationary case, the boundary value problem is defined by (1), (9), (19), (20), the radiation condition, and the edge conditions (if applicable). If the duct is in motion, then (1), (6), (7), (12), (18), radiation and edge conditions completely define the boundary value problem.

Boundary Integral Equation Formulation

In this section, we reformulate the boundary value problem by deriving one dimensional boundary integral equations in which the boundary functions $Q_s^{\pm}$ and $Q_N^{\pm}$ are unknown, where

$$Q_N^{\pm}(Z)=\left(\frac{\partial Q_s}{\partial N}\right)^{\pm}(Z). \tag{21}$$

Once the scattered boundary functions are determined, the scattered pressure in the sound field is calculated pointwise via a Helmholtz layer representation that satisfies the Sommerfeld radiation condition implicitly.

Helmholtz Layer Representation

The Green's function for the two dimensional

Helmholtz operator in (7) can be written

$$G(r,r',Z-Z') = \frac{1}{2\pi}\int_0^{\pi} \cos m\psi \frac{e^{-i\kappa R}}{R} d\psi \qquad (22)$$

where

$$R = \sqrt{r^2 + r'^2 - 2rr'\cos\psi + (Z-Z')^2}\,. \qquad (23)$$

Using results from Helmholtz potential theory[8] and (21-23), the solution of (7) is expressed as the sum of single and double layer Helmholtz potentials with densities $Q_N^{\pm}$ and $Q_s^{\pm}$, respectively. Thus,

$$\begin{aligned} Q_s(r,Z) = {} & s^+\left[Q_N^+\right](r,Z) - d^+\left[Q_s^+\right](r,Z) + \\ & s^-\left[Q_N^-\right](r,Z) - d^-\left[Q_s^-\right](r,Z) \end{aligned} \qquad (24)$$

Equation (24) is valid everywhere except for (r,Z) on the stretched duct surface. The field operators $s^{\pm}$ and $d^{\pm}$ are defined by

$$s^{\pm}[f](r,Z) = \frac{1}{2\pi}\int_a^b f(Z')\left[\lim_{r'\to r_0^{\pm}(Z')} G\right] J^{\pm}(Z')dZ' \qquad (25)$$

and

$$d^{\pm}[f](r,Z) = -\frac{1}{2\pi}\int_a^b f(Z')\left[\lim_{r'\to r_0^{\pm}(Z')} \frac{\partial G}{\partial N'}\right] J^{\pm}(Z')dZ' \qquad (26)$$

where f is some sufficiently smooth function and $J^{\pm}(Z')dZ'$ are the elements of arclength along the curves $r = r_0^{\pm}(Z')$.

If the boundary functions were known, then the scattered acoustic field could be obtained from (24).

Singular Boundary Operator Notation

In order to apply the boundary conditions to the field equation (24), it is necessary to evaluate the 2-D layer potentials and their derivatives on the stretched duct surface. The resulting 1-D boundary operators are singular. For $Z \in [a,b]$, define the following singular boundary operator - kernel pairs:

$$\begin{aligned} S^{\pm}[f](Z) &= \int_a^b f(Z')S^{\pm}(Z,Z')dZ' \\ S^{\pm}(Z,Z') &= \frac{1}{2\pi}J^{\pm}(Z')\lim_{\substack{r'\to r_0^{\pm}(Z') \\ r\to r_0^{\pm}(Z)}} G \end{aligned} \qquad (27)$$

$$\begin{aligned} D^{\pm}[f](Z) &= \int_a^b f(Z')D^{\pm}(Z,Z')dZ' \\ D^{\pm}(Z,Z') &= \frac{1}{2\pi}J^{\pm}(Z')\lim_{\substack{r'\to r_0^{\pm}(Z') \\ r\to r_0^{\pm}(Z)}} \frac{\partial G}{\partial N'} \end{aligned} \qquad (28)$$

$$\begin{aligned} S_N^{\pm}[f](Z) &= \int_a^b f(Z')S_N^{\pm}(Z,Z')dZ' \\ S_N^{\pm}(Z,Z') &= \frac{1}{2\pi}J^{\pm}(Z')\lim_{\substack{r'\to r_0^{\pm}(Z') \\ r\to r_0^{\pm}(Z)}} \frac{\partial G}{\partial N} \end{aligned} \qquad (29)$$

$$\begin{aligned} D_N^{\pm}[f](Z) &= \int_a^b f(Z')D_N^{\pm}(Z,Z')dZ' \\ D_N^{\pm}(Z,Z') &= \frac{1}{2\pi}J^{\pm}(Z')\lim_{\substack{r'\to r_0^{\pm}(Z') \\ r\to r_0^{\pm}(Z)}} \frac{\partial^2 G}{\partial N \partial N'} \end{aligned} \qquad (30)$$

$$\begin{aligned} S_Z^{\pm}[f](Z) &= \int_a^b f(Z')S_Z^{\pm}(Z,Z')dZ' \\ S_Z^{\pm}(Z,Z') &= \frac{1}{2\pi}J^{\pm}(Z')\lim_{\substack{r'\to r_0^{\pm}(Z') \\ r\to r_0^{\pm}(Z)}} \frac{\partial G}{\partial Z} \end{aligned} \qquad (31)$$

$$\begin{aligned} D_Z^{\pm}[f](Z) &= \int_a^b f(Z')D_Z^{\pm}(Z,Z')dZ' \\ D_Z^{\pm}(Z,Z') &= \frac{1}{2\pi}J^{\pm}(Z')\lim_{\substack{r'\to r_0^{\pm}(Z') \\ r\to r_0^{\pm}(Z)}} \frac{\partial^2 G}{\partial Z \partial N'} \end{aligned} \qquad (32)$$

Note that operators are denoted by bold face type. The kernels are singular for $Z - Z' = 0$. The nature of the singularities is examined below.

Singular Kernel Analysis

We list here, without proof, the asymptotic properties for $|Z-Z'| << 1$ of the above kernels. The singular character of the kernels is obtained by local analyses, the details of which will appear in a future publication:

$$S^{\pm}(Z,Z') = g_{13}^{\pm}(Z)\ln|Z-Z'| + K_1(Z,Z') \qquad (33)$$

$$D^{\pm}(Z,Z') = \frac{g_{12}^{\pm}(Z)}{Z-Z'} + g_{23}^{\pm}(Z)\ln|Z-Z'| + K_2(Z,Z') \qquad (34)$$

$$S_N^{\pm}(Z,Z') = \frac{g_{32}^{\pm}(Z)}{Z-Z'} + g_{33}^{\pm}(Z)\ln|Z-Z'| + K_3(Z,Z') \quad (35)$$

$$D_N^{\pm}(Z,Z') = \frac{g_{41}^{\pm}(Z)}{(Z-Z')^2} + \frac{g_{42}^{\pm}(Z)}{Z-Z'} + g_{43}^{\pm}(Z)\ln|Z-Z'| + K_4(Z,Z') \quad (36)$$

$$S_Z^{\pm}(Z,Z') = \frac{g_{52}^{\pm}(Z)}{Z-Z'} + g_{53}^{\pm}(Z)\ln|Z-Z'| + K_5(Z,Z') \quad (37)$$

$$D_Z^{\pm}(Z,Z') = \frac{g_{61}^{\pm}(Z)}{(Z-Z')^2} + \frac{g_{62}^{\pm}(Z)}{Z-Z'} + g_{63}^{\pm}(Z)\ln|Z-Z'| + K_6(Z,Z') \quad (38)$$

where $g_{ij}^{\pm}$, and K_i are known continuous functions.

The leading behavior for the single layer kernel (33) is logarithmic. Therefore, the associated operator is weakly singular. The leading terms for the kernels (34,35,37) are of the Cauchy type. Whilst, the kernels (36,38) are of the strongly singular Hadamard type. Consequently, integrals involved with the kernels (34-38) are divergent and must be interpreted in the finite part sense[10].

All of the above kernels have the logarithmic portions extracted. Integrations involving these terms are defined but difficult to achieve numerically. This problem is mitigated by the development of analytical results for the associated operators. Examples of this, as well as analytical results for the Cauchy and Hadamard terms, are presented in the results section.

Calculations involving the continuous portions of the kernels are performed by straightforward numerical integration.

Jump Relations from Potential Theory

Using the above operator notation, we state continuity properties for the single and double layers as a field point approaches the surface from the exterior of the duct. For sufficiently smooth f and $r_D^{\pm}$ (except possibly at $Z = a, b$), we have the following results[8] for $Z \in (a,b)$.

$$\lim_{r \to r_D^{\pm}(Z)} s^{\pm}[f](r,Z) = S^{\pm}[f](Z) \quad (39)$$

$$\lim_{r \to r_D^{\pm}(Z)} d^{\pm}[f](r,Z) = -\frac{1}{2}f(Z) + \mathbf{D}^{\pm}[f](Z) \quad (40)$$

$$\lim_{r \to r_D^{\pm}(Z)} \frac{\partial}{\partial N} s^{\pm}[f](r,Z) = \frac{1}{2}f(Z) + \mathbf{S}_N^{\pm}[f](Z) \quad (41)$$

$$\lim_{r \to r_D^{\pm}(Z)} \frac{\partial}{\partial N} d^{\pm}[f](r,Z) = \mathbf{D}_N^{\pm}[f](Z) \quad (42)$$

Boundary Integral Equations

A system of integral equations for $Q_s^{\pm}$ and $Q_N^{\pm}$ is derived by applying the boundary conditions (12) and (18) to (24) and (39-42).

We begin by deriving some preliminary results. From (1), (6a), (11a), (24), and (39-40) we write

$$Q_t^{\pm}(Z) = Q_t^{\pm}(Z) + S^{\pm}[Q_N^{\pm}](Z) + (\mathbf{I} - \mathbf{D}^{\pm})[Q_s^{\pm}](Z) \quad Z \in [a,b] \quad (43)$$

and

$$\frac{\partial Q_t^{\pm}}{\partial Z}(Z) = \frac{\partial Q_i^{\pm}}{\partial Z}(Z) + S_Z^{\pm}[Q_N^{\pm}](Z) + \frac{\partial Q_s^{\pm}}{\partial Z}(Z) - \mathbf{D}_Z^{\pm}[Q_s^{\pm}](Z) \quad Z \in [a,b] \quad (44)$$

Combining (1), (6a), (17), (24), and (41-42) yields

$$\left(\frac{\partial Q_t}{\partial N}\right)^{\pm}(Z) = \left(\frac{\partial Q_i}{\partial N}\right)^{\pm}(Z) + (\mathbf{I} + S_N^{\pm})[Q_N^{\pm}](Z) + \mathbf{D}_N^{\pm}[Q_s^{\pm}](Z) \quad Z \in [a,b] \quad (45)$$

Define the unknown surface vector functions $\bar{q}^{\pm}$ by

$$\bar{q}^{\pm}(Z) = \left(Q_s^{\pm}(Z), Q_N^{\pm}(Z)\right)^T. \quad (46)$$

Combining the boundary conditions (12) and (18) with results (33-46) yields the system of integral equations

$$\int_{-\infty}^{Z} e^{-i\frac{\kappa}{M_r}Z'} \mathbf{K}_1^{\pm}[\bar{q}^{\pm}](Z')dZ' + \mathbf{K}_2^{\pm}[\bar{q}^{\pm}](Z) = \bar{q}_i^{\pm}(Z) \quad Z \in (a,b) \quad (47)$$

for the four unknown surface functions. The vector function $\bar{q}_i^{\pm}$ is known from the incident pressure field and the integral operators $\mathbf{K}_1^{\pm}$ and $\mathbf{K}_2^{\pm}$ have the general form

$$A(Z)\bar{q}^{\pm}(Z)+B(Z)\frac{\partial\bar{q}^{\pm}(Z)}{\partial Z}+$$

$$C(Z)\int_a^b \frac{\bar{q}^{\pm}(Z')}{(Z-Z')^2}dZ'+D(Z)\int_a^b \frac{\bar{q}^{\pm}(Z')}{Z-Z'}dZ'+, \quad (48)$$

$$E(Z)\int_a^b \bar{q}^{\pm}(Z')\ln|Z-Z'|dZ'+K_B[\bar{q}^{\pm}](Z)$$

where **A**,...,**E** are matrices of known functions and K_B is an integral operator with continuous kernels. The matrix functions are determined from the coefficients in (33-38) and depend on the surface impedances and the duct curves $r=r_0^{\pm}(Z')$. Explicit expressions are lengthy and will not be presented here.

Examination of (48) indicates that (47) is a system of one dimensional, hypersingular, integro-differential equations of the second kind. As indicated previously, (47) must be augmented by a set of edge conditions if applicable. The authors are not aware of any theory that describes the solvability of (47). This subject is a matter of ongoing research. However, for certain simple cases, one of which is described in the next section, (47) is greatly simplified and solvability theorems do exist.

The characterization of the integral equation kernels by (48) greatly simplifies the numerical solution of (47). Analytical results for the logarithmic, Cauchy, and Hadamard kernels are available in many cases[11] and the continuous portions of the kernel can be computed by straightforward numerical integration.

Results

In this section, we consider the scattering of incident sound by an infinitesimally thin cylindrical duct of unit radius. The duct can be stationary or in motion. The interior and exterior walls of the duct are assumed to be hard. For this case, the complexity of the boundary integral equations is reduced significantly.

Boundary Integral Equation Formulation

From (12) and (18) the boundary conditions are

$$\int_{-\infty}^{Z} e^{-i\frac{\kappa}{M_r}Z'}\left(\frac{\partial Q_t}{\partial N}\right)^{\pm}(Z')dZ'=0 \quad Z\in[a,b]. \quad (49)$$

Differentiating (49) with respect to Z and using the relationships between total, scattered, and incident pressures yields the boundary equations

$$\left(\frac{\partial Q_t}{\partial N}\right)^{\pm}=Q_N^{\pm}\pm\left(\frac{\partial Q_i}{\partial\tau}\right)^{\pm}=0 \quad Z\in[a,b]. \quad (50)$$

Since the incident pressure and its derivatives are continuous across the duct surface we add the exterior and interior equations in (50) to get

$$Q_N^{+}+Q_N^{-}=0 \quad Z\in[a,b]. \quad (51)$$

Equation (51) is used below to simplify the field equation (24).

Define the jump in scattered pressure across the duct wall by

$$\Delta Q_s(Z)=Q_s^{+}(Z)-Q_s^{-}(Z) \quad Z\in[a,b]. \quad (52)$$

Referring to (25-26) observe that

$$d^{-}[f](r,Z)=-d^{+}[f](r,Z) \quad (53)$$

and

$$s^{-}[f](r,Z)=s^{+}[f](r,Z). \quad (54)$$

Thus, applying (51-54) to (24) produces the field equation

$$Q_s(r,Z)=-d[\Delta Q_s](r,Z). \quad (55)$$

Therefore, the scattered acoustic pressure in the sound field is written as a double layer with density given by the scattered pressure jump. Since the interior and exterior duct surfaces are the same, we have omitted the superscript on the double layer operator.

A single integral equation for ΔQ_s is obtained from (49) as follows: Use (42) to evaluate the normal derivative of (55) on the exterior wall, then combine this result with the exterior boundary condition in (49) to give

$$\int_{-\infty}^{Z} e^{-i\frac{\kappa}{M_r}Z'}D_N[\Delta Q_s](Z')dZ'=\int_{-\infty}^{Z} e^{-i\frac{\kappa}{M_r}Z'}\left.\frac{\partial Q_i}{\partial\tau}\right|_{r=1}(Z')dZ' \quad Z\in[a,b] \quad (56)$$

It is advantageous to rewrite (56) as the system of equations

$$D_N[\Delta Q_s](Z)=\left.\frac{\partial Q_i}{\partial\tau}\right|_{r=1}(Z) \quad Z\in[a,b] \quad (57a)$$

and

$$g[\Delta Q_s] = C_0, \tag{57b}$$

where the functional g is defined by

$$g[f] = \int_{-\infty}^{a} e^{-i\frac{\kappa}{M_r}Z'} D_N[f](Z')dZ' \tag{58}$$

and

$$C_0 = \int_{-\infty}^{a} e^{-i\frac{\kappa}{M_r}Z'} \left.\frac{\partial Q_i}{\partial \tau}\right|_{\tau=1} (Z')dZ'. \tag{59}$$

Equation (57a) is obtained by differentiating (56), and (57b) by evaluating (56) at the trailing edge. No information is lost by this reformulation. For the stationary case, (57b) is satisfied trivially. By performing a local analysis on the kernel in (57a) it can be shown to have the form

$$D_N(Z-Z') = \frac{A}{(Z-Z')^2} + \frac{}{B\ln|Z-Z'| + K_B(Z-Z')}, \tag{60}$$

where A and B are known constants and the kernel K_B is continuous and simple to evaluate numerically.

To obtain a unique solution to (57a,b), the behavior of the pressure jump at the duct leading and trailing edges is required. It is known that the jump in pressure has the following asymptotic behavior:

$$\Delta Q_s = \begin{cases} O\left(\sqrt{Z-a}\right) & Z \to a^+ \\ O\left(\dfrac{M_F}{\sqrt{b-Z}} + \sqrt{b-Z}\right) & Z \to b^- \end{cases} \tag{61}$$

Based on (61) we assume a solution of the form

$$\Delta Q_s(Z) = \alpha\sqrt{\frac{b-Z}{Z-a}} + \frac{}{\sqrt{(b-Z)(Z-a)}\,\gamma(Z)}, \tag{62}$$

where α is an unknown constant and γ is an unknown continuous function. Note that if the duct is stationary, then $\alpha = 0$.

A method is now developed in which the determination of γ is separated from the calculation of α. This yields an integral equation for γ that is relatively simple to solve. Use (62) in (57b) to obtain

$$\alpha = \frac{C_0 - g^{(1/2,1/2)}[\gamma]}{g^{(1/2,-1/2)}[1]}, \tag{63}$$

where

$$g^{(\eta,\xi)}[f] = g\left[(Z-a)^{\eta}(b-Z)^{\xi} f\right]. \tag{64}$$

The notation in (64) will be used with other integral operators in the remainder of this analysis. Substituting (62-62) in (57a) gives the first kind integral equation

$$K^{(1/2,1/2)}[\gamma](Z) = q(Z) \quad Z \in [a,b], \tag{65}$$

where

$$K^{(1/2,1/2)}[\gamma](Z) = D_N^{(1/2,1/2)}[\gamma](Z) - \frac{g^{(1/2,1/2)}[\gamma]}{g^{(1/2,-1/2)}[1]} D_N^{(1/2,-1/2)}[1](Z) \quad Z \in [a,b] \tag{66}$$

and

$$q(Z) = \left.\frac{\partial Q_i}{\partial \tau}\right|_{\tau=1} (Z) - \frac{C_0}{g^{(1/2,-1/2)}[1]} D_N^{(1/2,-1/2)}[1](Z) \quad Z \in [a,b] \tag{67}$$

The kernel for the operator in (66) has the same form as (60). After solving (65) for γ, (63) is used to calculate α.

Numerical Solution

Due to the edge behavior associated with γ, it is natural to expand γ in a series of Chebyshev polynomials of the second kind. Thus, constants $\{\gamma_j\}_{j=0}^{\infty}$ are sought such that

$$\gamma(Z) = \sum_{j=0}^{\infty} \gamma_j U_j\left(\frac{2Z-a-b}{b-a}\right), \tag{68}$$

where

$$U_j(x) = \frac{\sin\left[(j+1)\cos^{-1}x\right]}{\sin\left(\cos^{-1}x\right)}. \tag{69}$$

Golberg[9] has shown that if κ is not an eigenfrequency of **K**, then a unique convergent expansion such as (68) exists for integral equations with kernels of the type given in (60).

To solve (65) numerically, we truncate the expansion in (68) and apply the collocation method. Other popular projection techniques, such as Galerkin's method, require an additional numerical integration relative to collocation. With proper choice of collocation points and numerical quadrature scheme for the continuous portion of the kernel, Golberg[9] has shown that the accuracy obtained by Galerkin's method and collocation are equivalent for this problem. Thus, collocation yields the same accuracy as Galerkin's method, but with substantially less computational work.

The numerical solution begins by choosing the number of terms in the expansion (68), N_0+1. This number is a function of the modified wave number κ. If $\bar{\gamma}$ denotes the approximate solution, then

$$\bar{\gamma}(Z)=\sum_{j=0}^{N_0}\gamma_j U_j\left(\frac{2Z-a-b}{b-a}\right). \tag{70}$$

The collocation points, $\{Z_j\}_{j=1}^{N_0+1}$ are given by the zeroes of the N_0+1-th Chebyshev polynomial of the first kind and the numerical integration scheme for the continuous kernel is chosen as Gauss quadrature with weights and nodes based on second kind Chebyshev polynomials. Evaluating (65) at the collocation points yields the linear system

$$\sum_{i=0}^{N_0}\gamma_i K^{(1/2,1/2)}[U_i](Z_j)=q(Z_j) \qquad j=1,\ldots,N_0+1 \tag{71}$$

for the unknown expansion coefficients. The invertibility of the linear system has been established by Golberg.

To compute (71), integrals of the type

$$\int_{-1}^{1}\frac{\sqrt{1-x'^2}\,U_j(x')dx'}{(x-x')^2} \qquad x\in(-\infty,1], \tag{72}$$

$$\int_{-1}^{1}\sqrt{1-x'^2}\,U_j(x')\ln|x-x'|dx' \qquad x\in(-\infty,1], \tag{73}$$

$$\int_{-1}^{1}\sqrt{\frac{1+x'}{1-x'}}\frac{dx'}{(x-x')^2} \qquad x\in(-\infty,1], \tag{74}$$

and

$$\int_{-1}^{1}\sqrt{\frac{1+x'}{1-x'}}\ln|x-x'|dx' \qquad x\in(-\infty,1] \tag{75}$$

are encountered. Analytical results are obtained for (72-75) by applying the Plemelj-Sokhotski theorem[7] and its logarithmic analog to the complex function

$$R_j(w)=\left[w-\left(w^2-1\right)^{1/2}\right]^j$$

with branch cut

$$|\mathrm{Re}(w)|<1 \quad \mathrm{Im}(w)=0.$$

The branch is defined such that $(w^2-1)^{1/2}$ is real and positive if w is real and greater than one. This analysis yields the following results:

$$\int_{-1}^{1}\frac{\sqrt{1-x'^2}\,U_j(x')dx'}{(x-x')^2}=-\pi(j+1)\times \begin{cases} U_j(x) & x\in[-1,1] \\ \dfrac{\left(x+\sqrt{x^2-1}\right)^{j+1}}{\sqrt{x^2-1}} & x<-1 \end{cases}, \tag{76}$$

$$\int_{-1}^{1}\sqrt{1-x'^2}\,U_0(x')\ln|x-x'|dx'= \frac{\pi}{2}\begin{cases} \dfrac{1}{2}T_2(x)-\ln 2 & x\in[-1,1] \\ \dfrac{1}{2}\left(x+\sqrt{x^2-1}\right)^2+ \\ \quad \ln\left(-x+\sqrt{x^2-1}\right) & x<-1 \end{cases}, \tag{77}$$

$$\int_{-1}^{1}\sqrt{1-x'^2}\,U_j(x')\ln|x-x'|dx'= \frac{\pi}{2}\begin{cases} \dfrac{T_{j+2}(x)}{j+2}-\dfrac{T_j(x)}{j} & x\in[-1,1] \\ \dfrac{\left(x+\sqrt{x^2-1}\right)^{j+2}}{j+2}-\dfrac{\left(x+\sqrt{x^2-1}\right)^{j}}{j} & x<-1 \quad j>0 \end{cases}, \tag{78}$$

$$\int_{-1}^{1} \sqrt{\frac{1+x'}{1-x'}}\,\frac{dx'}{(x-x')^2} = \pi\begin{cases} 0 & x \in [-1,1] \\ \dfrac{1}{(1-x)\sqrt{x^2-1}} & x < -1 \end{cases}, \qquad (79)$$

and

$$\int_{-1}^{1} \sqrt{\frac{1+x'}{1-x'}}\,\ln|x-x'|dx' = -\pi\begin{cases} x+\ln 2 & x \in [-1,1] \\ x+\ln 2-\sqrt{x^2-1}+\ln\left(-x+\sqrt{x^2-1}\right) & x < -1 \end{cases}. \qquad (80)$$

In the above, T_j is the j-th order Chebyshev polynomial of the first kind

$$T_j(x) = \cos\left(j\cos^{-1}x\right). \qquad (81)$$

Examples

The analysis leading to the BIEM is independent of the fan noise source description. For illustrative purposes, it is expedient to assume simplified source mechanisms with analytical expressions for the incident field. In the results presented here, a collection of N_B equally spaced point axial dipoles of unit strength located inside the duct at a radial distance $0.9r_D$ and spinning with angular speed Ω are used to simulate the loading noise produced by the fan (see figure 2). An analytical description exists for the incident field induced by this configuration[1]. The use of more sophisticated source processes is considered in the conclusion section.

To demonstrate the versatility of the BIEM, several studies were conducted for the above problem. In each study, continuous portions of the total acoustic pressure field in the unstretched, moving frame were calculated. The numerical methods described in (66-81) were implemented on a Cray YMP computer at NASA Langley Research Center. For each set of parameters considered in the studies, the computational time for both field and integral equation calculations was 2-8 minutes. The acoustic fields displayed are composed of 20,000-50,000 observer point calculations.

In the first study, $N_B = 20$ point sources with tip Mach number $M_{TIP} = 1.2$, were used to simulate the fan noise. Four forward flight Mach numbers (M_F = 0.0, 0.2, 0.4, and 0.6) were considered. Field calculations in a plane perpendicular to the fan plane and parallel to the duct axis are presented in figure 3a-d.

An examination of the pressure fields inside the duct reveals that the wavelengths of axial modes propagating in the direction of motion decreases with increasing M_F. A spectral analysis of the axial wave structure is beyond the scope of this work. However, the number of waves per unit length of the dominant axial mode present can be approximated by visual inspection. In table 1, these observations are compared to the axial wave numbers for the first radial mode from classical spinning mode theory for ducts of infinite length. If ν represents the smallest zero of the function J'_m, then the theoretical axial wave numbers are given by the formula[12]

$$k_z = \frac{\kappa}{\beta}\left[-M_F \pm \sqrt{1-\left(\frac{\nu}{\kappa}\right)^2}\right], \qquad (82)$$

where J_m is the m-th order Bessel function of the first kind. Only propagating modes are considered. Note that $k_z < 0$ corresponds to axial waves traveling from the fan face to the inlet. The computed results appear to be in agreement with theory.

It is also noted that the angle between the line of peak noise and the duct axis decreases with increasing Mach number. This agrees qualitatively with the results of Rice, etal.[13].

M_F	κ	$k_z/2\pi$ (Theory)	$k_z/2\pi$ (Observed)
0.0	24.0	-1.44, +1.44	-1.5, +1.5
0.2	24.5	-2.47, +0.88	-2.5
0.4	26.2	-4.23, +0.59	-4.0
0.6	30.0	-7.59, +0.43	-7.5, +0.5

Table 1: Propagation Properties for Figure 3 Results
($M_{TIP} = 1.2 \quad L_D = 1.0 \quad m = N_B$)

Using the same source configuration as above, the effects of increasing tip Mach number for fixed flight Mach number $M_F = 0.8$ were examined (see figure 4a-d and table 2). With regard to propagation and radiation characteristics, similar comments as in the previous study apply for cases 4a and 4b.

In cases 4c-d, the waves moving forward in the duct are in agreement with the theoretical results.

However, waves traveling toward the exit are present that are not accounted for in the theory. The modified frequencies for these two cases are relatively close to some eigenfrequencies for the interior Dirichlet problem. That is, the eigenfrequencies are occurring at the zeroes of J_m. There appear to be resonant radial modes present. Condition numbers for the linear system (71) at these frequencies increase significantly. The numerical results are therefore questionable. This phenomenon has been well studied in the literature and is usually associated with ficticious interior eigenfrequencies while solving exterior problems. The interested reader is referred to the work of Kleinman and Roach[14] for a comprehensive theoretical discussion on the removal of the ficticious eigenfrequencies. In the present work, the interior is real and the eigenfrequencies are not necessarily ficticious. Research into the subject is ongoing. The authors believe that the ill conditioning can be mitigated by the use of singular value decomposition methods. We further contend that acoustic treatment of the duct interior will eliminate the problem entirely.

M_{TIP}	κ	$k_z/2\pi$ (Theory)	$k_z/2\pi$ (Observed)
0.5	16.7	none	none
0.7	23.3	-3.06, -6.84	-6.5
0.9	30.0	-1.02, -11.71	-11.5, +3.0
1.1	36.7	-0.04, -15.52	-15.0, +6.0

Table 2: Propagation Properties for Figure 4 Results
($M_F = 0.8 \quad L_D = 0.5 \quad m = N_B$)

The third example was chosen to demonstrate the capability of the BIEM to computer higher harmonics and different portions of the acoustic field (figure 5a-c). In this case, $N_B = 16$, $M_F = 0.2$, and $M_{TIP} = 1.7$. Sound pressure levels are plotted in an observer plane two duct diameters beneath the duct. The kinematic properties and the observer locations were selected to correspond to those used for tests conducted with the Langley ducted propeller simulator[15]. Direct comparisons with the results in reference 15 are not possible because of the simplified source model used for the BIEM. The results do show, however, the ability of the BIEM to compute the sound field in regions of interest.

Conclusions

The results presented here demonstrate that the BIEM is a versatile and computationally efficient tool for predicting ducted fan engine noise. Qualitative radiation and duct propagation results can be obtained by using simplified source models such as spinning point or line sources. By tuning the strengths of the resulting monopoles and dipoles to account for fan loading and thickness effects, it is believed that the BIEM can produce results that are useful for quantitative studies.

Other boundary integral techniques have been developed for the problem of scattering of incident sound by a thin duct with hard walls[1-5]. The BIEM developed here is valid for many situations of interest and features extensive mathematical analyses on the integral equation kernels. The analyses yield expressions for singular and logarithmic integral operators that can be evaluated in terms of known functions and continuous portions that can be evaluated by simple numerical quadrature schemes. This versatility and depth of analysis, absent in the referenced works, simplify the calculations considerably.

Realistic duct geometry is included in the boundary integral equation formulation. Implementation of an arbitrary duct profile requires the solution of a system of two hypersingular integral equations. The inclusion of a duct centerbody produces another integral equation with the same properties. Both the duct profile and centerbody have interior regions that produce ficticious eigenfrequencies for the Neumann or Dirichlet boundary value problems. This difficulty can be alleviated in several ways. The method of Burton and Miller[16] appears to be adaptable to the BIEM presented here. Ficticious eigenfrequencies are not present if the engine components are acoustically lined.

The use of passive noise control techniques are included in the BIEM. A spatially varying, locally reactive liner model appears in the boundary conditions. This property makes the BIEM attractive for active and passive noise control design studies.

References

1. J. Lan: Acoustic Shielding from a Short Rigid Duct Around a Propeller, Master's Thesis, The George Washington University, August 1993.

2. J. Buhler: A New Boundary Integral Method for Predicting the Acoustic Field Generated by Ducted Rotating Sources, Master's Thesis, The George Washington University, August 1994.

3. R. Martinez: Aeroacoustic Diffraction and Dissipation by a Short Propeller Cowl in Subsonic Flight. NASA CR 190801, April 1993.

4. R. Martinez: A Boundary Integral Formulation for Thin-walled Shapes of Revolution, J. Acous. Soc. Am., 87(2), February 1990.

5. M.A. Hamdi and J.M. Ville: Development of a Sound Radiation Model for a Finite Length Duct of Arbitrary Shape, AIAA Journal, Vol. 20, No. 12, December 1982, pgs. 1687-1692.

6. M.K. Myers: On the Acoustic Boundary Condition in the Presence of Flow, Journal of Sound and Vibration, 71(3), 1980, pgs. 429-434.

7. F.D. Gakhov: Boundary Value Problems, Dover Publications, Inc., New York, 1966.

8. V.I. Smirnov: A Course of Higher Mathematics, Vol. IV, Pergamon Press, Oxford, 1964.

9. M. Golberg: The Convergence of Several Algorithms for Solving Integral Equations with Finite-Part Integrals, Journal of Integral Equations 5, 1983, pgs. 329-340.

10. F. Farassat: Introduction to Generalized Functions with Applications in Aerodynamics and Aeroacoustics, NASA TP 3428, May 1994, (Corrected Copy - February 1996)

11. A.C. Kaya and F. Erdogan: On the Solution of Integral Equations with Strongly Singular Kernels, Quarterly of Applied Mathematics, Volume XLV, Number 1, April 1987, pgs. 105-122.

12. Walter Eversman: Theoretical Models for Duct Acoustic Propagation and Radiation, Chapter 13, Aeroacoustics of Flight Vehicles: Theory and Practice, Vol. 2: Noise Control, NASA RP 1258, August 1991.

13. E.J. Rice, M.F. Heidmann, and T.G. Sofrin: Modal Propagation Angles in a Circular Duct with Flow and their relation to Sound Radiation, 17th Aerospace Sciences Meeting Paper AIAA-79-0183, New Orleans, 1979.

14. R.E. Kleinman and G.E. Roach: Boundary Integral Equations for the Three-Dimensional Helmholtz Equation, SIAM Rev., Vol. 16, No. 2, 1974.

15. R.H. Thomas, C.H. Gerhold, F. Farassat, O.L. Santa Maria, W.E. Nuckolls, and D.W. De Vilbiss : Far Field Noise of the 12 Inch Advanced Ducted Propeller Simulator, 33rd Aerospace Sciences Meeting and Exhibit Paper AIAA-95-0722, Reno, 1995.

16. A.J. Burton and G.F. Miller: The Application of Integral Equation Methods to the Numerical Solution of Some Exterior Boundary Value Problems, Proc. Roy. Soc. Ser. A. 323, 1971, pgs. 201-210.

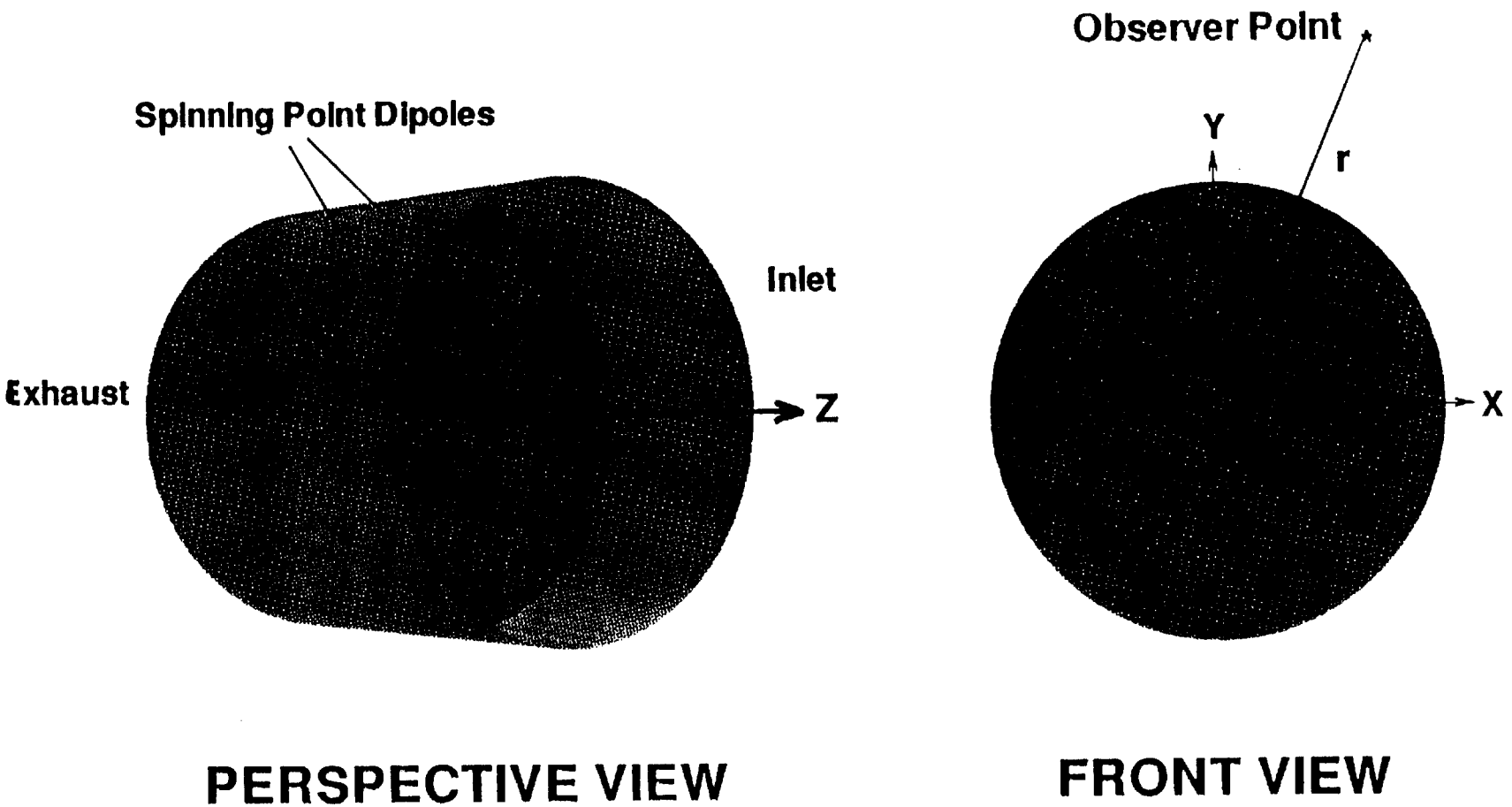

Figure 2: Geometry and Coordinate Definitions for
BIEM Noise Prediction

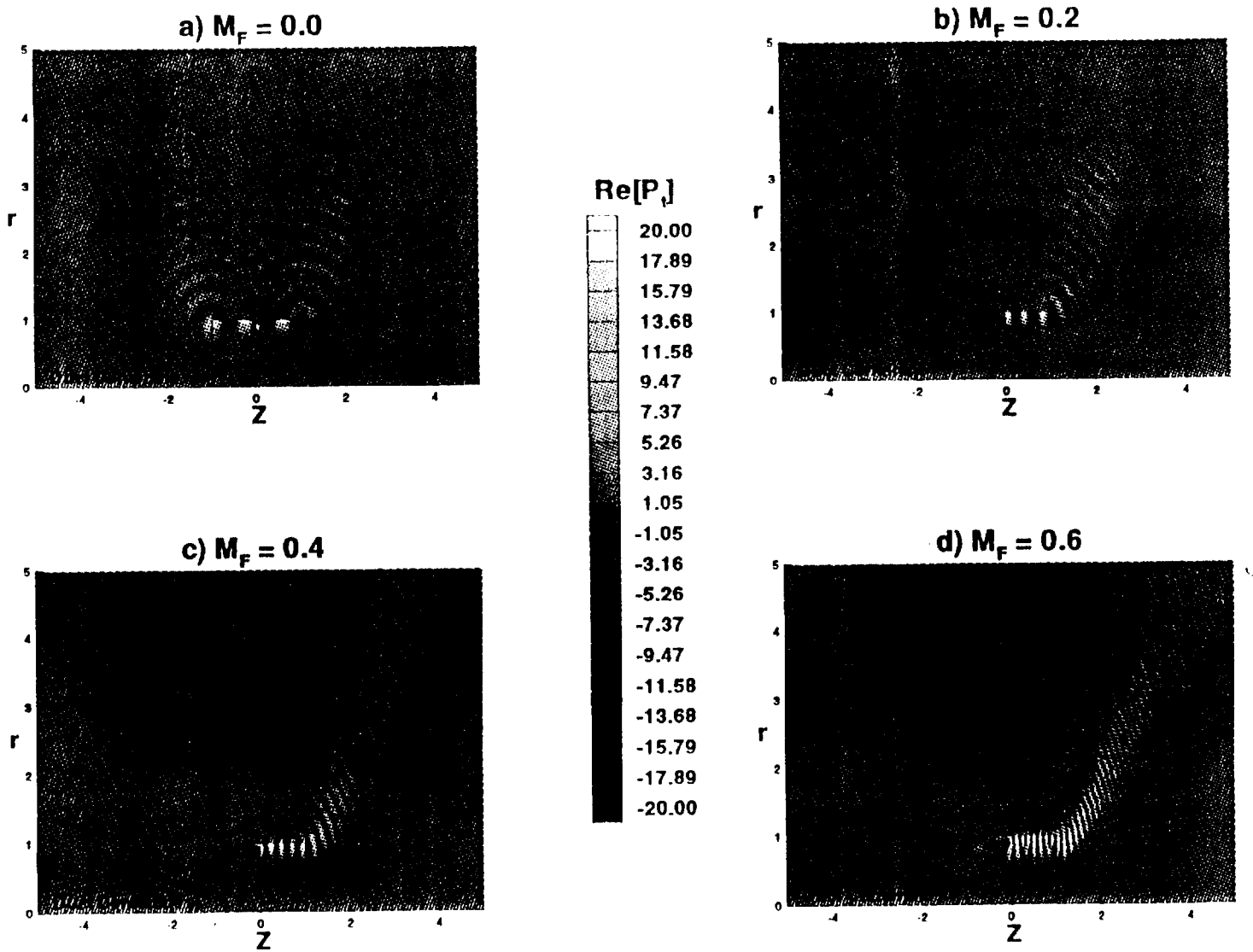

Figure 3: Total Pressure Field

$m = 20 \quad M_{TIP} = 1.2 \quad L_D = 1.0$

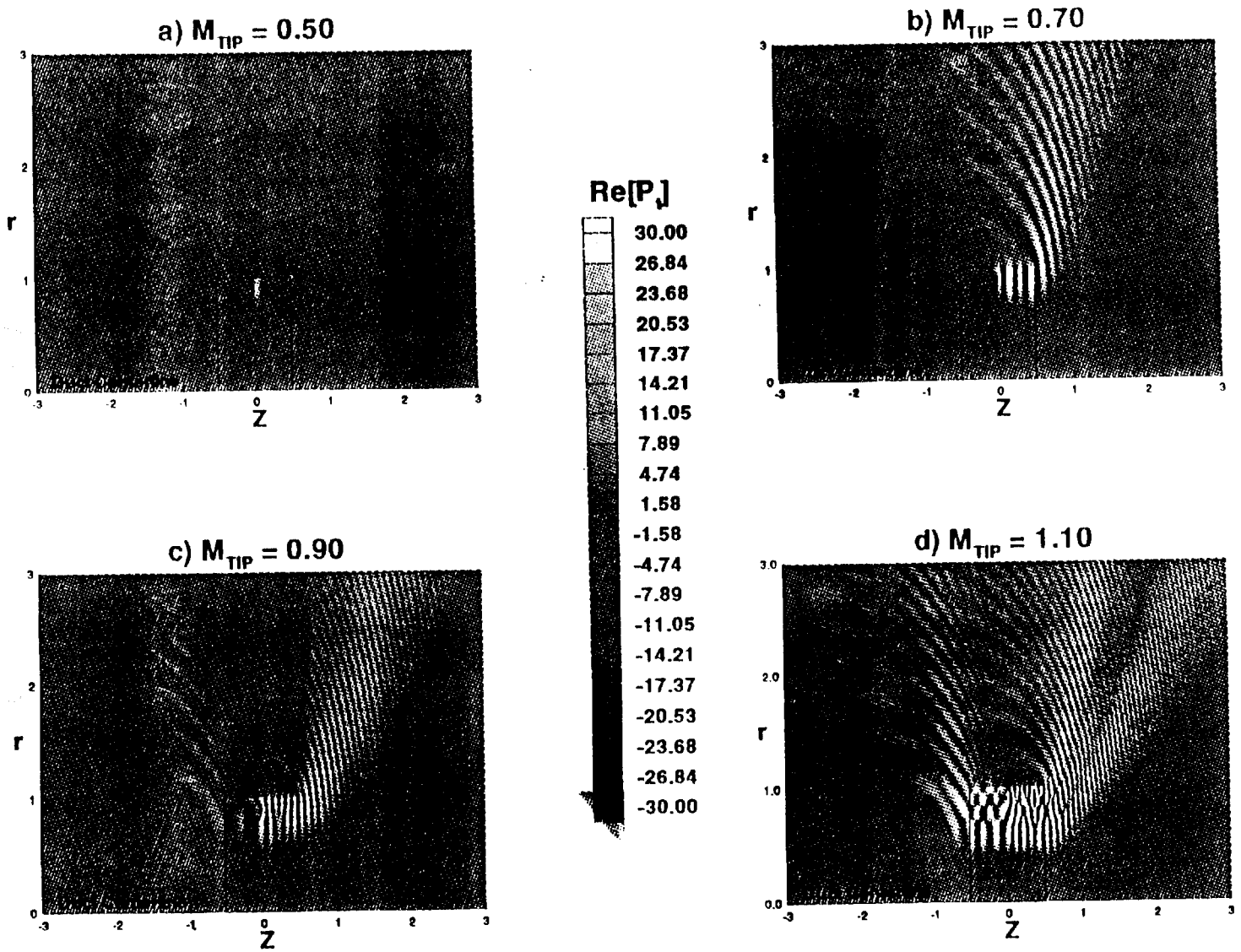

Figure 4: Total Pressure Field

$m = 20 \quad M_F = 0.8 \quad L_D = 0.5$

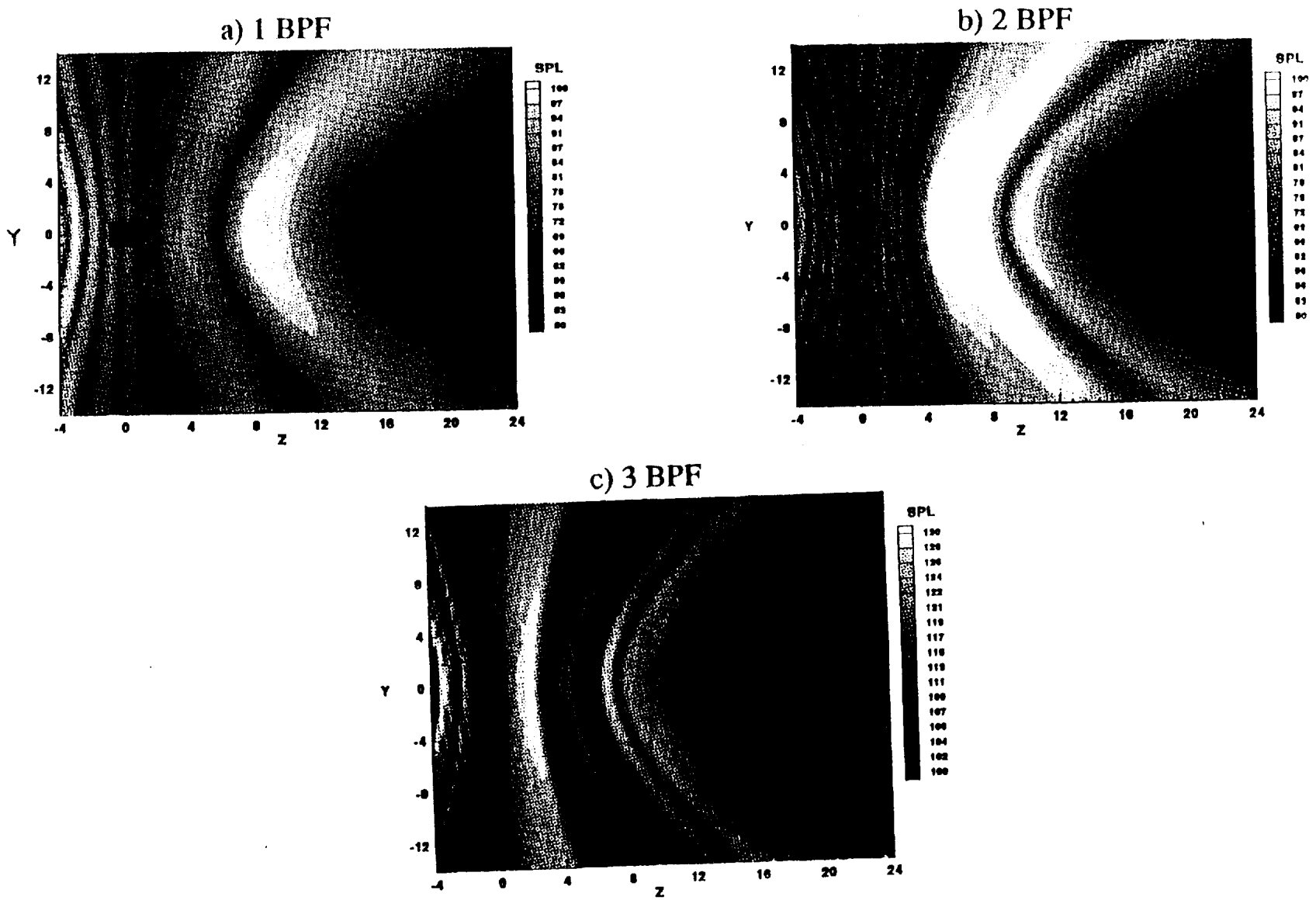

Figure 5: Noise Footprint for Langley Ducted Fan Rig

$N_B = 16 \quad M_F = 0.2 \quad M_{TIP} = 1.7$

Acoustic Radiation and Propagation for an Acoustically Treated Engine Duct Via a Boundary Integral Equation Method

M. H. Dunn and J. Tweed
Old Dominion University
Norfolk, VA

F. Farassat
NASA Langley Research Center
Hampton, VA

Abstract

The prediction of ducted fan engine noise using a boundary integral equation method (BIEM) is presented. Governing equations for the BIEM are based on the assumption that the duct is approximated by a thin, finite length circular cylinder. Acoustic processes are assumed to be linear, generate spinning modes, and occur in a uniform flow field. A mixed boundary value problem (BVP) is defined that describes the scattering of incident sound by the cylinder. The boundary condition on the duct interior wall allows for an axially segmented locally reacting liner. Using potential theory, the BVP is recast as a system of hypersingular boundary integral equations for the unknown single and double layer potential densities. BIEM derivations and solution methodology are demonstrated for the scattering of incident sound generated by simple sources in a low speed uniform flow field. The key features of the BIEM are its computational speed and efficiency, versatility, validity over a wide range of frequencies, and the ability to compute rapidly any portion of the sound field without the need to compute the entire field. Propagation results obtained are in agreement with the classical results of spinning mode theory for infinite ducts. Various calculations are presented to illustrate the utility of the BIEM as a tool for conducting active and passive noise control studies.

Notation

$\sim$	denotes that a quantity is dimensional when appearing over a variable
a	axial coordinate of duct trailing edge in stretched, moving frame
b	axial coordinate of duct leading edge in stretched, moving frame
$\tilde{c}, c$	ambient sound speed
k	$= mM_{TIP}$ characteristic wave number of m-th circumferential mode
L_D	ratio of duct length to duct diameter
m	circumferential mode number
M_F	$= \tilde{V}_F / \tilde{c}$ forward flight Mach number
M_{TIP}	$= \tilde{r}_D \tilde{\Omega} / \tilde{c}$ tip Mach number
N_B	number of fan blades
p'	Eulerian description of total acoustic pressure field
p_i'	Eulerian description of incident acoustic pressure field
p_s'	Eulerian description of scattered acoustic pressure field
(r, ψ, z)	cylindrical coordinates in stationary frame
$\tilde{r}_D$	duct radius
$\tilde{t}, t$	time
$\vec{u}'$	Eulerian description of acoustic velocity field
$\tilde{V}_F, V_F$	forward flight speed
Z	axial coordinate in stretched, moving frame
$\alpha^{\pm}$	specific surface acoustic admittance on duct exterior (interior)
β	$= \sqrt{1 - M_F^2}$ stretching parameter

κ $= k/\beta$ stretched characteristic wave number

$\tilde{\rho}_0$ ambient density

$\tilde{\Omega}$ shaft speed (radians/second)

Introduction

The reduction of tonal noise radiated by turbofans is a subject of ongoing aeroacoustics research. Advanced analytical tools for predicting the sound radiated from engine ducts can facilitate the design of active and passive noise abatement technology. To be useful in design studies, prediction tools should be fast, versatile, accurate, valid for a wide range of frequencies and engineering situations, and implementable on mainstream computer systems. The ability to compute any portion of the sound field without the need to calculate the entire field is an important attribute in this regard. Computational approaches such as Finite Element Methods, CFD, and Computational Aeroacoustics lack this property. Therefore, their usefulness for parametric noise reduction studies is limited.

In this paper, a Boundary Integral Equation Method (BIEM) for the prediction of ducted fan engine noise is presented. The work is an extension of the BIEM discussed in reference 1***. The method is based on the equations of linearized acoustics with uniform inflow, and features analytical and computational techniques that minimize the consumption of computer resources. We validate the BIEM by reproducing qualitative propagation results from infinite duct theory. Various computational studies are presented to demonstrate the effectiveness of the BIEM as a tool in the study of active and passive noise control.

It is assumed that the engine duct is approximated by an infinitesimally thin, circular cylinder of finite length. We adopt a scattering approach in which the acoustic pressure field is split into known incident and unknown scattered components. The acoustic source processes are assumed to generate an incident pressure field that can be represented by a superposition of spinning modes.

In a frame of reference moving with the engine duct and in regions of space not occupied by scattering surfaces, the modal components of scattered acoustic pressure satisfy Helmholtz' equation. An exterior boundary value problem for the scattered pressure is obtained by including a far field radiation condition and boundary conditions on the interior and exterior cylinder surfaces. The boundary conditions allow for hard walls or a locally reacting liner that can be uniform or segmented.

We solve the boundary value problem by expressing the scattered pressure field as a sum of double and single layer Helmholtz potentials with unknown densities. Application of the boundary conditions to the layer representation yields a system of one-dimensional, singular boundary integral equations for the layer densities. For uniqueness, conditions on the densities at the duct leading and trailing edges must be imposed. The source terms for the system are related to the known incident pressure and its normal and tangential derivatives. The system of boundary integral equations, edge conditions, and method of solution comprise the BIEM.

***CITE DIFFERENCES WITH PREVIOUS WORK ON INTEGRAL EQUATION METHODS FOR DUCTED FAN NOISE PREDICTION - MARTINEZ & THE FRENCH GUYS - NAMELY, DEPTH OF KERNEL ANALYSIS, SOLVABILITY RESULTS, NOTATION, DESIGN TOOL.

Boundary Value Problem Derivation

We consider an engine fan surrounded by an infinitesimally thin, finite length circular cylinder translating in the $+\tilde{z}$ (axial) direction with uniform speed $\tilde{V}_F$. The fan is composed of N_B equally spaced blades and rotates with shaft speed $\tilde{\Omega}$. The incident acoustic pressure field generated by the fan is given. Linear conditions are assumed to apply and the inflow is uniform.

In the analysis that follows, all quantities are nondimensional: length by $\tilde{r}_D$, mass by $\tilde{\rho}_0\tilde{r}_D^3$, and time by $\tilde{\Omega}^{-1}$.

Governing Differential Equations

The total acoustic pressure in the sound field is split into known incident and unknown scattered parts

$$p'(r,\psi,z,t) = p'_i(r,\psi,z,t) + p'_s(r,\psi,z,t). \tag{1}$$

In regions of space that contain no scattering surfaces, p'_s is governed by the homogeneous wave equation

$$\left[\frac{1}{c^2}\frac{\partial^2}{\partial t^2} - \frac{1}{r}\frac{\partial}{\partial r}\left(r\frac{\partial}{\partial r}\right) - \frac{1}{r^2}\frac{\partial^2}{\partial \psi^2} - \frac{\partial^2}{\partial z^2}\right]p'_s = 0. \tag{2}$$

Acoustic pressure and velocity are related through the acoustic momentum equation

$$\frac{\partial \vec{u}'}{\partial t} + \nabla p' = 0. \tag{3}$$

In a frame of reference moving with the duct, all dependent acoustic variables can be expressed as linear superpositions of spinning modes. For example, the scattered pressure has the form

$$p'_s(r,\psi,Z,t) = \sum_{m/N_B=l}^{\infty} P_s^m(r,Z)e^{im(t-\psi)} \tag{4a}$$

and the total acoustic velocity is written

$$\vec{u}'(r,\psi,Z,t) = \sum_{m/N_B=l}^{\infty} \vec{U}^m(r,Z)e^{im(t-\psi)}, \tag{4b}$$

where the stretched, moving axial coordinate Z is given by

$$Z = \frac{z - V_F t}{\beta}. \tag{5}$$

Incident and total acoustic pressures are written similarly.

Modal amplitudes in the BIEM are calculated term by term. For notational convenience, the superscript m on the modal coefficients is dropped hereafter.

Define the dependent variables Q, Q_s, Q_i, and V_r by

$$Q(r,Z) = P(r,Z)e^{ikM_F Z} \tag{6a}$$

$$Q_s(r,Z) = P_s(r,Z)e^{i\kappa M_F Z} \tag{6b}$$

$$Q_i(r,Z) = P_i(r,Z)e^{i\kappa M_F Z} \tag{6c}$$

$$V_r(r,Z) = U_r(r,Z)e^{i\kappa M_F Z} \tag{6d}$$

Combining (4-6) with (2) yields the two dimensional Helmholtz equation

$$\left[\frac{1}{r}\frac{\partial}{\partial r}\left(r\frac{\partial}{\partial r}\right)+\frac{\partial^2}{\partial Z^2}-\frac{m^2}{r^2}+\kappa^2\right]Q_s = 0 \tag{7}$$

for the m-th scattered coefficient. Using (3-6a), the m-th radial component of the momentum equation (3) can be written as

$$e^{-i\frac{\kappa}{M_F}Z}V_r(r,Z) = \frac{\beta M_{TIP}}{M_F}\int_{-\infty}^{Z} e^{-i\frac{\kappa}{M_F}Z'}\frac{\partial Q}{\partial r}(r,Z')dZ' . \tag{8}$$

If the duct is stationary, then (7) and (8) reduce to

$$\left[\frac{1}{r}\frac{\partial}{\partial r}\left(r\frac{\partial}{\partial r}\right)+\frac{\partial^2}{\partial z^2}-\frac{m^2}{r^2}+k^2\right]P_s = 0 \tag{9}$$

and

$$U_r(r,z) = \frac{i}{m}\frac{\partial P}{\partial r}(r,z) . \tag{10}$$

Equations (7-10) are valid for points not lying on the stretched duct.

Boundary Conditions

To meet FAA noise certification levels, it is necessary to treat the engine duct with noise suppression devices. In this work, the duct treatment is modeled by a uniform or axially segmented locally reacting liner. We consider the case of a hard exterior surface and lined (or hard) interior. To simulate actual duct treatment, we impose hard wall conditions at and near the leading and trailing edges on the interior wall.

Let $f(r,Z)$ be an arbitrary field function. Define the surface function $f^{\pm}(Z)$ by

$$f^{\pm}(Z) = \lim_{r \to 1^{\pm}} f(r,Z) \qquad Z \in (a,b). \tag{11}$$

In reference 2***Myers BC*** it is shown that if and α represents the piecewise constant specific acoustic surface admittance on the interior, then in the stretched, moving frame of reference, the boundary modal coefficients of velocity and pressure satisfy the boundary equations

$$V_r^+(Z) = 0 \qquad Z \in (a,b) \tag{12a}$$

and

$$-V_r^-(Z) + \frac{iM_F \alpha(Z)}{\beta^2 \kappa} \frac{d}{dZ}\left(e^{-i\frac{\kappa}{M_F}Z} Q^- \right)(Z) = 0 \qquad Z \in (a,b) \ . \tag{12b}$$

In the absence of flow, the boundary conditions reduce to

$$U_r^+(z) = 0 \qquad z \in (a,b). \tag{13a}$$

and

$$-U_r^-(z) + \alpha(z) P^-(z) = 0 \qquad z \in (a,b). \tag{13b}$$

We use the acoustic momentum equation (8) to eliminate the normal velocity from the (12):

$$\left(\frac{\partial Q}{\partial r} \right)^+ (Z) = 0 \qquad Z \in (a,b), \tag{14a}$$

$$-e^{-i\frac{\kappa}{M_F}Z} \left(\frac{\partial Q}{\partial r} \right)^- (Z) + \frac{iM_F^2 \alpha(Z)}{\beta^3 M_{TIP} \kappa} \frac{d^2}{dZ^2}\left(e^{-i\frac{\kappa}{M_F}Z} Q^- \right)(Z) = 0 \qquad Z \in (a,b), \tag{14b}$$

and

$$\int_{-\infty}^{a} e^{-i\frac{\kappa}{M_F}Z'} \frac{\partial Q}{\partial r}(1,Z')dZ' = 0 \tag{15}$$

Note that (15) is satisfied trivially for $M_F \to 0$ and provides no information.

The thin duct approximation produces a surface with discontinuous tangents at the duct leading and trailing edges. Consequently, there are infinitely many solutions to (14-15). For uniqueness, we must constrain the acoustic pressure at the duct edges. At the trailing edge we impose the Kutta condition

$$\lim_{Z\to a^+}\left[Q^-(Z)-Q^-(Z)\right]=0. \tag{16}$$

For $M_F>0$, the Kutta condition ensures infinite pressure at the leading edge. For physically reasonable solutions to exist we require the acoustic pressure to be integrable in any region of space about the leading edge.

The boundary value problem is finalized by specifying the behavior of the acoustic pressure in the farfield. To ensure that the acoustic field consists only of outgoing waves at infinity we impose the Sommerfeld radiation condition

$$\lim_{\rho=\sqrt{r^2+Z^2}\to\infty}\sqrt{\rho}\left(\frac{\partial Q}{\partial\rho}+i\kappa Q\right)=0. \tag{17}$$

Using (1) and assuming that the functions Q_i and its derivatives are known, satisfy (17), and are continuous on the duct surface, we rewrite the boundary value problem in terms of the scattered pressure:

$$\left[\frac{1}{r}\frac{\partial}{\partial r}\left(r\frac{\partial}{\partial r}\right)+\frac{\partial^2}{\partial Z^2}-\frac{m^2}{r^2}+\kappa^2\right]Q_s=0 \tag{18a}$$

$$\left(\frac{\partial Q_s}{\partial r}\right)^+(Z)=-\frac{\partial Q_i}{\partial r}(1,Z)\qquad Z\in(a,b) \tag{18b}$$

$$\begin{aligned}\left(\frac{\partial Q_s}{\partial r}\right)^+(Z)-\left(\frac{\partial Q_s}{\partial r}\right)^-(Z)+\frac{iM_F^2\alpha(Z)}{\beta^3\kappa M_{TIP}}\left[e^{i\frac{\kappa}{M_F}Z}\frac{d^2}{dZ^2}\left(e^{-i\frac{\kappa}{M_F}Z}Q_s\right)\right]^-(Z)=\\ -\frac{iM_F^2\alpha(Z)}{\beta^3\kappa M_{TIP}}e^{i\frac{\kappa}{M_F}Z}\frac{\partial^2}{\partial Z^2}\left(e^{-i\frac{\kappa}{M_F}Z}Q_i\right)(1,Z)\qquad Z\in(a,b)\end{aligned} \tag{18c}$$

$$\int_{-\infty}^{a}e^{-i\frac{\kappa}{M_F}Z'}\frac{\partial Q_s}{\partial r}(1,Z')dZ'=-\int_{-\infty}^{a}e^{-i\frac{\kappa}{M_F}Z'}\frac{\partial Q_i}{\partial r}(1,Z')dZ' \tag{18d}$$

$$\lim_{Z\to a^+}\left[Q_s^+(Z)-Q_s^-(Z)\right]=0 \tag{18e}$$

$$\int_{\Re} |Q_s| d\Re < \infty \qquad \Re \text{ any region in } r - Z \text{ plane} \tag{18f}$$

$$\lim_{\rho=\sqrt{r^2+Z^2}\to\infty} \sqrt{\rho}\left(\frac{\partial Q_s}{\partial \rho} + i\kappa Q_s\right) = 0 . \tag{18g}$$

Boundary Integral Equation Formulation

In this section, we convert the boundary value problem (18a-g) to a system of boundary integral equations.

Helmholtz Potential Representation

The Green's function for the two dimensional Helmholtz operator that satisfies the radiation condition (18g) can be written as

$$G(r,r',Z-Z') = \frac{1}{2\pi}\int_0^{\pi} \cos m\psi \frac{e^{-i\kappa R}}{R} d\psi \tag{19}$$

where

$$R = \sqrt{r^2 + r'^2 - 2rr'\cos\psi + (Z-Z')^2}\,. \tag{20}$$

For an arbitrary surface function f, we define the single and double layer operators, $\mathbf{s}$ and $\mathbf{d}$, by the equations

$$\mathbf{s}[f](r,Z) = \int_a^b f(Z')s(r,Z-Z')dZ' \tag{21}$$

and

$$\mathbf{d}[f](r,Z) = \int_a^b f(Z')d(r,Z-Z')dZ'\,, \tag{22}$$

where the kernels s and d are given by

$$s(r,Z-Z') = G(r,1,Z-Z') \tag{23}$$

and

$$d(r,Z-Z') = -\frac{\partial G}{\partial r'}(r,1,Z-Z')\,. \tag{24}$$

The integrals in (21-22) are well defined for points (r,Z) not on the stretched duct surface.

We define additional field operators by calculating radial and axial derivatives of $\mathbf{s}$ and $\mathbf{d}$. Denote by $\mathbf{s}_r$ the operator

$$\mathbf{s}_r[f](r,Z) = \frac{\partial}{\partial r}\mathbf{s}[f](r,Z) = \int_a^b f(Z')s_r(r,Z-Z')dZ'\,, \tag{25}$$

where

$$s_r(r, Z - Z') = \frac{\partial s}{\partial r}(r, Z - Z'). \tag{26}$$

Define the field operators $\mathbf{s}_z$, $\mathbf{s}_{zz}$, $\mathbf{d}_r$, $\mathbf{d}_z$, $\mathbf{d}_{zz}$ and associated kernels in a similar fashion.

Using results from Helmholtz potential theory (reference ***Courant & Hilbert***), the scattered pressure can be written as a sum of single and double layer Helmholtz potentials.

$$Q_s(r, Z) = \mathbf{s}[Q_1](r, Z) + \mathbf{d}[Q_2](r, Z) \tag{27}$$

Equations (18a) and (18g) are satisfied by (27). The layer densities Q_1 and Q_2 are unknown surface functions. Once the densities are determined, (27) is used to obtain the scattered field at any desired location. We will show later that Q_1 is related to the jump in the normal derivative of scattered pressure across the duct surface and Q_2 is related to the jump in scattered pressure.

Surface Operator Notation

In order to apply the boundary conditions (18b-c) to (27), it is necessary to evaluate directly the single and double layer potentials and their derivatives on the stretched duct surface. The resulting one dimensional surface operators have both singular and nonsingular parts.

For $Z \in [a, b]$ and sufficiently smooth f, we define the surface operators $\mathbf{S}$ and $\mathbf{D}$ by

$$\mathbf{S}[f](Z) = \int_a^b f(Z')S(Z - Z')dZ' \tag{28}$$

and

$$\mathbf{D}[f](Z) = \int_a^b f(Z')D(Z - Z')dZ', \tag{29}$$

where the kernels S and D are given by

$$S(Z - Z') = s(1, Z - Z') \tag{30}$$

and

$$D(Z - Z') = d(1, Z - Z'). \tag{31}$$

The operators $\mathbf{S}_r$, $\mathbf{S}_z$, $\mathbf{S}_{zz}$, $\mathbf{D}_r$, $\mathbf{D}_z$, $\mathbf{D}_{zz}$ and associated kernels are similarly defined.

Singular Kernel Analysis

All of the above kernels are singular for $Z - Z' = 0$. We list without proof the asymptotic behavior of the kernels for $|Z - Z'| << 1$. The singular portions of the kernels are obtained by local analyses of the Green's function (19) and its derivatives. All kernels are written as sums of singular and bounded terms. Bounded kernels are denoted by the superscript B.

$$S(Z - Z') = -\frac{1}{2\pi} ln|Z - Z'| + S^B(Z - Z') \tag{32}$$

$$S_r(Z - Z') = \frac{1}{4\pi} ln|Z - Z'| + S_r^B(Z - Z') \tag{33}$$

$$S_z(Z - Z') = \frac{1}{2\pi(Z' - Z)} + S_z^B(Z - Z') \tag{34}$$

$$S_{zz}(Z - Z') = \frac{1}{2\pi(Z - Z')^2} + \frac{4(\kappa^2 - m^2) + 1}{16\pi} ln|Z - Z'| + S_{zz}^B(Z - Z') \tag{35}$$

$$D(Z - Z') = -\frac{1}{4\pi} ln|Z - Z'| + D^B(Z - Z') \tag{36}$$

$$D_r(Z - Z') = -\frac{1}{2\pi(Z - Z')^2} + \frac{4(\kappa^2 - m^2) + 3}{16\pi} ln|Z - Z'| + D_r^B(Z - Z') \tag{37}$$

$$D_z(Z - Z') = \frac{1}{4\pi(Z' - Z)} + D_z^B(Z - Z') \tag{38}$$

$$D_{zz}(Z - Z') = \frac{1}{4\pi(Z - Z')^2} + \frac{4(\kappa^2 - 3m^2) + 3}{32\pi} ln|Z - Z'| + D_{zz}^B(Z - Z') \tag{39}$$

The leading behavior for the kernels (32), (33), and (36) is logarithmic. Therefore, the associated operators are weakly singular. The leading terms for the kernels (34) and (38) are of the Cauchy type. While the kernels (35), (37), and (39) are of the strongly singular Hadamard type. Integrals with Cauchy and Hadamard kernels are divergent and must be interpreted in the finite part sense.

All of the above kernels have the logarithmic portions extracted. Integrations involving these terms are well defined theoretically but difficult to achieve numerically. This problem is mitigated by the development of analytical results for the associated operators. Examples of this, as well as analytical results for the Cauchy and Hadamard terms, are presented in a later section. Calculations involving the continuous portions of the kernels are performed by straightforward numerical integration.

Layer Continuity Properties

Using the above operator notation, we state well-known continuity properties for the single and double layers and their derivatives as a field point approaches the stretched duct surface from the interior or exterior of the duct. For sufficiently smooth $f(Z)$ with $Z \in (a,b)$, we have the following results (see reference ***Courant & Hilbert***):

$$\lim_{r \to l^{\pm}} \mathbf{s}[f](r,Z) = \mathbf{S}[f](Z) \tag{40}$$

$$\lim_{r \to l^{\pm}} \mathbf{d}[f](r,Z) = \mp \frac{1}{2} f(Z) + \mathbf{D}[f](Z) \tag{41}$$

$$\lim_{r \to l^{\pm}} \mathbf{s}_{\mathbf{r}}[f](r,Z) = \mp \frac{1}{2} f(Z) + \mathbf{S}_{\mathbf{r}}[f](Z) \tag{42}$$

$$\lim_{r \to l^{\pm}} \mathbf{d}_{\mathbf{r}}[f](r,Z) = \mathbf{D}_{\mathbf{r}}[f](Z) \tag{43}$$

$$\lim_{r \to l^{\pm}} \mathbf{s}_{\mathbf{Z}}[f](r,Z) = \mathbf{S}_{\mathbf{Z}}[f](Z) \tag{44}$$

$$\lim_{r \to l^{\pm}} \mathbf{s}_{\mathbf{ZZ}}[f](r,Z) = \mathbf{S}_{\mathbf{ZZ}}[f](Z) \tag{45}$$

$$\lim_{r \to l^{\pm}} \mathbf{d}_{\mathbf{Z}}[f](r,Z) = \mp \frac{1}{2} \frac{df}{dZ}(Z) + \mathbf{D}_{\mathbf{Z}}[f](Z) \tag{46}$$

$$\lim_{r \to l^{\pm}} \mathbf{d}_{\mathbf{ZZ}}[f](r,Z) = \mp \frac{1}{2} \frac{d^2 f}{dZ^2}(Z) + \mathbf{D}_{\mathbf{ZZ}}[f](Z) \tag{47}$$

By applying (40-43) to (27) we establish the previously mentioned relationships between the layer densities and scattered pressure surface quantities.

$$Q_s^+(Z) - Q_s^-(Z) = -Q_2(Z) \tag{48}$$

$$\left(\frac{\partial Q_s}{\partial r}\right)^+(Z) - \left(\frac{\partial Q_s}{\partial r}\right)^-(Z) = -Q_1(Z) \tag{49}$$

Boundary Integral Equations

Equations (18a-c) and (18g) are replaced by an equivalent system of integral equations for Q_1 and Q_2. Using the operator notation (28-29, etc.) and the continuity results (40-47), the boundary conditions (18b-c) can be written as

$$\left(-\frac{1}{2}\mathbf{I} + \mathbf{S}_\mathbf{r}\right)[Q_1](Z) + \mathbf{D}_\mathbf{r}[Q_2](Z) = -\frac{\partial Q_1}{\partial r}(1,Z) \quad Z \in (a,b) \tag{50a}$$

and

$$\begin{aligned}\left\{-e^{-i\frac{\kappa}{M_F}Z}\mathbf{I} + \frac{iM_F^2\alpha(Z)}{\beta^3\kappa M_{TIP}}\frac{d^2}{dZ^2}\left(e^{-i\frac{\kappa}{M_F}Z}\mathbf{S}\right)\right\}[Q_1](Z) + \frac{iM_F^2\alpha(Z)}{\beta^3\kappa M_{TIP}}\frac{d^2}{dZ^2}\left[e^{-i\frac{\kappa}{M_F}Z}\left(\frac{1}{2}\mathbf{I} + \mathbf{D}\right)\right][Q_2](Z) \\ = -\frac{iM_F^2\alpha(Z)}{\beta^3\kappa M_{TIP}}\frac{\partial^2}{\partial Z^2}\left(e^{-i\frac{\kappa}{M_F}Z}Q_1\right)(1,Z) \qquad Z \in (a,b)\end{aligned} \tag{50b}$$

where $\mathbf{I}$ is the identity operator.

To obtain a unique solution of the system (50a-b), we must establish requirements on the layer densities at the duct leading and trailing edges. This information is provided by the as yet unsatisfied BVP equations (18d-f). Applying the layer representation for the scattered pressure to (18d-f) yields

$$\int_{-\infty}^{a} e^{-i\frac{\kappa}{M_F}Z'}\left\{\mathbf{s}_\mathbf{r}[Q_1](1,Z') + \mathbf{d}_\mathbf{r}[Q_2](1,Z')\right\}dZ' = -\int_{\infty}^{a} e^{-i\frac{\kappa}{M_F}Z'}\frac{\partial Q_1}{\partial r}(1,Z')dZ' \ , \tag{55c}$$

$$Q_2(a) = 0 \ , \tag{50d}$$

and

$$\int_{\Re}\left|\mathbf{s}[Q_1](r,Z) + \mathbf{d}[Q_2](r,Z)\right|d\Re < \infty \qquad \Re \text{ any region in } r - Z \text{ plane} \ . \tag{50e}$$

The boundary value problem (18a-g) is thus replaced by the equivalent boundary integral equation formulation (50a-e). Equations (50a-b) comprise a system of strongly singular integro-differential equations.

Elaborate techniques are required to solve (50). For clarity, we consider the solution of (50) under simplified circumstances of practical interest. For $\alpha \equiv 0$ (hard interior wall) in (50b), we obtain the result $Q_1(Z) \equiv 0$. This yields the classical Neumann boundary integral equation

$$\mathbf{D}_{\mathbf{r}}[Q_2](Z) = -\frac{\partial Q_1}{\partial r}(1,Z) \qquad Z \in (a,b) \tag{51a}$$

and auxiliary conditions

$$\int_{-\infty}^{a} e^{-i\frac{\kappa}{M_F}Z'} \mathbf{d}_{\mathbf{r}}[Q_2](1,Z')dZ' = -\int_{-\infty}^{a} e^{-i\frac{\kappa}{M_F}Z'} \frac{\partial Q_1}{\partial r}(1,Z')dZ' \quad , \tag{51b}$$

$$Q_2(a) = 0 \quad , \tag{51c}$$

$$\int_{\Re} \left|\mathbf{d}[Q_2](r,Z)\right| d\Re < \infty \qquad \Re \text{ any region in } r-Z \text{ plane} \quad . \tag{51d}$$

Note that (51b) is satisfied trivially for $M_F = 0$.

The solution of (51) for cylindrical ducts has been studied in the literature recently (references ***-***). The referenced works differ in their derivations, depth of kernel analyses, and solution techniques. In reference ***AIAA paper***, the analyses and techniques similar to those presented here were applied to (51). For the first time using boundary integral techniques, continuous portions of the acoustic field were calculated quickly (several minutes on a PC) and accurately. This was made possible by applying advanced analytical and numerical methods to the singular integrals in (51).

Also of interest are "small" inflow Mach number situations. Such conditions occur at take-off and landing for example. Ignoring terms in (50) smaller than $O(1)$ for $M_F \to 0$, yields the approximate system

$$\left(-\frac{1}{2}\mathbf{I}+\mathbf{S}_{\mathbf{r}}\right)[Q_1](Z)+\mathbf{D}_{\mathbf{r}}[Q_2](Z)=-\frac{\partial Q_1}{\partial r}(1,Z) \quad Z\in(a,b) \tag{52a}$$

$$-\left\{\mathbf{I}+\frac{im\alpha(Z)}{\beta^4}\mathbf{S}\right\}[Q_1](Z)-\frac{im\alpha(Z)}{\beta^4}\left(\frac{1}{2}\mathbf{I}+\mathbf{D}\right)[Q_2](Z)=\frac{im\alpha(Z)}{\beta^4}Q_1(1,Z) \qquad Z\in(a,b) \tag{52b}$$

CHECK THIS ONE OUT FOR THE HARD WALL CASE

$$\mathbf{s}_{\mathbf{r}}[Q_1](1,a^-)+\mathbf{d}_{\mathbf{r}}[Q_2](1,a^-)=-\frac{\partial Q_1}{\partial r}(1,a) \ , \tag{52c}$$

$$Q_2(a)=0 \ , \tag{52d}$$

$$\int_{\Re}\left|\mathbf{s}[Q_1](r,Z)+\mathbf{d}[Q_2](r,Z)\right|d\Re<\infty \qquad \Re \text{ any region in } r-Z \text{ plane} \ . \tag{52e}$$

In (52c) the notation a^- implies the limit as Z approaches a from the left.

In the next section, the solution of (52) will be examined in detail. The validity of the approximate equations for $0\le M_F\le 0.4$ *** THIS RANGE MAY CHANGE - NEED SOME HARD WALL CALCULATIONS TO VERIFY*** is demonstrated in the results section. The solution of the full equations (50) will be considered in future research by the authors.

TBIEM3D

A Computer Program for Predicting Ducted Fan Engine Noise

Version 1: May 1997

M.H. Dunn
Department of Mathematics and Statistics
Old Dominion University
Norfolk, VA

Contents

List of Symbols 3

Introduction 5

Limitations and Comments 8

Operating Instructions 9

Examples 10

References 11

Tables and Figures 12

List of Symbols

a	axial coordinate of duct trailing edge in moving frame
b	axial coordinate of duct leading edge in moving frame
c	ambient sound speed
k	$= mN_B M_{TIP}$ nondimensional characteristic wave number of m-th circumferential mode
L_D	ratio of duct length to diameter
m	circumferential mode number
M	$= V/c$ flight Mach number
M_{TIP}	$= r_D \Omega / c$ tip Mach number (based on duct radius)
N_B	number of fan blades
N_L	number of liner segments
N_{OBS}	number of observers for TBIEM3D output
P	total acoustic pressure
P^m	m-th circumferential coefficient of total pressure
P_i	incident acoustic pressure
P_i^m	m-th circumferential coefficient of incident pressure
P_s	scattered acoustic pressure
P_s^m	m-th circumferential coefficient of scattered pressure
(r, ψ, Z)	cylindrical coordinates in frame of reference attached to duct
r_D	duct radius
r_0	radial coordinate of spinning point dipoles
t	time

T	thrust from fan
V	duct speed
$\{Z_j\}_{j=1}^{N_L+1}$	axial locations of liner segments
$\alpha(Z)$	$= \rho_0 c[\xi(Z) - i\sigma(Z)]$ segmented, specific acoustic admittance on interior duct wall
$\{\alpha_j\}_{j=1}^{N_L}$	piecewise specific acoustic admittances
β	$= \sqrt{1 - M^2}$ compressibility (stretching) parameter
κ	$= k/\beta$ nondimensional stretched characteristic wave number
ρ_0	ambient density
$\sigma(Z)$	segmented, acoustic susceptance on interior duct wall
$\xi(Z)$	segmented, acoustic conductance on interior duct wall
Ω	shaft speed (radians/second)

Introduction

This document describes the ducted fan noise prediction computer program TBIEM3D (Thin duct, Boundary Integral Equation Method, 3 Dimensional). The scattering of fan generated noise by a finite length, infinitesimally thin circular cylinder in a uniform flow field is considered. The program, based on a boundary integral equation method (BIEM), calculates circumferential modal coefficients of the acoustic pressure at user specified field locations. TBIEM3D features include versatility, rapid calculations, and ease of use. Theoretical and computational details can be found in references 1-4.

In a frame of reference attached to the duct, the fan generates spinning acoustic modes. The thrust component of fan loading noise is approximated by a collection of spinning point thrust dipoles. A precise mathematical representation for the acoustic field due to this configuration has been implemented. In many cases, TBIEM3D can be easily adapted to accommodate other source fields.

TBIEM3D employs cylindrical coordinates in a frame of reference attached to the engine (figures 1-3). The coordinate origin is at the center of the fan disc. The fan and duct translate in the $+Z$ (axial) direction with uniform speed V. N_B equally spaced blades comprise the fan. The shaft rotates with speed Ω (figure 2).

The total acoustic pressure in the sound field is split into known incident and unknown scattered parts:

$$P'(r,\psi,Z,t) = P_s'(r,\psi,Z,t) + P_i'(r,\psi,Z,t) \quad . \tag{1}$$

Assuming linear conditions, all dependent acoustic variables can be expressed as superpositions of spinning modes. For example, the scattered pressure has the form

$$P_s'(r,\psi,Z,t) = \sum_{m=-\infty}^{\infty} P_s^m(r,Z)\, e^{imN_B(\Omega t-\psi)} \quad . \tag{2}$$

Incident and total acoustic pressures are written similarly. Modal amplitudes are calculated term by term. The TBIEM3D code must be run separately for each desired mode.

The duct exterior is hard and the interior may be hard or lined. Passive noise treatment is modeled by an axisymmetric, locally reactive, segmented liner with user specified admittances. The definition of specific acoustic admittance used by TBIEM3D

$$\alpha(Z) = \rho_0 c\left[\xi(Z) - i\sigma(Z)\right] \tag{3}$$

is consistent with the time factor $e^{-imN_B\Omega t}$ in (2). Regions of the duct interior near the leading and trailing edges are assumed hard (figure 3). Any interior wall segment may also be rigid. These comments are summarized by the equation

$$\alpha(Z) = \begin{cases} 0 & Z \in [a, Z_1] \cup \left[Z_{N_L+1}, b\right] \\ \alpha_j & Z \in \left(Z_j, Z_{j+1}\right) \quad j = 1, \ldots N_L \end{cases} \tag{4}$$

BIEM methodology is a three step process: Step 1) A Helmholtz boundary value problem (BVP) for the modal coefficients in (2) is derived. Step 2) Using layered Helmholtz potentials, the BVP is converted to a boundary integral equation formulation that features a set of hypersingular integral equations for the unknown Helmholtz layers. Step 3) The integral equations are solved and the acoustic field calculated from the Helmholtz potential representation.

The TBIEM3D code is written in the FORTRAN programming language and employs IMSL mathematical library routines. TBIEM3D should be implementable on any computer that can accommodate FORTRAN and IMSL. Some code modification may be required. For minimally adequate computational performance, a Pentium 133 processor (or equivalent) with 32 megabytes of RAM is recommended.

TBIEM3D input is relatively simple. Geometric, kinematic, and liner parameters are required. If a source description other than the one described above is desired, then the user must supply FORTRAN subroutines for the calculation of the incident field and its radial derivative. Output from TBIEM3D consists of the modal coefficients of the complex pressure components [see equations (1-2)] at user specified field points. Postprocessing of results is left to the user.

The key feature of TBIEM3D is the ability to compute any portion of the sound field without the need to calculate the entire field. Competing methods such as finite differences and finite elements lack this property. Other positive attributes include reduced consumption of computational resources, enhanced numerical accuracy, versatility, coupling of radiation and propagation both forward and aft, and validity over a wide range of frequencies. Consequently, the TBIEM3D code is well suited for parametric calculations. Many engineering studies of interest can be handled by TBIEM3D.

Questions, comments, and requests for discussions should be addressed to **mhd314@aol.com**

Limitations and Comments

1) At present, the TBIEM3D code can treat "small" Mach number inflow. Results obtained for $M > 0.4$ may be questionable. TBIEM3D with no inflow restrictions will be made available when complete.

2) For large values of κ, TBIEM3D computational time and storage requirements can increase considerably. Therefore, at typical fan operating conditions, it is recommended that the user calculate a maximum of three circumferential modes. Efforts are underway to improve TBIEM3D performance for high frequencies.

3) It is well known from the theory of wave propagation in an infinite, hard walled duct that resonance occurs at certain discrete frequencies. At these eigenfrequencies, the infinite duct problem is unsolvable. Theoretically, the finite, hard walled interior duct is solvable at all frequencies. Ill-conditioning in the TBIEM3D numerical system, however, is experienced at and near the infinite duct eigenfrequencies. TBIEM3D results at these eigenfrequencies show evidence of resonance but appear plausible. The numerical correctness of TBIEM3D at resonance has not been established. Therefore users should examine TBIEM3D results carefully when the hard wall interior option is activated.

4) For some applications, it may be convenient to place the sources outside the duct. This is easily achieved with TBIEM3D. The user must have either $a > 0$, $b < 0$, and/or $r_0 > r_D$.

5) Since the duct is approximated by an infinitely thin cylinder, the acoustic pressure is discontinuous across the duct surface. Consequently, evaluation of the acoustic pressure on the duct wall is ambiguous. It is recommended that if the pressure on the interior duct surface is required, then the user should place the observer a small distance off the duct toward the interior.

Operating Instructions

TBIEM3D operating parameters consist of a one line identifier, output file name and path, and physical parameters. The code generates one output file containing values of program parameters and the complex modal coefficients of incident, scattered, and total pressure at user specified field points. The output file is associated with logical unit 9. Access of unit 9 elsewhere in the calling program can lead to errors and should be avoided. COMMON statements in TBIEM3D should be examined to avoid conflicts with the user program.

To activate TBIEM3D, the user's calling program must have the FORTRAN statement

$$\begin{aligned} &\textbf{CALL TBIEM3D(}\ \mathit{ident}\ ,\ \mathit{outfile}\ ,\ m\ ,\ N_B\ ,\ RPM\ ,\ r_D\ ,\ a\ ,\ b\ ,\ r_0\ ,\ T\ ,\ c\ ,\ \rho_0\ ,\ V\ , \\ &\quad N_L\ ,\ \left\{Z_J\right\}_{J=1}^{N_{L+1}}\ ,\ \left\{\alpha_J\right\}_{J=1}^{N_L}\ ,\ N_{OBS}\ ,\ \left\{r_J\right\}_{J=1}^{N_{OBS}}\ ,\ \left\{\overline{Z}_J\right\}_{J=1}^{N_{OBS}}\ \ \textbf{)} \end{aligned} \tag{5}$$

*

The notation $\left\{x_J\right\}_{J=1}^{N}$ in (5) denotes a one dimensional array of length N. Variables in the argument list are described in table 1. SI units are required for dimensional variables.

The TBIEM3D output file contains the case identifier and program parameters followed by N_{OBS} formatted lines containing the dimensional (pascals) complex modal coefficients of incident, scattered, and total acoustic pressure. For each observer point, TBIEM3D writes the pressure components according to the following FORTRAN statements:

WRITE(6,600) $r\ ,\ Z\ ,\ Re\left[P_i^m\right],\ Im\left[P_i^m\right],\ Re\left[P_s^m\right],\ Im\left[P_s^m\right],\ Re\left[P^m\right],\ Im\left[P^m\right]$

600 **FORMAT(8E11.4)** .

Examples

Three examples are presented in this section to demonstrate TBIEM3D features and usage. Kinematic parameters were chosen to simulate actual ducted fan engine operating conditions ($M_F = 0.40$, $M_{TIP} = 1.22$, $N_B = 20$, $L_D = 0.50$). The examples differ in the acoustic treatment on the duct interior. Admittances for the three cases are given below. All calculations were performed on a Pentium 133 laptop computer with 32 megabytes of RAM. Graphical results displayed here are not part of TBIEM3D.

For each of the three cases, two dimensional portions of the sound field are computed. Acoustic pressure and sound pressure level contours for the first modal coefficient are plotted in figures 5-7. The specific acoustic admittances used for the calculations do not necessarily correspond to actual conditions but were chosen for demonstrative purposes. Figure 4 contains the FORTRAN calling program that generated the results for figures 5-7.

Example 1 Hard inlet and hard exhaust. See figures 5a-b. Three minutes computational time required for 15000 field points.

Admittance: $\alpha(Z) = 0 \quad Z \in [a,b]$

Example 2 Lined inlet (one segment) and hard exhaust. See figures 6a-b. Five minutes computational time required for 15000 field points.

Admittance: $$\alpha(Z) = \begin{cases} 1-i & Z \in (0,0.475) \\ 0 & \text{elsewhere} \end{cases}$$

Example 3 Lined inlet (one segment) and lined exhaust (one segment). See figures 7a-b. Five minutes computational time required for 15000 field points.

Admittance: $$\alpha(Z) = \begin{cases} 1-i & Z \in (0,0.475) \\ 0.5 & Z \in (-0.475,0) \\ 0 & \text{elsewhere} \end{cases}$$

In figures 8a-b, comparisons between the three cases in both the nearfield and farfield are displayed. Sound pressure levels for the first modal coefficient on an arc of 200 field points about the duct center are calculated. The radius of the arc is ten meters for the farfield example (figure 8a) and one meter for the nearfield example (figure 8b) and extends from the forward duct axis to the aft duct axis. The results are plotted to show the effects of passive noise treatment. Calculations required approximately one minute.

References

[1] M.H. Dunn, J. Tweed, and F. Farassat: The Prediction of Ducted Fan Engine Noise Via a Boundary Integral Equation Method; AIAA Paper 96-1770; Dunn, Tweed, and Farassat, April 1996.

[2] M.H. Dunn, J. Tweed, and F.Farassat: The Prediction of Radiated Tonal Noise from an Acoustically Treated Engine Duct; In Progress.

[3] R. St. John, M.H. Dunn, and J. Tweed: Acoustic Scattering Problems in Two Dimensions; In Progress.

[4] J. Tweed, M.H. Dunn, and R. St. John: On the convergence of Algorithms for the Numerical Solution of a Finite-Part Integral Equation; In progress.

Variable	Description	Comments
ident	Character*80 variable; case identifier	80 ASCII characters maximum
outfile	Character*80 variable; output file name	80 ASCII characters maximum; file path may be included
m	Integer; Circumferential mode number	See (2) and limitation 2)
N_B	Integer; Number of fan blades	See figures 1-3; $N_B > 0$
RPM	Real; shaft speed (revolutions per minute)	$\Omega = (\pi\, RPM)/30$
r_D	Real; duct radius (meters)	See figures 1-3
a	Real; axial coordinate of duct trailing edge (meters)	See figures 1-2
b	Real; axial coordinate of duct leading edge (meters)	See figures 1-2
r_0	Real; radial location of spinning dipoles (meters)	See figures 2-3
T	Real; thrust from fan (kilonewtons)	
c	Real; Ambient sound speed (meters per second)	
ρ_0	Real; Ambient density (kilograms per cubic meter)	
V	Real; Engine speed (meters per second)	$V/c < 1$; see limitation 1)
N_L	Integer; number of liner segments	For hard wall interior set $N_L = 0$ in which case limitation 3) may apply
$\{Z_j\}_1^{N_L+1}$	Real; axial coordinates of liner segments (meters)	See (3-4) and figure 3; if $N_L = 0$, then omit; $a < Z_i < Z_{i-1} < b \quad i = 1,\ldots N_L$
$\{\alpha_j\}_1^{N_L}$	Complex; acoustic admittances (non dimensional) for segmented liner	See (3-4) and figure 3; if $N_L = 0$, then omit; some segments may be hard, i.e., $\alpha_i = 0$
N_{OBS}	Integer; number of observers for output	$0 < N_{OBS} \le 10^5$; Large values of N_{OBS} can lead to excessive computational time
$\{r_j\}_1^{N_{OBS}}$	Real; radial coordinates of observer points (meters)	See limitation 5)
$\{\bar{Z}_j\}_1^{N_{OBS}}$	Real; axial coordinates of observer points (meters)	

Table 1: TBIEM3D Input Parameters

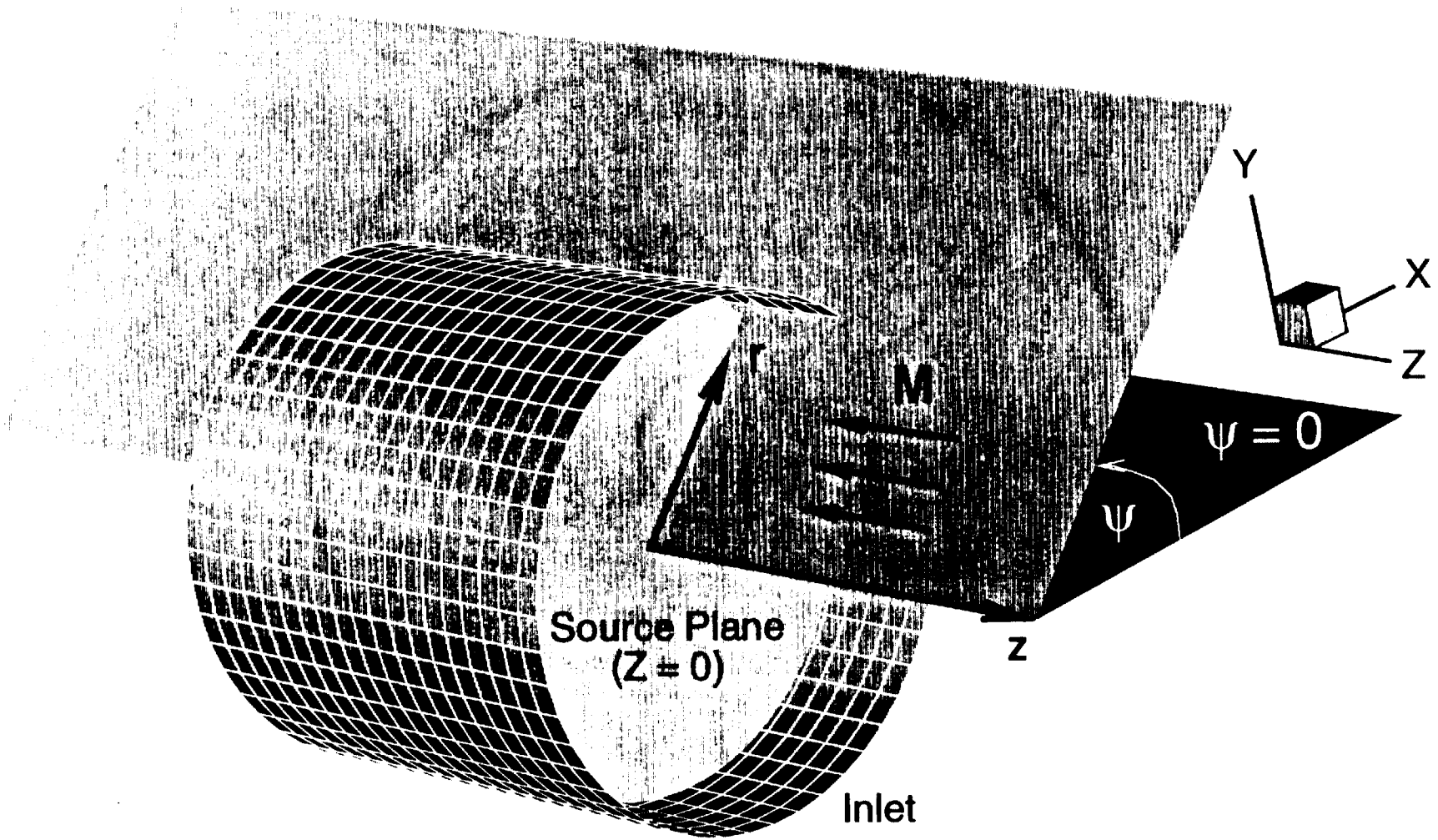

Figure 1: Duct Geometry and Coordinate Definitions
Cylindrical Frame Fixed to Duct

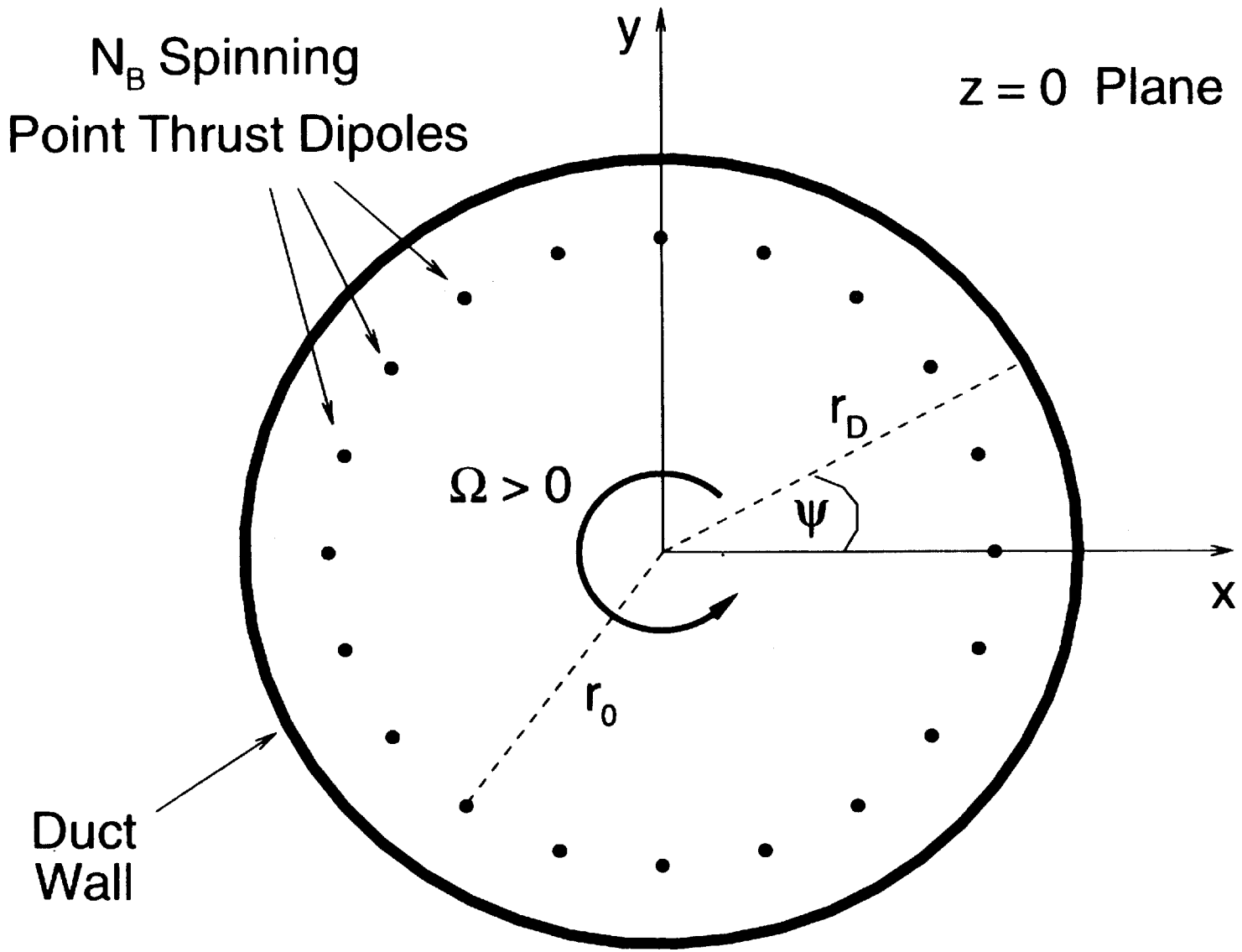

Figure 2: Source Plane Geometry
View from Inlet into Duct

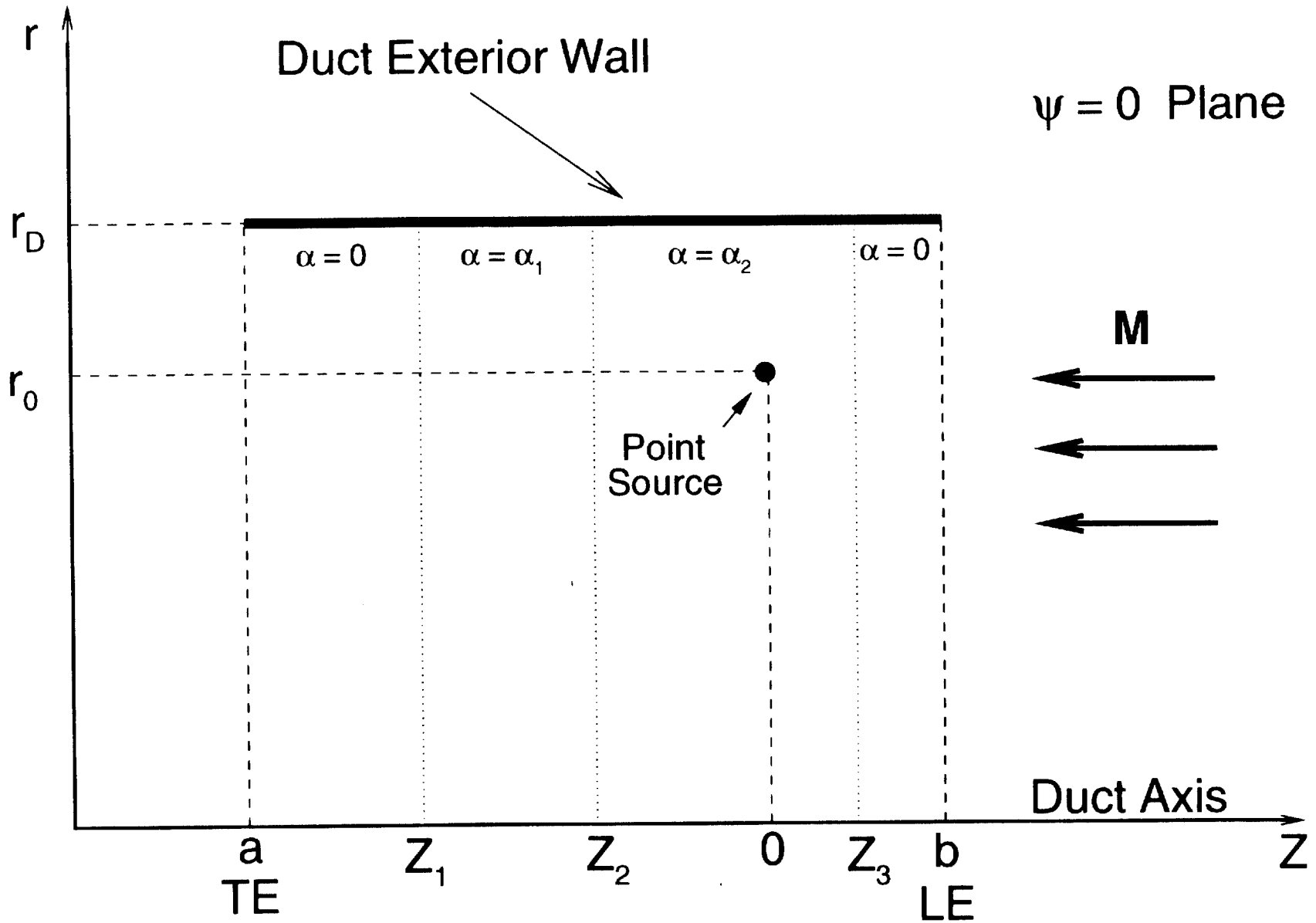

Figure 3: Duct and Liner Geometry (Side View)
Two Piece Segmented Liner

Figure 4: Calling Program for TBIEM3D Examples 1-3

```
c
c+++++++++++++++++++++++++++++++++++++++++
c TBIEM3D examples for user document
c+++++++++++++++++++++++++++++++++++++++++
c
   program myBIEM
   dimension ZOBS(100000),rOBS(100000)
   dimension Zliner(100)
   complex admit(100)
   character*80 ident,outfile
   ident = 'TBIEM3D Example #1'
   outfile = 'c:\myBIEM.txt'
   pref = 2.*10.**(-5.)
   nharm = 1
   nblades = 20
   rpm = 3500.
   radiusd = 1.0
   zte = -0.5
   zle = 0.5
   radius0 = 0.95
   thrustc = 27.0
   sposnd = 300.
   density = 0.4
   V = 120.
c
c-----------------------------------------
c Define observer points for r-Z field
c calculations
c-----------------------------------------
c
   nz = 150
   nr = 100
   NOBS = nz*nr
   zmin = -2.
   zmax = 2.
   dz = (zmax-zmin)/float(nz-1)
   rmin = 0.
   rmax = 3.
   dr = (rmax-rmin)/float(nr-1)
   kount = 0
   do i = 1,nz
      z = zmin+(i-1.)*dz
      do j = 1,nr
         kount = kount+1
         r = rmin+(j-1.)*dr
         ZOBS(kount) = z
         rOBS(kount) = r
         enddo
      enddo
c
c-----------------------------------------
c Example 1: Hard Wall Interior
c-----------------------------------------
c
   NL = 0
   call TBIEM3D(ident,outfile,nharm,nblades,rpm,
  1 radiusd,zte,zle,radius0,thrustc,sposnd,
  2 density,V,NL,Zliner,admit,NOBS,ZOBS,rOBS)
```

Figure 4 (Continued): Calling Program for TBIEM3D Examples 1-3

```
c*********************************************
c Begin postprocessing for user document
c graphics - NOT part of TBIEM3D
c*********************************************
   open(unit=10,file='c:\fort10.txt',status=
  1'unknown')
   write(10,*)'zone t = "1", i = ',nr,', j = ',nz
   rewind(9)
   do j = 1,15
      read(9,*)
      enddo
   do iobs = 1,NOBS
      read(9,600)zz,rr,res,ais,rei,aii,ret,ait
      pmag = sqrt(ret**2+ait**2+1.e-12)
      spl = 10.*alog10(pmag/pref)
      write(10,*)zz,rr,spl,ret
      enddo


c*************************************************
c End postprocessing
c*************************************************
c
c-------------------------------------------------
c Example 2: Lined inlet with one segment
c-------------------------------------------------
c
   NL = 1
   Zliner(1) = 0
   Zliner(2) = 0.475
   admit(1) = cmplx(1.,-1.)
   rewind(9)
    call TBIEM3D(ident,outfile,nharm,nblades,rpm,radiusd,
    1   zte,zle,radius0,thrustc,sposnd,density,V,NL,
    2   Zliner,admit,NOBS,ZOBS,rOBS)
c*************************************************
c Begin postprocessing for user document
c graphics - NOT part of TBIEM3D
c*************************************************
   write(10,*)'zone t = "1", i = ',nr,', j = ',nz
   rewind(9)
   do j = 1,15
      read(9,*)
      enddo
   do iobs = 1,NOBS
      read(9,600)zz,rr,res,ais,rei,aii,ret,ait
      pmag = sqrt(ret**2+ait**2+1.e-12)
      spl = 10.*alog10(pmag/pref)
      write(10,*)zz,rr,spl,ret
      enddo
c*************************************************
c End postprocessing
c*************************************************
c
c-------------------------------------------------
c Example 3: Lined exhaust with one segment and
```

Figure 4 (Continued): Calling Program for TBIEM3D Examples 1-3

```
c             lined inlet with one segment
c-------------------------------------------------------
c
   NL = 2
   Zliner(1) = -0.475
   Zliner(2) = 0.
   Zliner(3) = 0.475
   admit(1) = cmplx(.5,0.)
   admit(2) = cmplx(1.,-1.)
   rewind(9)
    call TBIEM3D(ident,outfile,nharm,nblades,rpm,radiusd,
    1       zte,zle,radius0,thrustc,sposnd,density,V,NL,
    2       Zliner,admit,NOBS,ZOBS,rOBS)
c*********************************************************
c Begin postprocessing for user document
c graphics - NOT part of TBIEM3D
c*********************************************************
   write(10,*)'zone t = "1", i = ',nr,', j = ',nz
   rewind(9)
   do j = 1,15
      read(9,*)
      enddo
   do iobs = 1,NOBS
      read(9,600)zz,rr,res,ais,rei,aii,ret,ait
      pmag = sqrt(ret**2+ait**2+1.e-12)
      spl = 10.*alog10(pmag/pref)
      write(10,*)zz,rr,spl,ret
      enddo
c************************************
c End postprocessing
c************************************
   stop
600   format(8e11.4)
   end
```

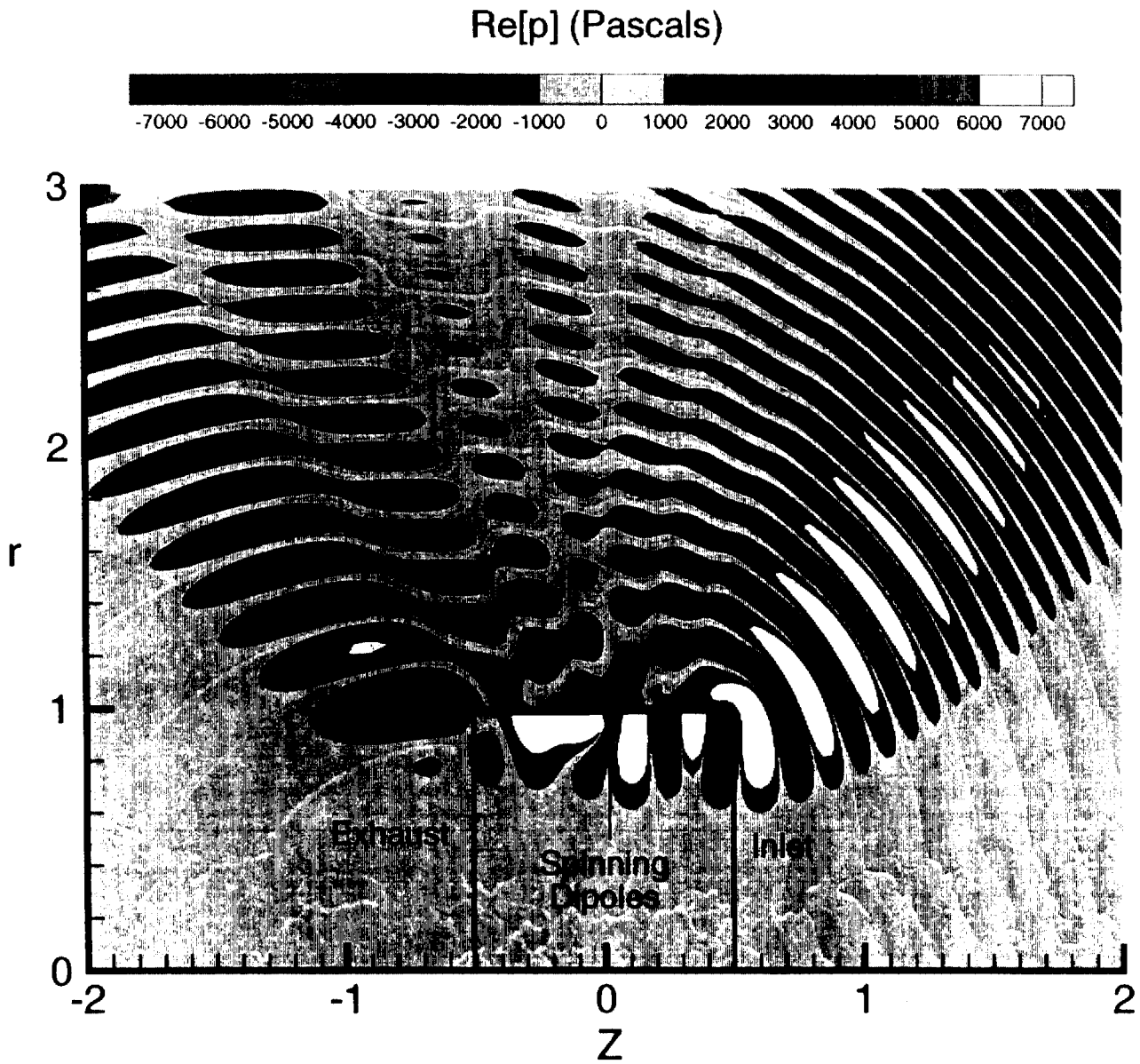

Figure 5a: BIEM Example #1 - Hard Inlet and Hard Exhaust
Acoustic Pressure
$M_F = 0.40$ $M_{TIP} = 1.22$ $L_D = 0.5$ $N_B = 20$

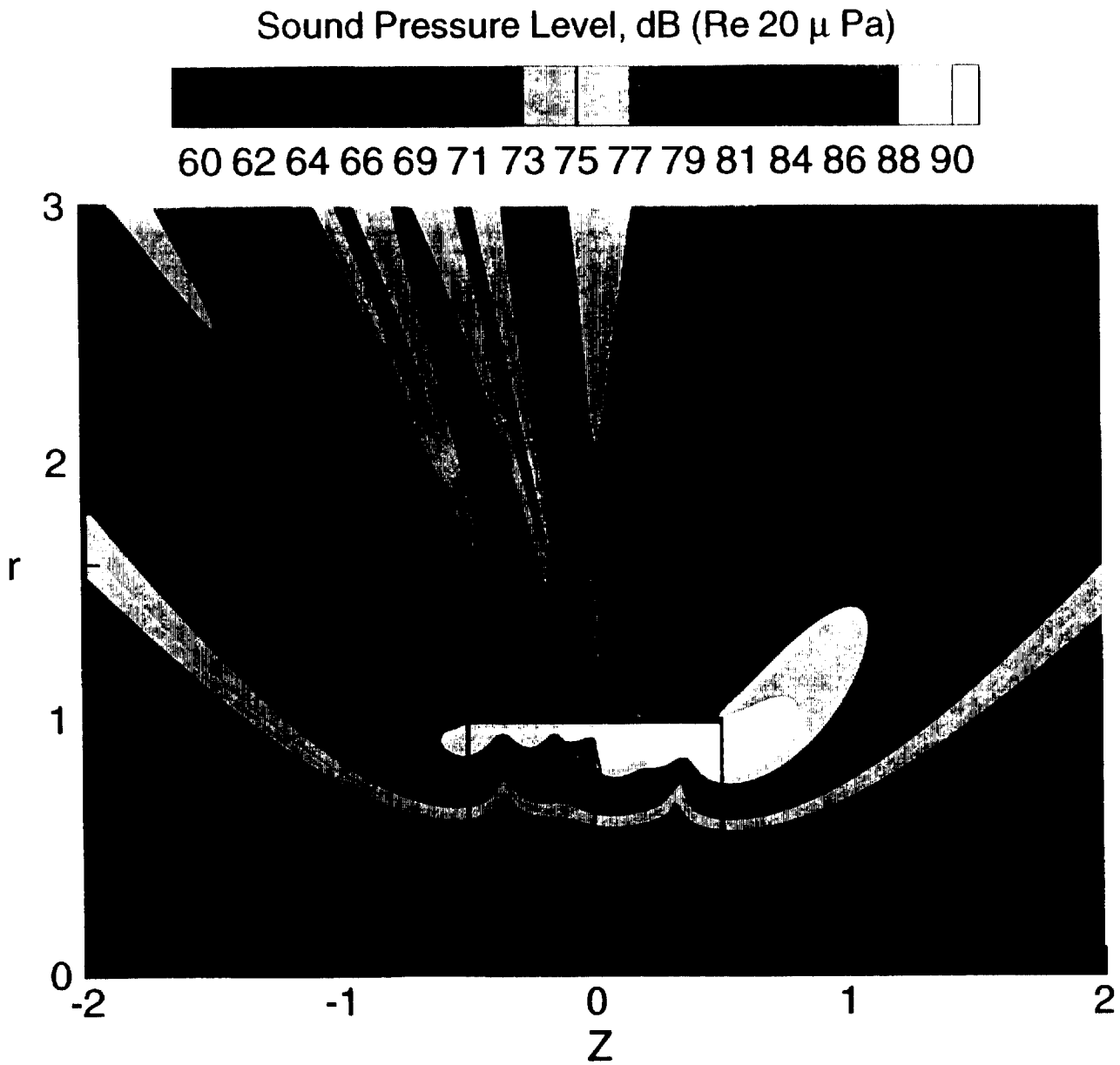

Figure 5b: BIEM Example #1 - Hard Inlet and Hard Exhaust
Sound Pressure Levels

$M_F = 0.40$ $M_{TIP} = 1.22$ $L_D = 0.5$ $N_B = 20$

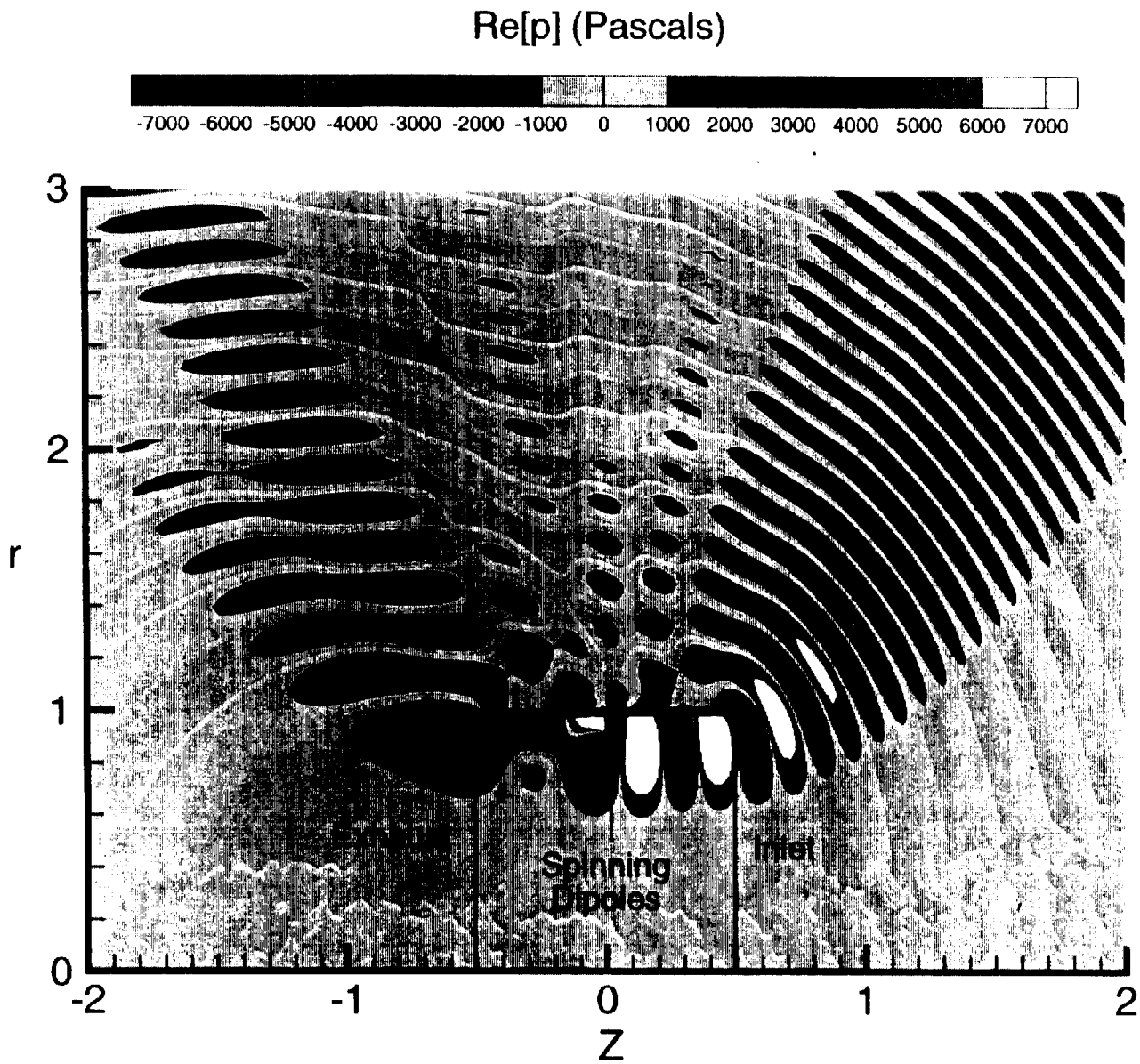

Figure 6a: BIEM Example #2 - Lined Inlet and Hard Exhaust
Acoustic Pressure
$M_F = 0.40$ $M_{TIP} = 1.22$ $L_D = 0.5$ $N_B = 20$

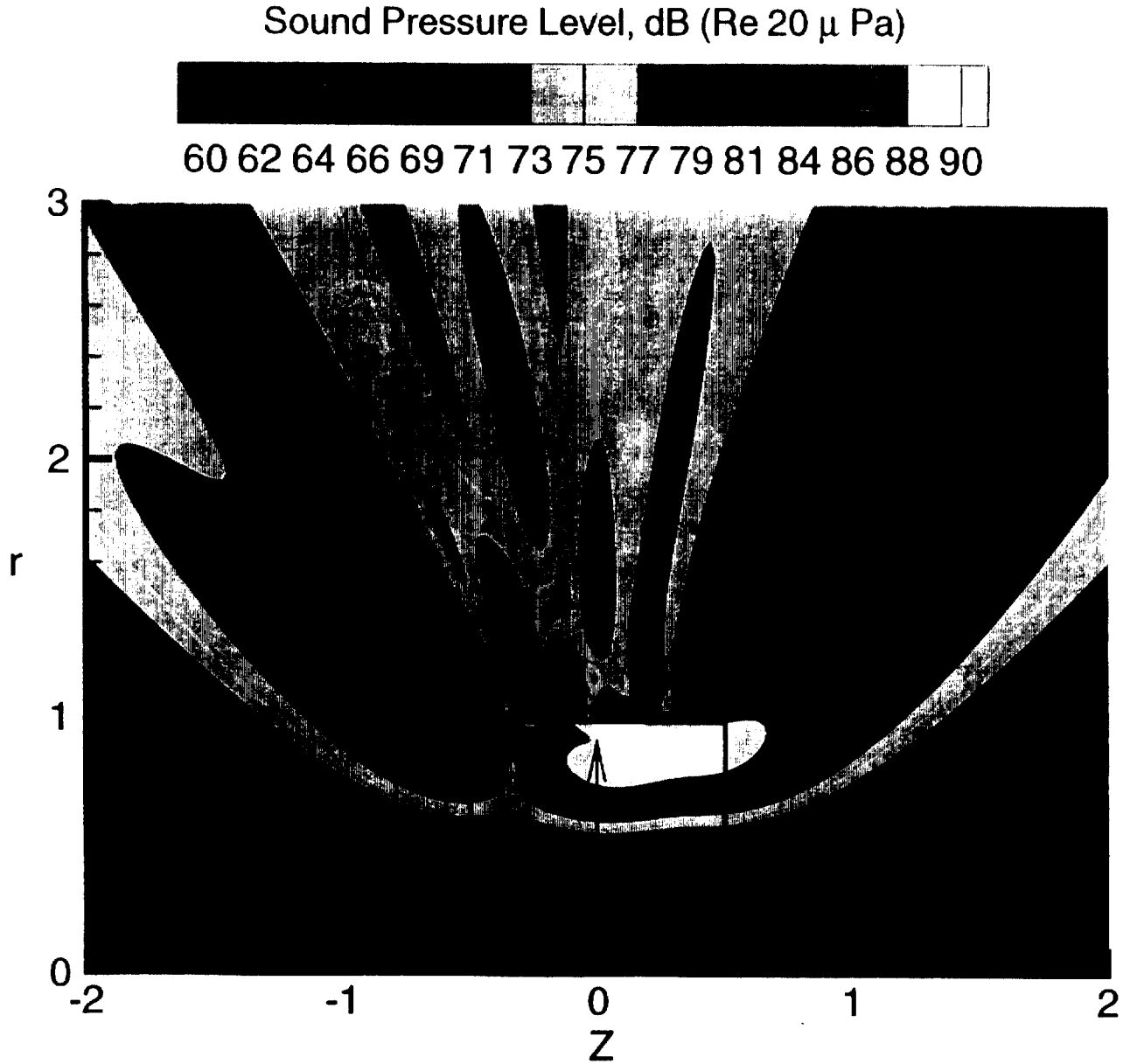

Figure 6b: BIEM Example #2 - Lined Inlet and Hard Exhaust
Sound Pressure Levels

$M_F = 0.40$ $M_{TIP} = 1.22$ $L_D = 0.5$ $N_B = 20$

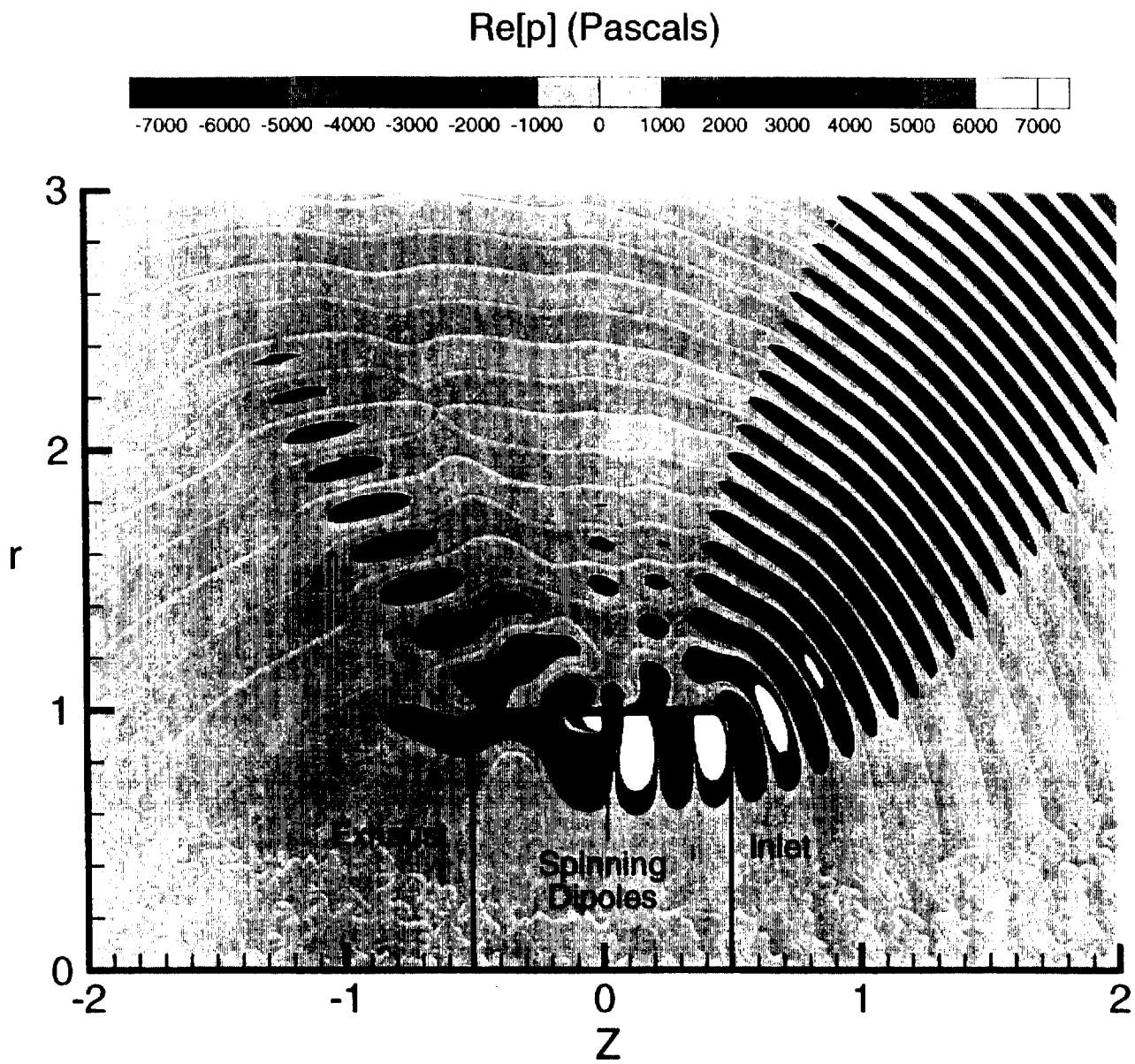

Figure 7a: BIEM Example #3 - Lined Inlet and Lined Exhaust
Acoustic Pressure
$M_F = 0.40$ $M_{TIP} = 1.22$ $L_D = 0.5$ $N_B = 20$

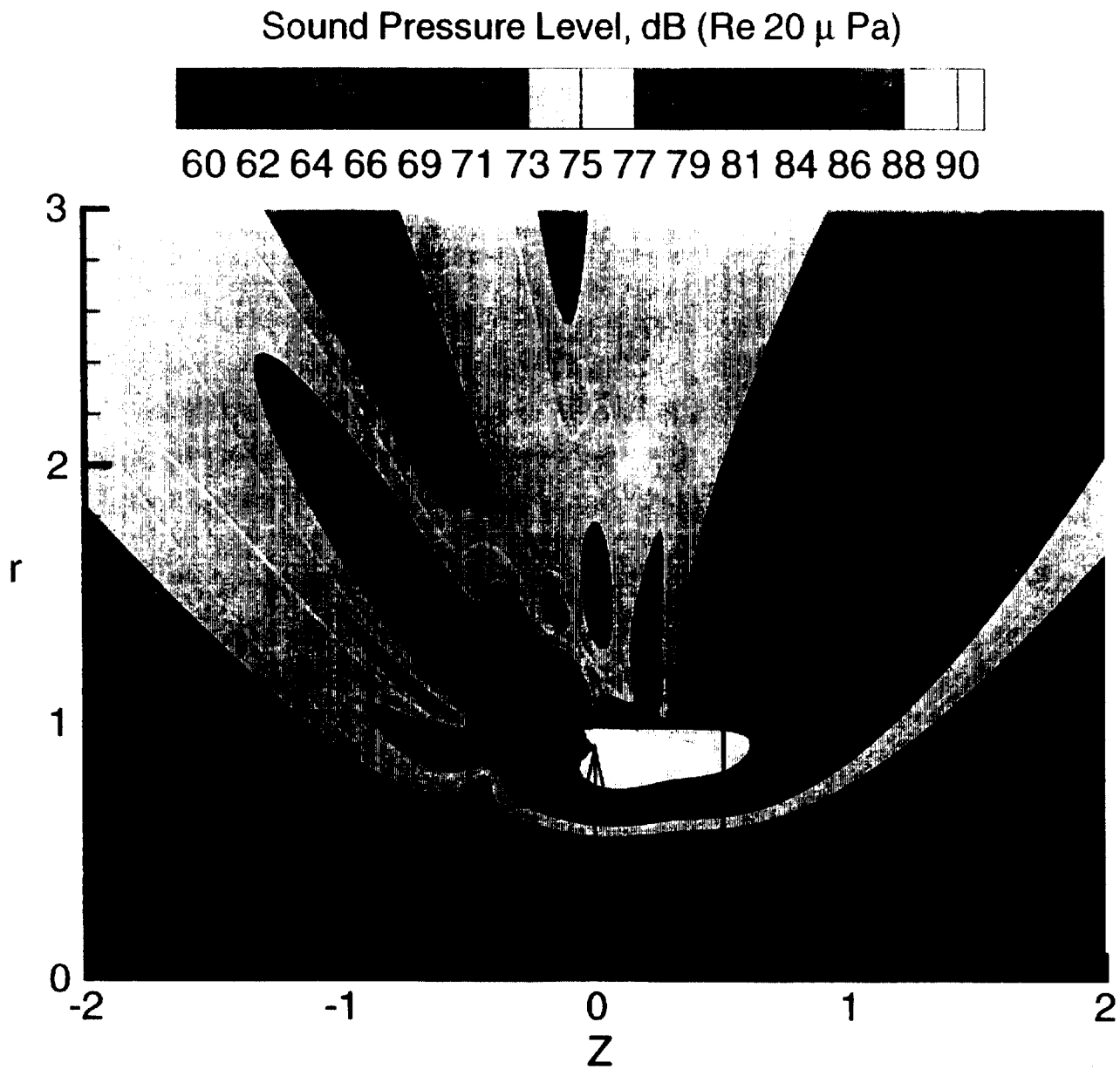

Figure 7b: BIEM Example #3 - Lined Inlet and Lined Exhaust
Sound Pressure Levels

$M_F = 0.40$ $M_{TIP} = 1.22$ $L_D = 0.5$ $N_B = 20$

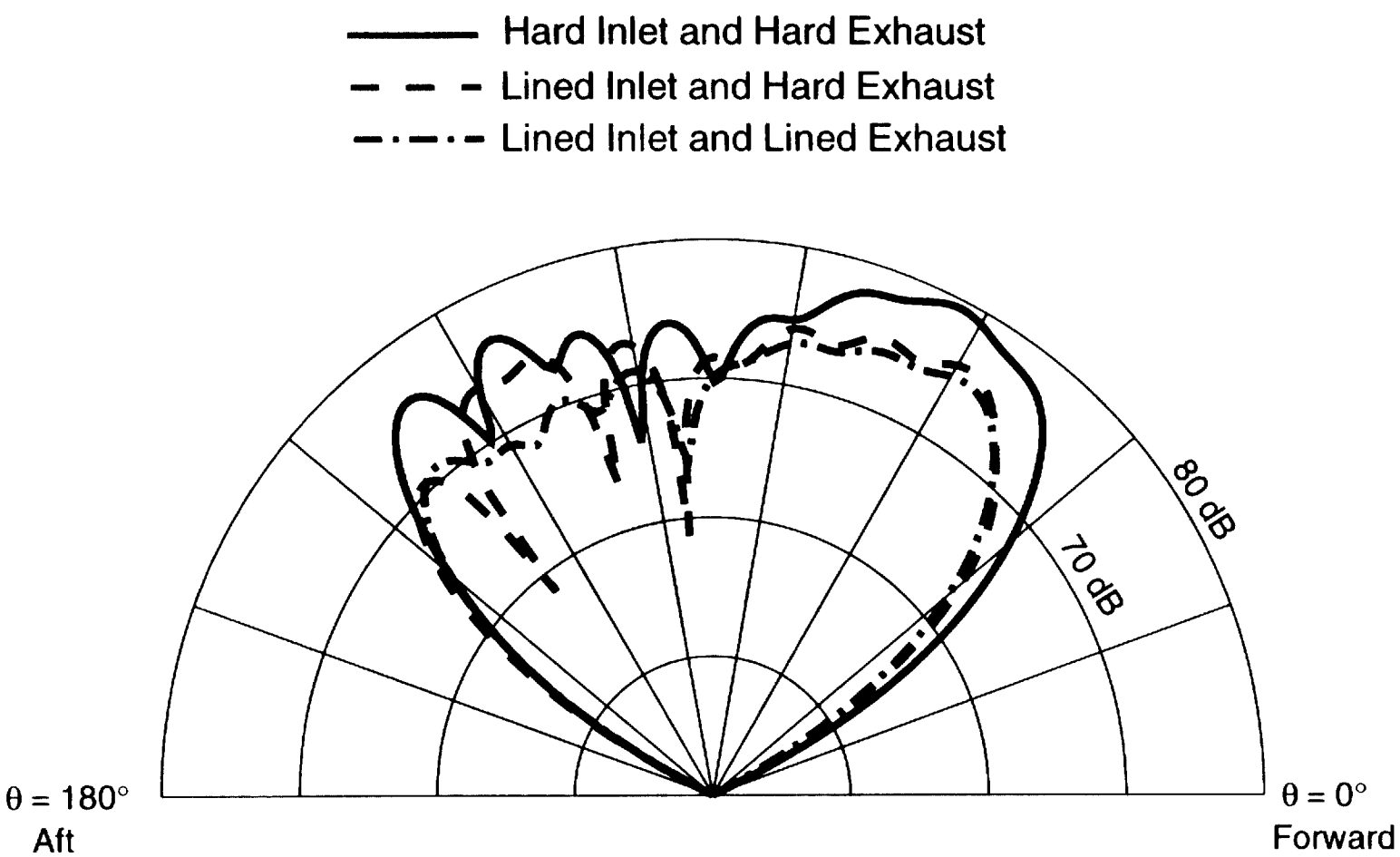

Figure 8a: Effect of Passive Noise Treatment
on Farfield Radiated Sound
$M_F = 0.4$ $M_{TIP} = 1.22$ $N_B = 20$ $L_D = 0.5$ $r_{OBS} = 10m$

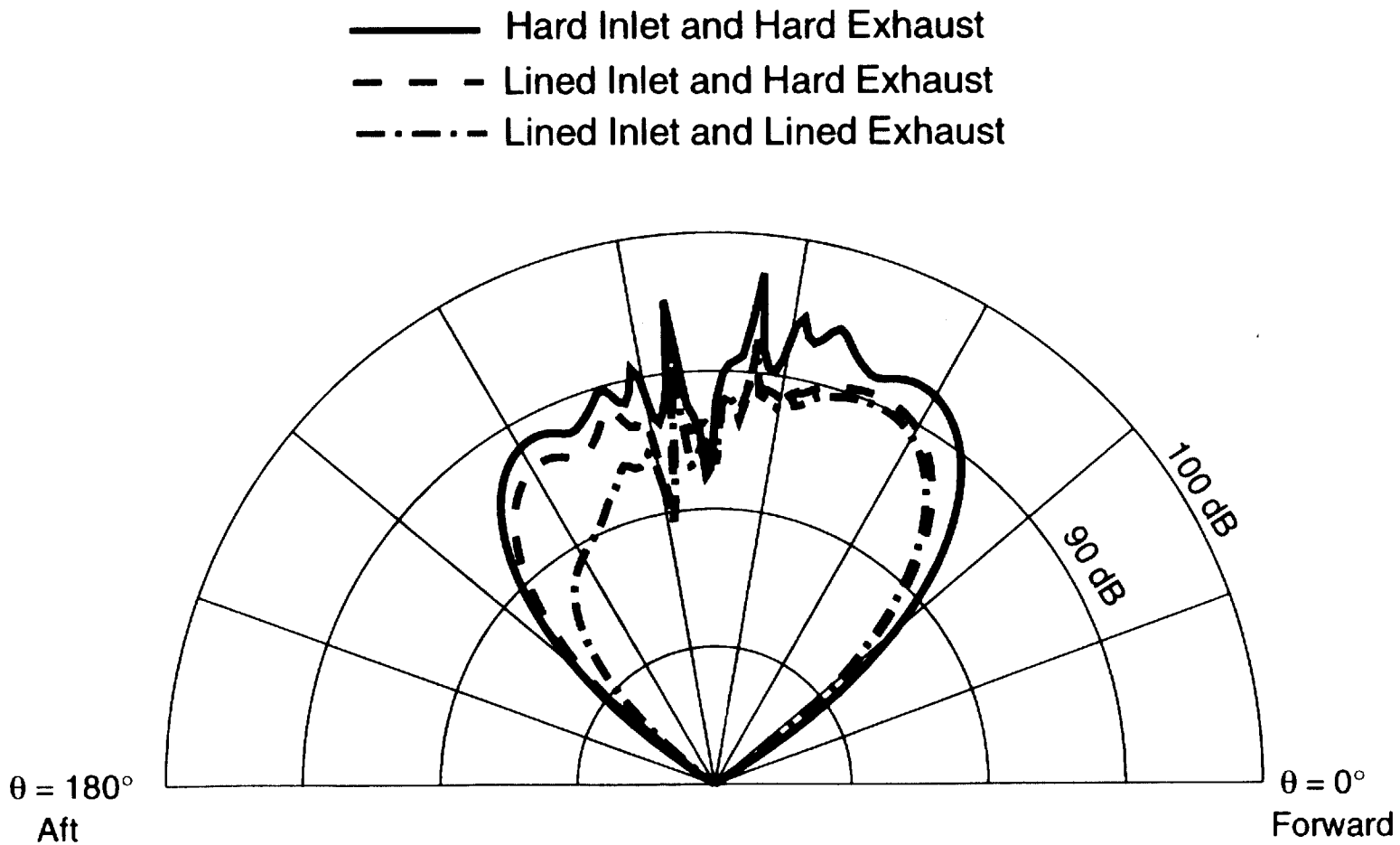

Figure 8b: Effect of Passive Noise Treatment
on Nearfield Radiated Sound

$M_F = 0.4$ $M_{TIP} = 1.22$ $N_B = 20$ $L_D = 0.5$ $r_{OBS} = 1m$

A Study of Noise Radiation from a Two Dimensional Scarf Inlet

M.H. Dunn and Richard St. John
Old Dominion University, Norfolk, Virginia

1.0 Introduction

The scarf inlet and exhaust have been recommended for the control of the noise radiation directivity from a ducted fan engine. There has been some experimental evidence that a scarf inlet does affect the directivity of the noise radiation pattern from the inlet and therefore, it is a promising passive noise control tool for aeroengines. Recently a computer code was developed at the Old Dominion University based on the boundary integral equation method (BIEM) for noise radiation from finite thin two dimensional ducts which allows the study scarf inlets and exhausts. The noise source inside the duct is taken as a point dipole source. We study the effect of the scarf inlet on noise radiation pattern from the inlet and the exhaust of a short duct with a conventional exhaust. The duct wall is assumed rigid and only one configuration of scarf inlet is studied. It is shown that the directivity of noise radiation from the inlet and exhaust is influenced by the presence of scarf inlet over a large range of frequency. The main part of the present study is for a stationary duct. However, we present some results at duct forward Mach number of $M = 0.4$ which indicate that the scarf inlet also influences the noise directivity even when the duct is in motion.

2.0 The Scarf Inlet

Figure 1 shows the two dimensional scarf inlet used in this study. Note that the upper wall is longer than the lower wall. Only one configuration of scarf inlet with conventional exhaust was studied. The design is based on the longest and the shortest axial nacelle length of the Langley 12 inch ducted fan model used in the scarf inlet test. This figure is to scale and the three circles of radii 0.2, 2.0 and 6.0 (nondimensionalized with respect to the duct width) indicate the arcs on which the acoustic pressure levels were calculated. The dipole point source is at the center of these circles and is located at the axial

position of the rotor center in the model test. The dipole source models the thrust of the rotor with the dipole axis along the duct axis. The axial position of the dipole corresponds to the rotor position in the Langley 12 inch ducted fan model.

3.0 The Acoustic Code (TBIEM2D)

The acoustic code used in this study was developed at the Old Dominion University. It is called TBIEM2D (Thin-duct BIEM 2 Dimensional). The duct is assumed finite in length, infinitely thin and can be in uniform forward motion. The interior of the duct can be lined and the two duct walls do not need to be of equal length. The liner can be segmented. In the examples given here we have used rigid duct wall option.

The duct propagation and radiation problem is modeled as follows. The acoustic pressure is written as the sum of the incident and scattered pressures. The scattered acoustic pressure in the frame fixed to the moving duct satisfies the convected wave equation which is Fourier transformed in time into a Helmholtz partial differential equation. The boundary condition for this equation is obtained from the incident wave and the locally reacting liner property. The problem is then reformulated as a coupled system of one dimensional hypersingular linear integral equations with single and double layer sources of unknown strengths on the duct wall. The radiation condition is automatically satisfied in the derivation of these equations but additional conditions are imposed to insure uniqueness and physical validity of the solution.

The system of the integral equations are solved by the collocation method for the unknown source strengths of the single and the double layer sources on the duct wall. The scattered acoustic pressure is then calculated at any point in the radiation field from integrals on the duct surface whose integrands depend on the known strengths of the single and the double layer sources. This is essentially equivalent to using the Kirchhoff formula for moving surfaces. The method of finding the scattered acoustic pressure is known as the boundary integral equation method (BIEM). The scattered pressure is added to the incident pressure to get the total acoustic pressure at the observer point.

One of the most important advantages of our approach is that the acoustic pressure can be calculated at any point in the field without the need for calcu-

lating the acoustic pressure elsewhere. This is in contrast to the finite difference and finite element methods which require the gridding of the space between the duct and the observer position and calculating the acoustic pressure at each grid point as well as at the observer position of interest. Thus the boundary integral equation method results in a very efficient computation tool for the acoustic pressure. The code TBIEM2D is run on a PC and has a simple input for point source excitation. The entire acoustic radiation field can be computed at a fixed observer time or at many observer times and then animated to see the propagation of the acoustic waves in the medium as well as the region of intense acoustic intensity and shadows.

4.0 Scarf Inlet Acoustic Results

We present our results below using nondimensional length and wave numbers as follows. All lengths are nondimensionalized by the duct width $W = 0.30$ m. The nondimensional wave number is defined as $k = \omega W/c$ where ω and c are the radian frequency and the speed of sound taken as 340 m/s. In all the calculations presented here, the source strength of the dipole inside the duct is kept fixed. Therefore, the relative levels of the acoustic pressure for the scarfed and conventional (unscarfed) inlet remain unchanged at the same nondimensional distance from the duct.

Figure 2 presents the directivity of the acoustic pressure level at the distances 0.2, 2.0 and 6.0 from the source and at the wave numbers $k = 18$ for both the scarf and conventional inlets at $M_F = 0$. Figures 3 and 4 show similar results at $k = 27$ and 36, respectively. We first consider the results of Fig. 2 at $k = 18$. The circle at the radius R = 0.2 is inside the duct and the directivity of the acoustic pressure level is clearly very similar to an axial dipole in the free field for both scarfed and unscarfed inlets. In the inlet radiation field, the scarf inlet radiation pattern becomes asymmetric with respect to the duct axis with a slight noise reduction in the upper and lower quadrants at angles of about 60° at radii R = 2 and R = 6. At R = 6, there is a slight increase in the acoustic pressure level of the noise radiated from the exhaust in the lower quadrant from the duct in scarf inlet. At $k = 27$ and $k = 36$, there are more lobes in the inlet and the exhaust radiation patterns of the two ducts. The asymmetry of the radiation pattern of the scarf inlet, as compared to the conventional inlet, is clearly visible in Figs. 3 and 4. In the inlet radiation field, there is a reduction of the noise levels in the upper quadrant and an increase in the lower

quadrant for the scarf inlet as compared to the unscarfed inlet. This effect is seen at large angles to the duct axis. There is some small changes in the exhaust radiation field by the scarf inlet at large angles to the duct axis.

Figures 5 to 7 show the directivity of the acoustic pressure level at three radial distances from the source and at three wave numbers for the scarf and conventional inlets at $M_F = 0.4$. The effect of the motion of the duct on the radiation pattern inside the duct is now much more pronounced than at $M_F = 0$. In the exterior of the duct and for the inlet radiation, there is a reduction on of the noise level in the upper quadrant and an increase in the noise level in the lower quadrant for the scarf inlet as compared to the conventional inlet at large angles from the duct axis. More surprising is the change in radiation pattern from the exhaust for the two inlet designs, particularly at $k = 18$. This may have important implication for the a real engine noise radiation.

As suggested by Dr. Robert Dougherty of the Boeing Commercial Airplane Group, a study of the relative acoustic power radiated in different quadrants can be useful in assessing the effect of scarf inlet on the control of noise radiation from ducted fans. We define an indicator of the acoustic power by the following relation for $M_F = 0$:

$$P = \int_{\psi_0}^{\psi_0 + \pi/2} p'^2(R, \psi) d\psi,$$

where ψ_0 is 0, $\pi/2$, π and $3\pi/2$ for the first to fourth quadrants, respectively. Note that the first and the fourth quadrants correspond to the upper and lower inlet quadrants, respectively. In figures 8 to 11, we present $20 \log\left[\frac{P_u}{P_s}\right] = \Delta_{SPL}$ for a large range of values of wave number k in the four quadrants where subscripts u and s refer to the unscarfed and scarfed inlets. A positive value of this quantity indicates that the conventional inlet radiates more acoustic power than the scarf inlet in that quadrant. From these figures, it is seen that for the range of frequencies considered, the scarf inlet radiates less acoustic power in the upper quadrant of the inlet and more

power in the lower quadrant than the conventional inlet. This is clearly seen in Fig. 12 where we have plotted Figs. 8 and 11 on the same plot. It is seen that the radiated power in each of the inlet quadrants is a function of the wave number. Also there is an interesting symmetry with respect to the 0 dB line in this figure which indicates that the function of the scarf inlet is essentially to redirect the acoustic power from the upper quadrant to the lower quadrant. Figures 9 and 10 show the relative acoustic power radiation in the upper and the lower quadrants of the exhaust. There are both an increase and a decrease of acoustic power radiation of the duct with scarf inlet as compared to the conventional inlet depending on the wave number. There is no clear trend emerging from power radiated from the exhaust in our study.

In Figures 8 to 11, we have shown the condition number of the matrix of the coefficients of a set of functions used in the boundary integral equation method. Large condition numbers indicate sensitivity to errors of the inversion of the matrix. except at isolated wave numbers, it appears that the condition numbers are generally small and the precision of our calculations can be trusted.

5.0 Concluding Remarks

In this study, we have shown that the scarf inlet has the potential of redirecting the acoustic power into the quadrant with shorter inlet length. This behavior extends to a large range of wave numbers and appears to be also effective at forward speed. There are also changes in the exhaust radiation pattern which do not appear to follow a clear trend. These changes require further studies. We have also shown the usefulness of the boundary integral equation method code TBIEM2D used in our study. All calculations were performed on a PC at a short execution time.

2-D Duct with Scarfed Inlet

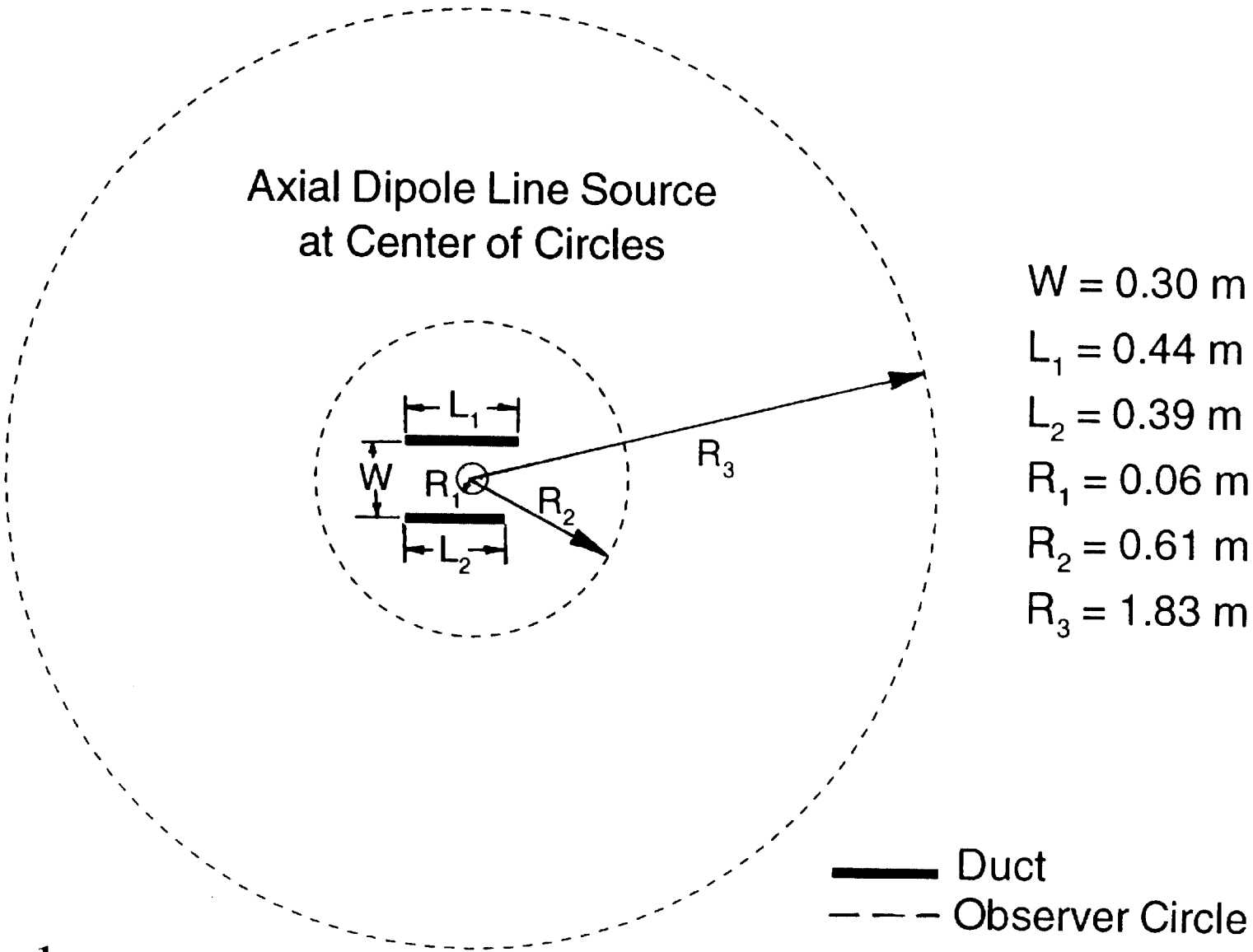

Figure 1

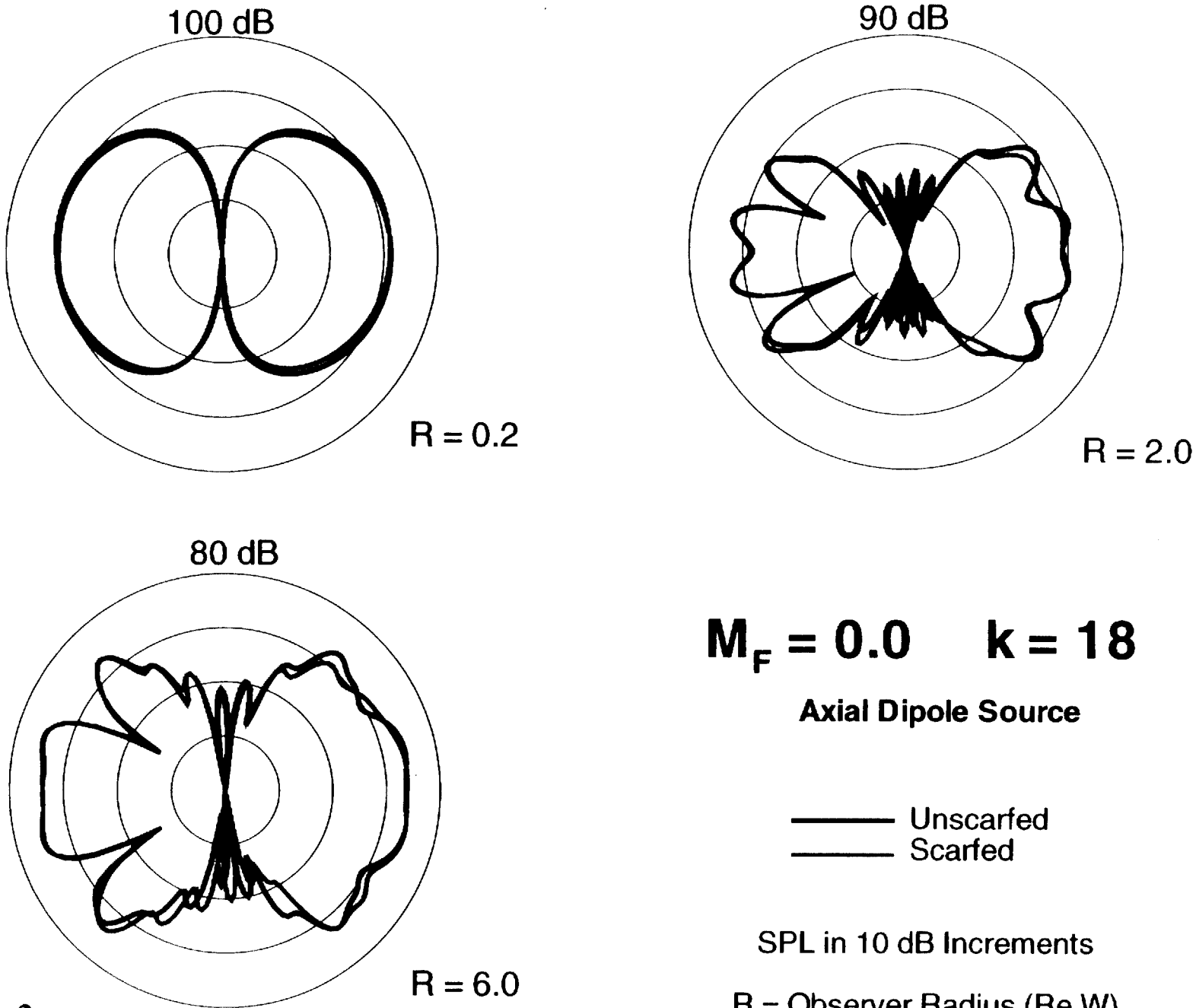
100 dB
R = 0.2
90 dB
R = 2.0
80 dB
R = 6.0
$M_F = 0.0$ k = 18
Axial Dipole Source
Unscarfed
Scarfed
SPL in 10 dB Increments
R = Observer Radius (Re W)

Figure 2

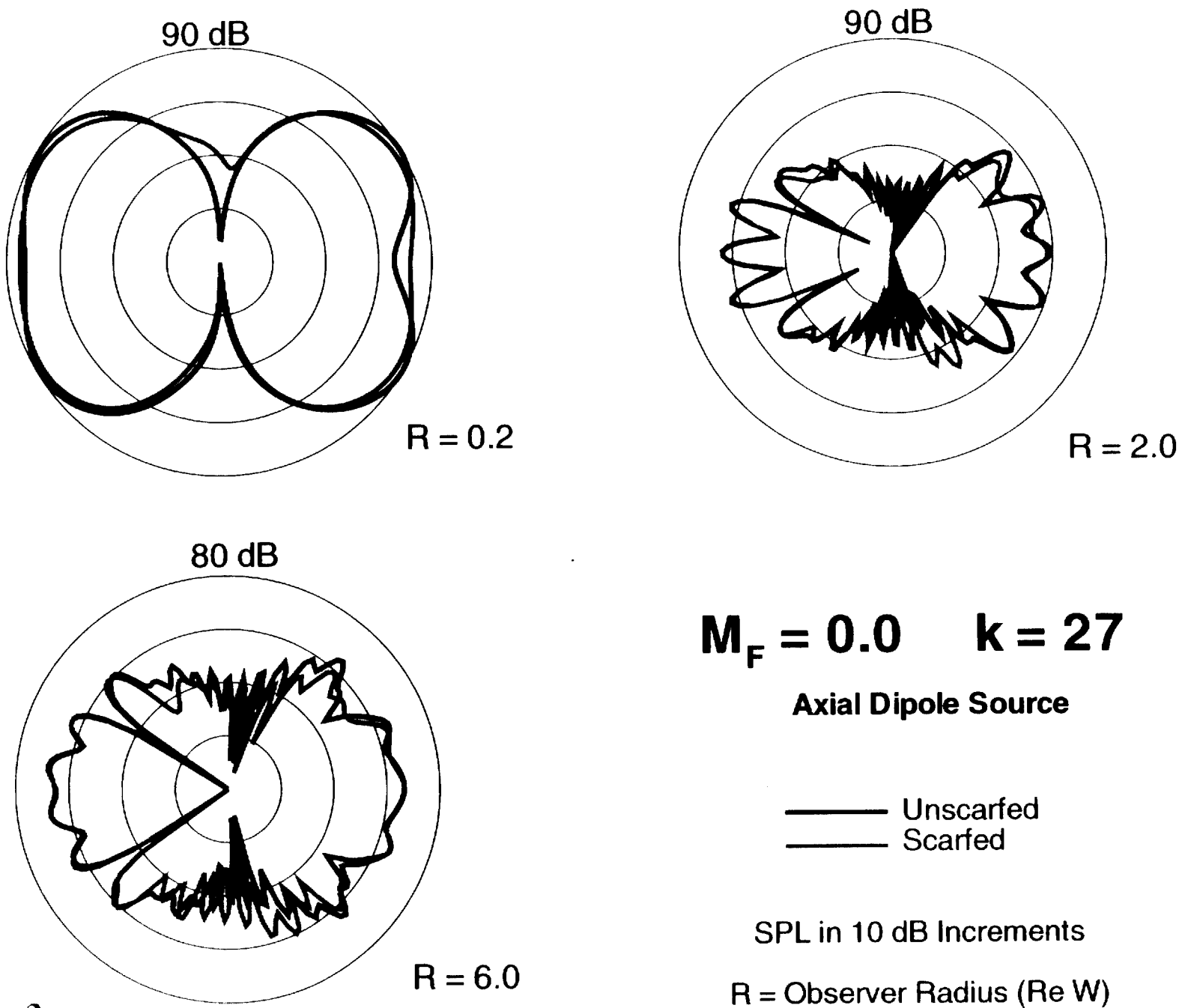
90 dB
R = 0.2
90 dB
R = 2.0
80 dB
R = 6.0
$M_F = 0.0$ k = 27
Axial Dipole Source
Unscarfed
Scarfed
SPL in 10 dB Increments
R = Observer Radius (Re W)

Figure 3

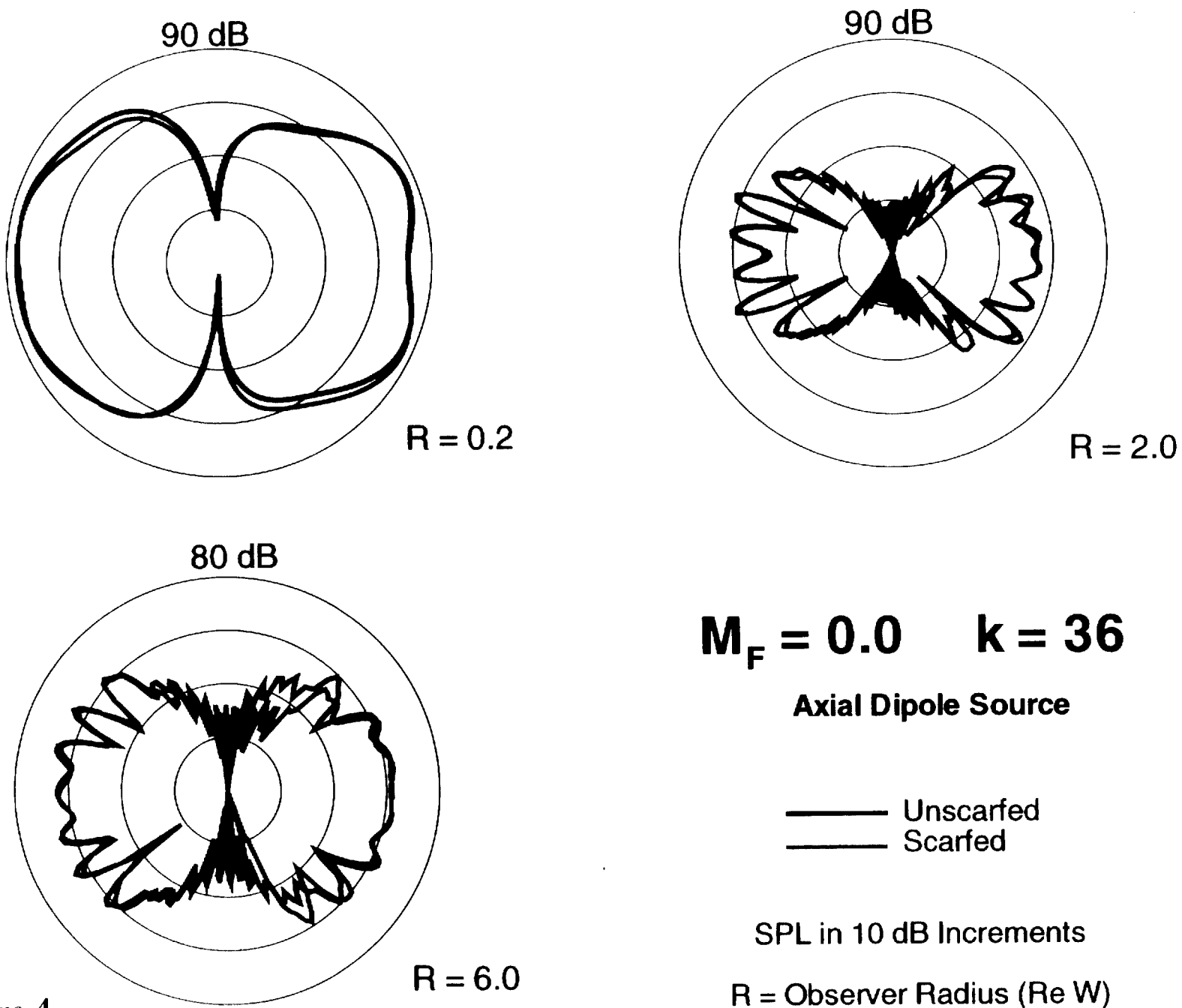
90 dB
R = 0.2
90 dB
R = 2.0
80 dB
R = 6.0
$M_F = 0.0$ k = 36
Axial Dipole Source
Unscarfed
Scarfed
SPL in 10 dB Increments
R = Observer Radius (Re W)

Figure 4

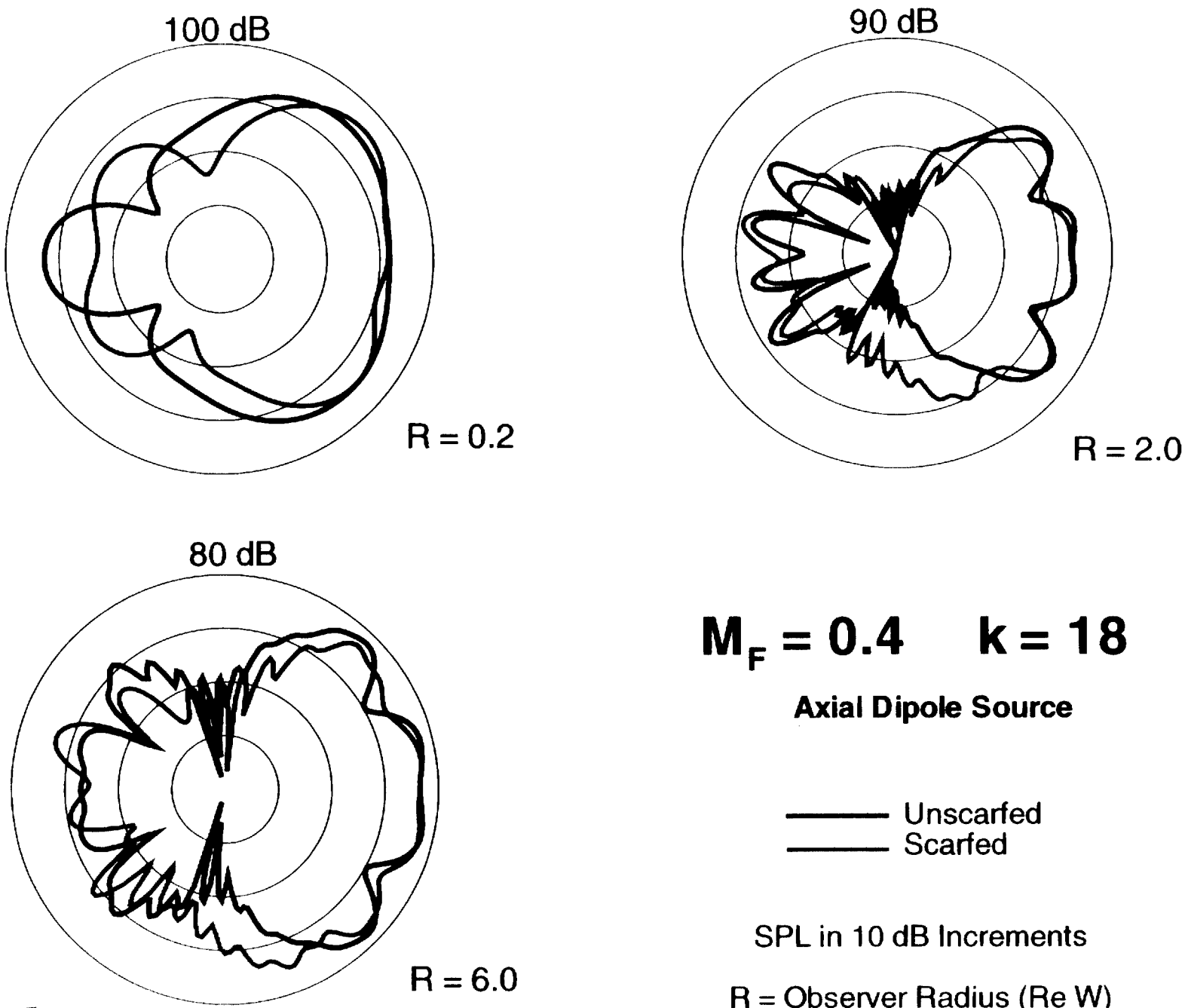
100 dB
R = 0.2
90 dB
R = 2.0
80 dB
R = 6.0
$M_F = 0.4$ k = 18
Axial Dipole Source
Unscarfed
Scarfed
SPL in 10 dB Increments
R = Observer Radius (Re W)

Figure 5

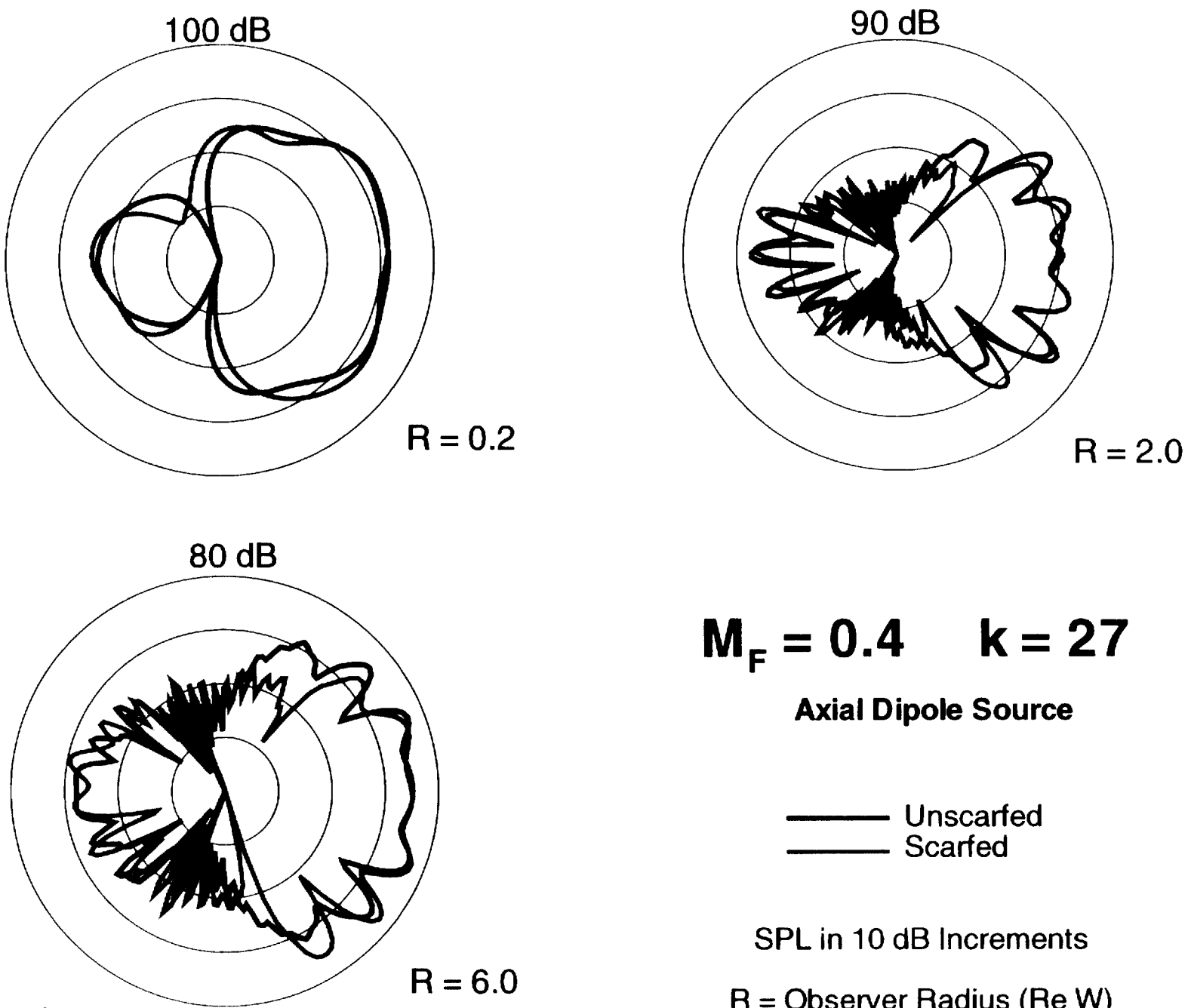
100 dB
R = 0.2
90 dB
R = 2.0
80 dB
R = 6.0
$M_F = 0.4$ k = 27
Axial Dipole Source
Unscarfed
Scarfed
SPL in 10 dB Increments
R = Observer Radius (Re W)

Figure 6

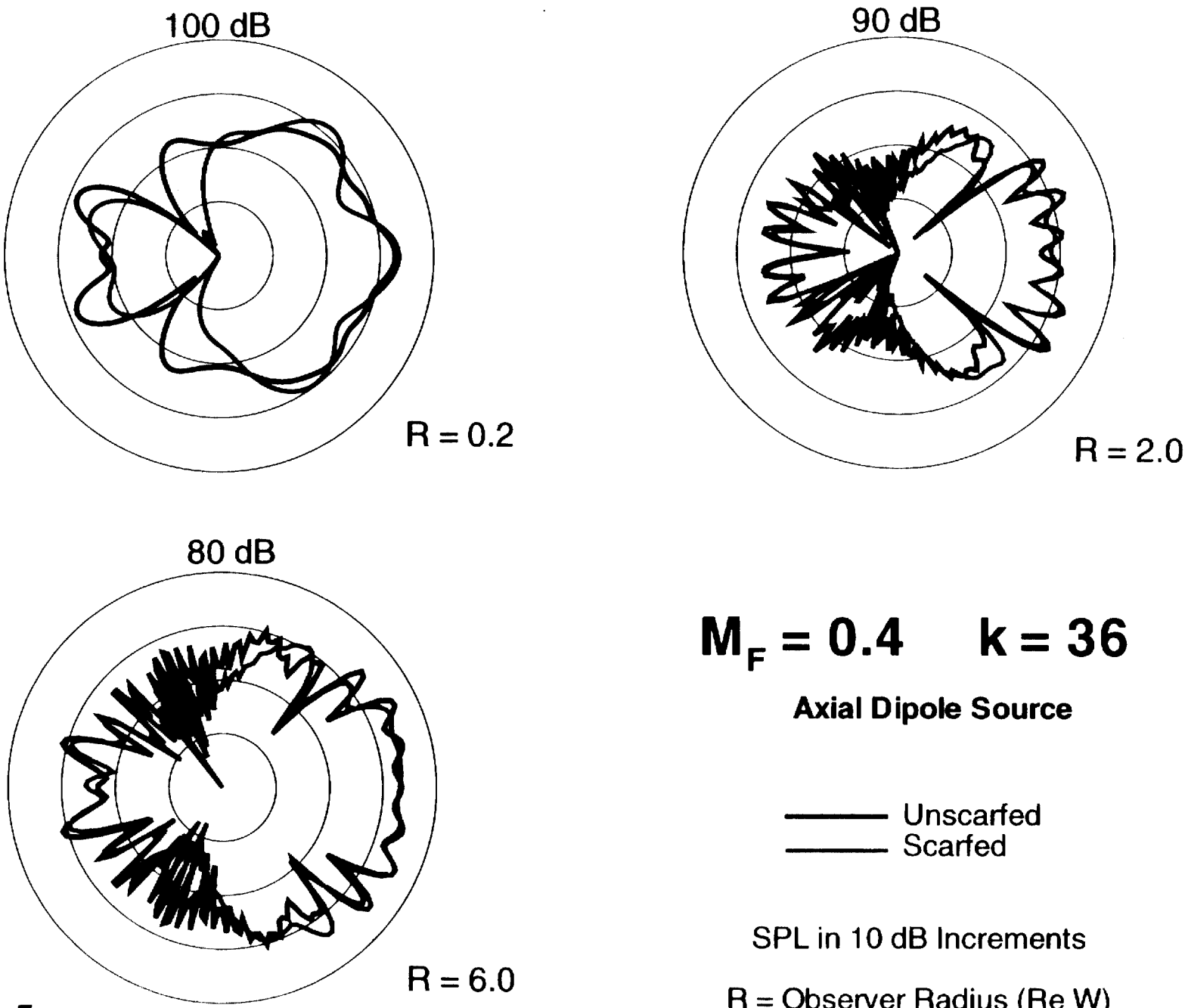
100 dB
R = 0.2
90 dB
R = 2.0
80 dB
R = 6.0
$M_F = 0.4$ k = 36
Axial Dipole Source
Unscarfed
Scarfed
SPL in 10 dB Increments
R = Observer Radius (Re W)

Figure 7

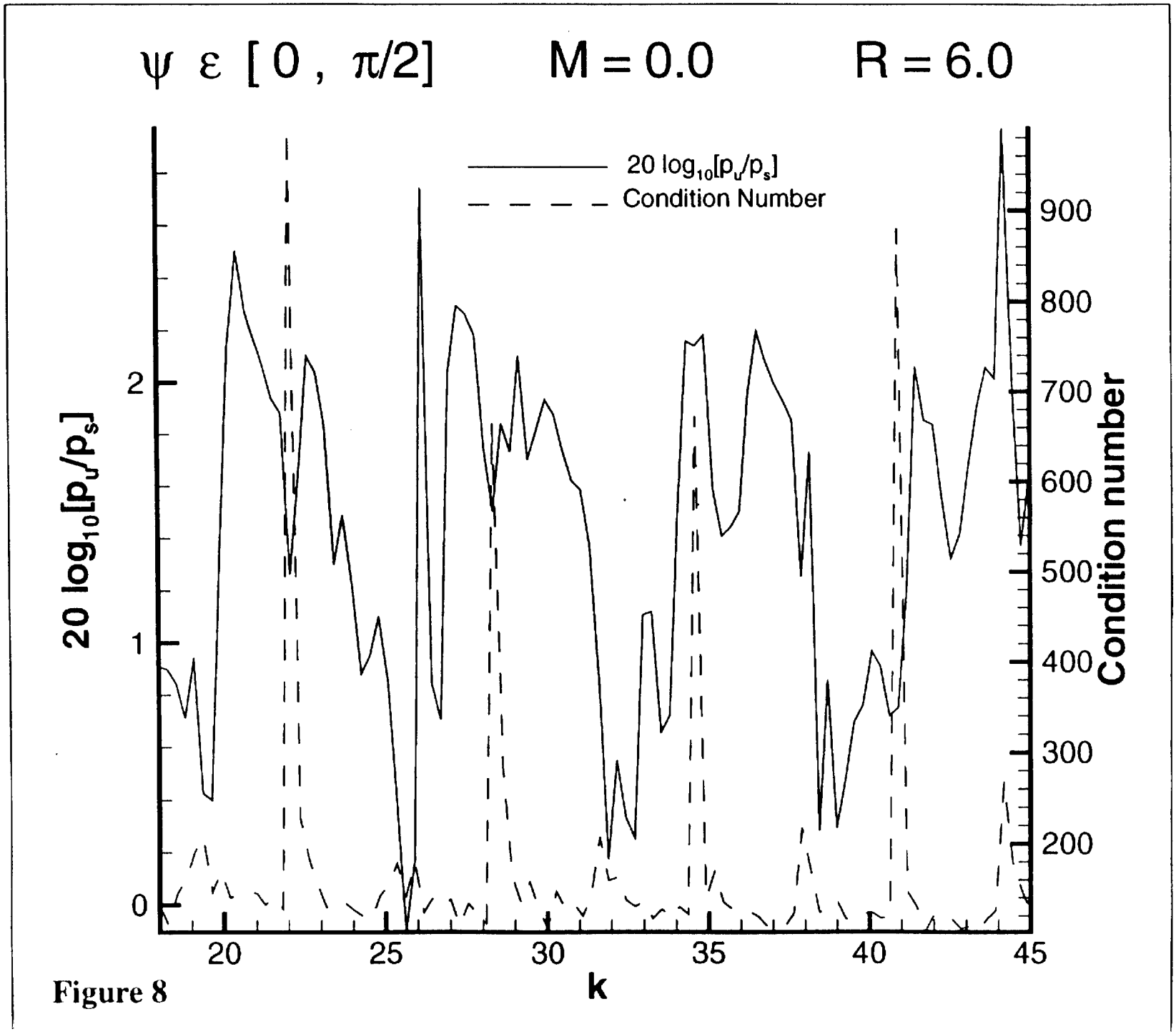
ψ ε [0 , π/2]
M = 0.0
R = 6.0
20 log10[pu/ps]
Condition Number
20 log10[pu/ps]
Condition number
k
0
1
2
200
300
400
500
600
700
800
900
20
25
30
35
40
45

Figure 8

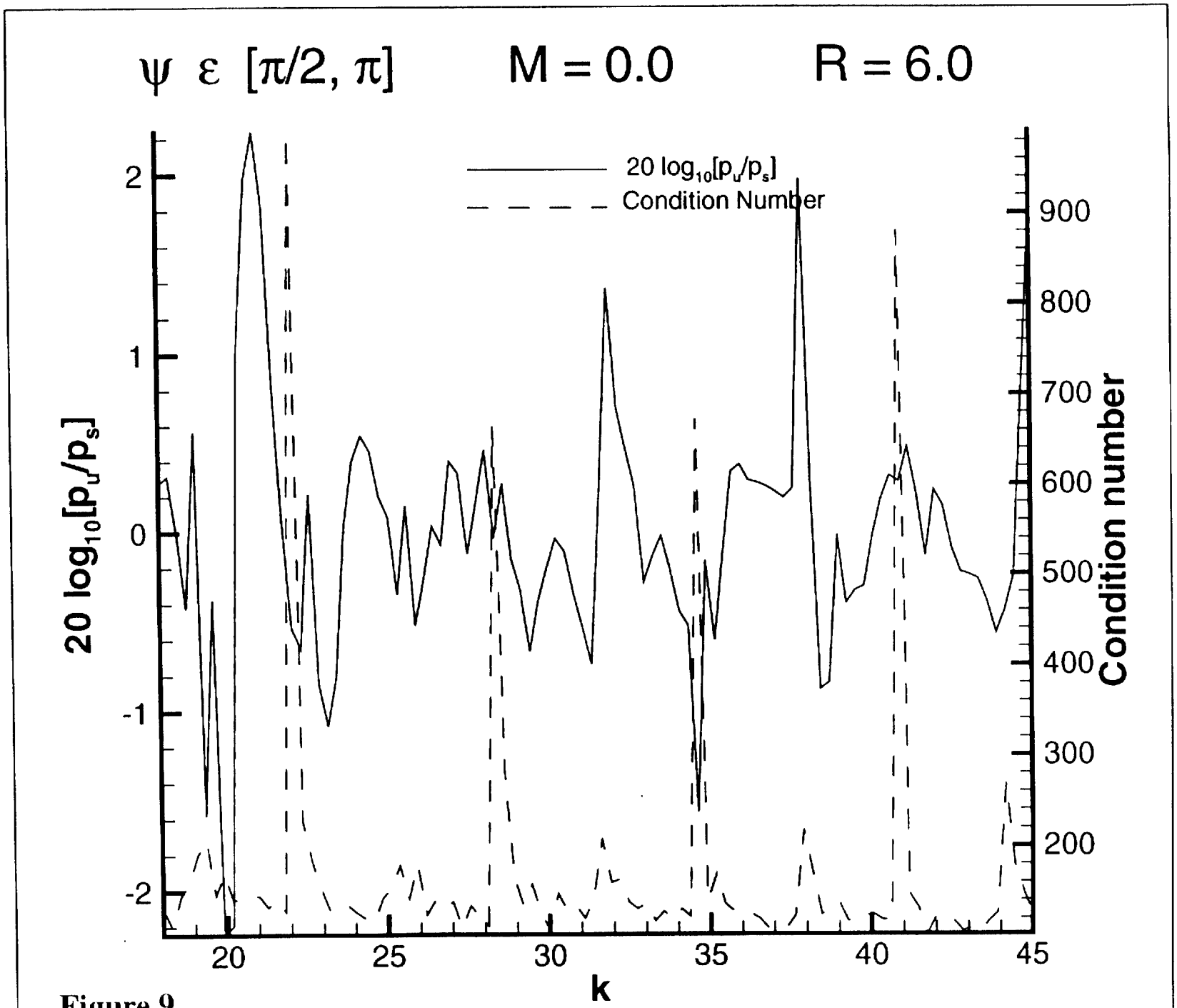
ψ ε [π/2, π]
M = 0.0
R = 6.0
20 log10[pu/ps]
Condition Number
20 log10[pu/ps]
Condition number
k
2
1
0
-1
-2
900
800
700
600
500
400
300
200
20
25
30
35
40
45

Figure 9

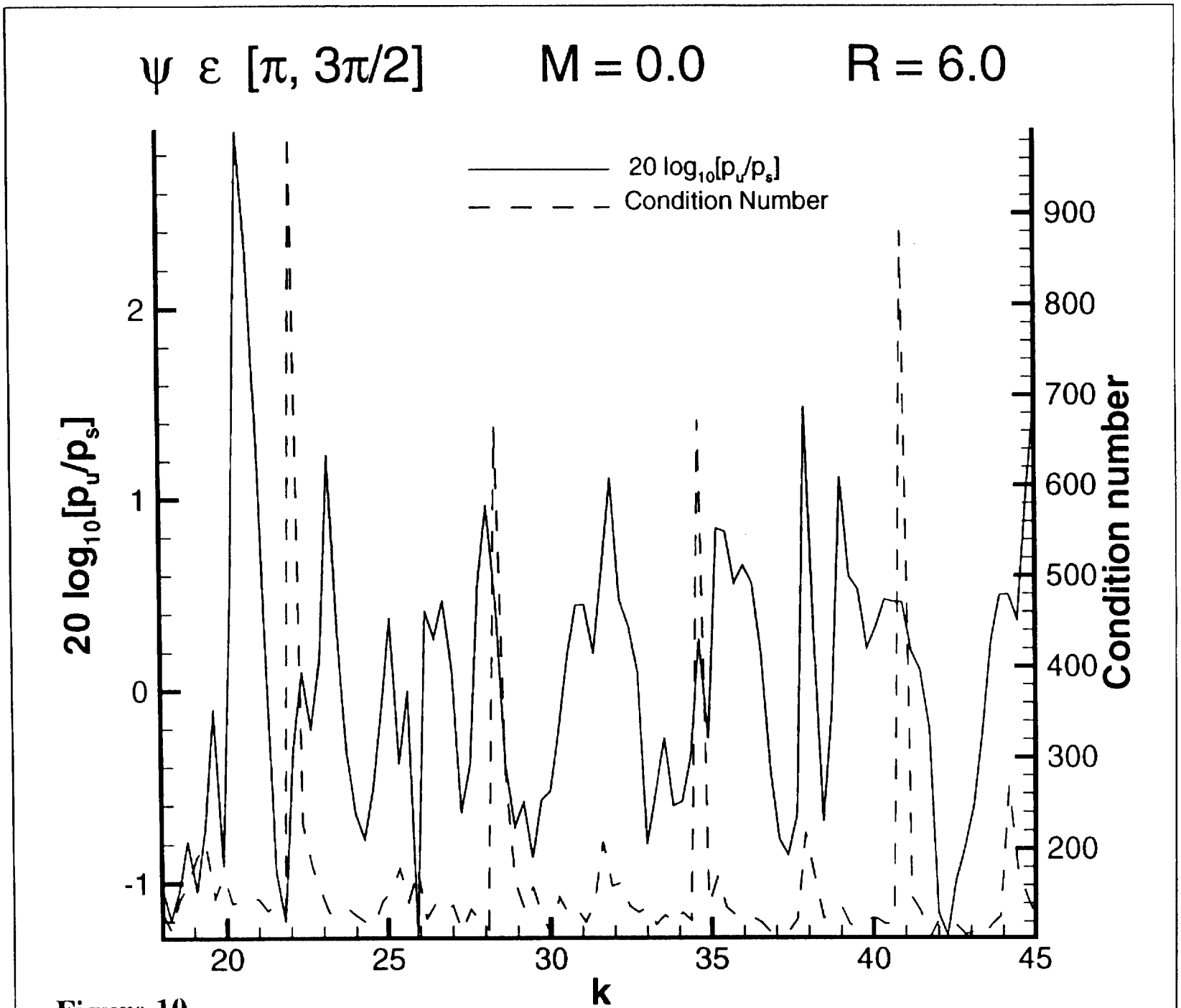
ψ ε [π, 3π/2]
M = 0.0
R = 6.0
20 log10[pu/ps]
Condition Number
20 log10[pu/ps]
Condition number
k
2
1
0
-1
900
800
700
600
500
400
300
200
20
25
30
35
40
45

Figure 10

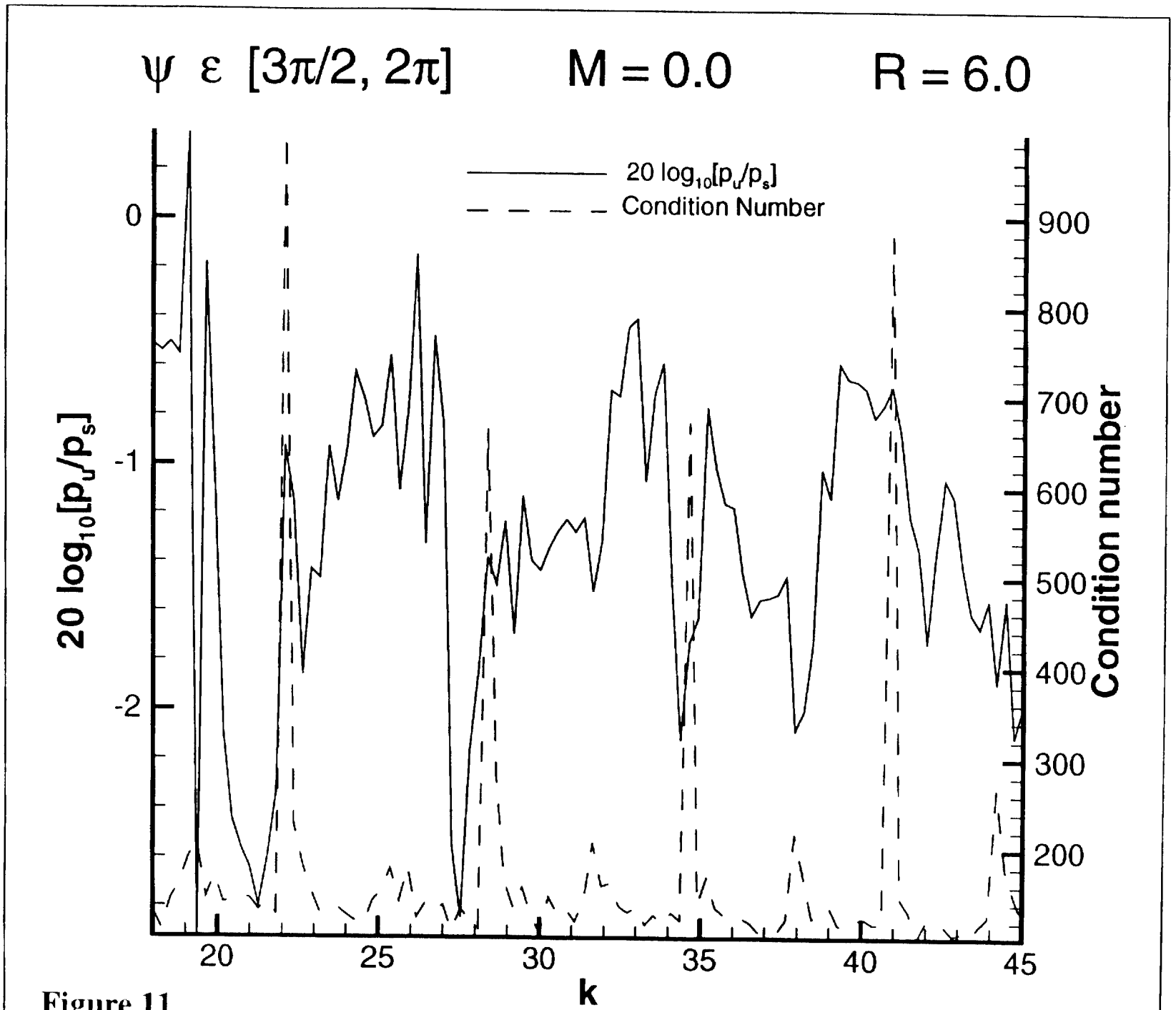
ψ ε [3π/2, 2π]
M = 0.0
R = 6.0
20 log10[pu/ps]
Condition Number
20 log10[pu/ps]
Condition number
k
0
-1
-2
900
800
700
600
500
400
300
200
20
25
30
35
40
45

Figure 11

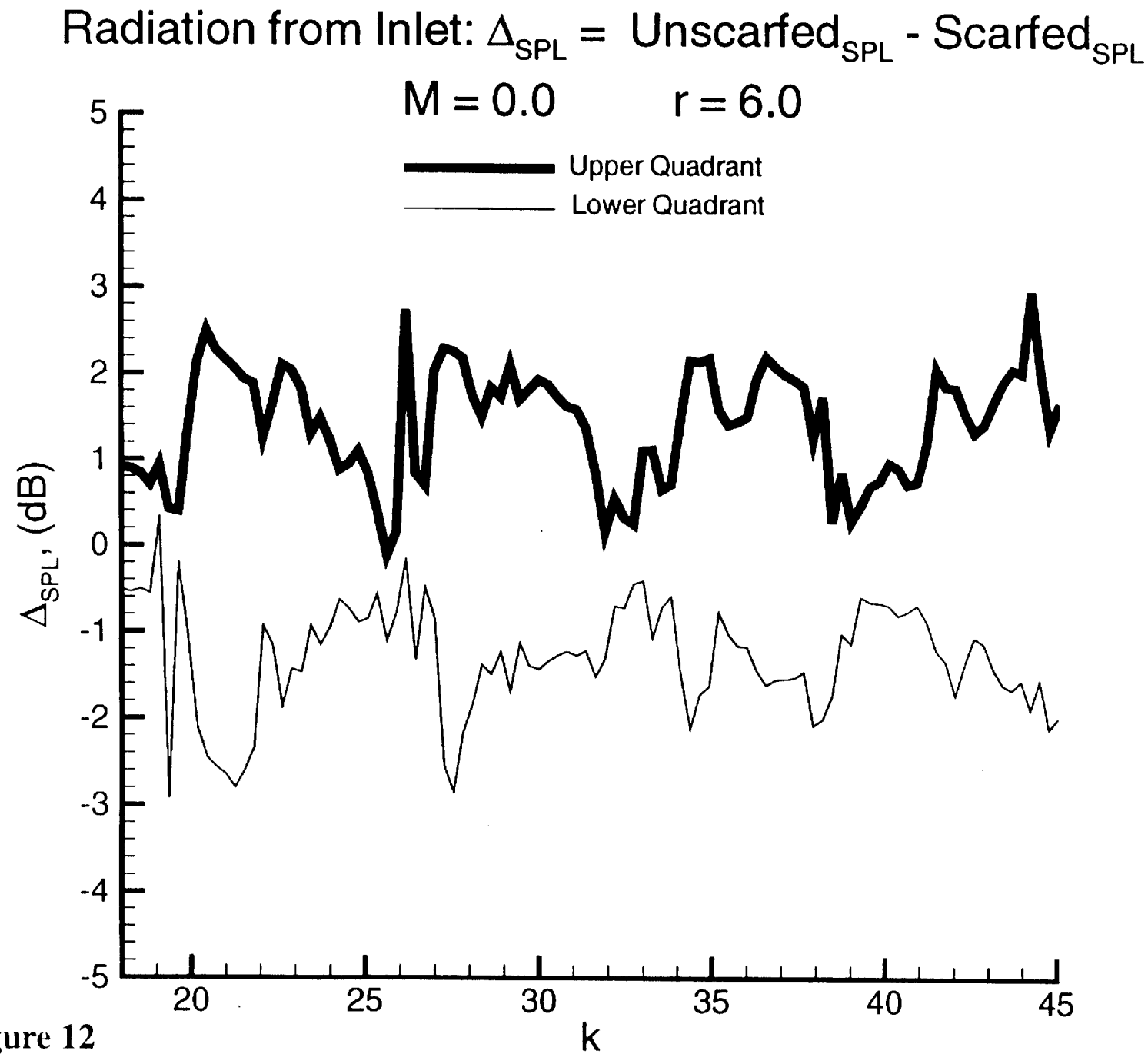
Radiation from Inlet: Δ_{SPL} = Unscarfed$_{SPL}$ - Scarfed$_{SPL}$
M = 0.0 r = 6.0
Upper Quadrant
Lower Quadrant
Δ_{SPL}, (dB)
5
4
3
2
1
0
-1
-2
-3
-4
-5
20
25
30
35
40
45
k

Figure 12